1972

Experimental Studies of the Metal-Nonmetal Transition in Nickel-Sulfide.

Jeffrey Francis Trahan
Louisiana State University and Agricultural & Mechanical College

INFORMATION TO USERS

This dissertation was produced from a microfilm copy of the original document. While the most advanced technological means to photograph and reproduce this document have been used, the quality is heavily dependent upon the quality of the original submitted.

The following explanation of techniques is provided to help you understand markings or patterns which may appear on this reproduction.

1. The sign or "target" for pages apparently lacking from the document photographed is "Missing Page(s)". If it was possible to obtain the missing page(s) or section, they are spliced into the film along with adjacent pages. This may have necessitated cutting thru an image and duplicating adjacent pages to insure you complete continuity.

2. When an image on the film is obliterated with a large round black mark, it is an indication that the photographer suspected that the copy may have moved during exposure and thus cause a blurred image. You will find a good image of the page in the adjacent frame.

3. When a map, drawing or chart, etc., was part of the material being photographed the photographer followed a definite method in "sectioning" the material. It is customary to begin photoing at the upper left hand corner of a large sheet and to continue photoing from left to right in equal sections with a small overlap. If necessary, sectioning is continued again – beginning below the first row and continuing on until complete.

4. The majority of users indicate that the textual content is of greatest value, however, a somewhat higher quality reproduction could be made from "photographs" if essential to the understanding of the dissertation. Silver prints of "photographs" may be ordered at additional charge by writing the Order Department, giving the catalog number, title, author and specific pages you wish reproduced.

University Microfilms

300 North Zeeb Road
Ann Arbor, Michigan 48106

A Xerox Education Company

Experimental Studies of the Metal-Nonmetal Transition in Nickel Sulfide

A Dissertation

Submitted to the Graduate Faculty of the
Louisiana State University and
Agricultural and Mechanical College
in partial fulfillment of the
requirements for the degree of
Doctor of Philosophy

in

The Department of Physics and Astronomy

by
Jeffrey Francis Trahan
B.S., Tulane University, 1963
May, 1972

ACKNOWLEDGEMENTS

The author wishes to thank Dr. Roy G. Goodrich for suggesting the problem and providing guidance and assistance throughout the course of the experiment. Thanks are due to Drs. Claude G. Grenier and Steven Watkins for many informative discussions.

The author wishes to express thanks to the staffs of the machine and electronics shops for assistance in preparation and running of the experiments. Special thanks are due to the author's wife, Jean Trahan, who was lovingly coerced into typing and proofreading this manuscript.

The author wishes to acknowledge the United States Atomic Energy Commission (Contract #AT-(40-1)-30087) for partial financial support of the experiment. Financial assistance received from the Dr. Charles E. Coates Memorial Fund of the L.S.U. Foundation donated by George H. Coates for preparation of this manuscript is gratefully acknowledged.

ABSTRACT

Experimental measurements were conducted on stoichiometric samples of hexagonal NiS to aid in understanding the metal-nonmetal transition which occurs at 263°K. Methods of preparing stoichiometric samples and of etching and chemically polishing single crystals are presented such that the polished surfaces are suitable for optical measurements.

An x-ray crystal structure determination was conducted on sintered samples. The symmetry of the unit cell was found changed from $P6_3/mmc$ in the metallic state to $P6_3/mc$ in the semiconducting phase.

The specific heat of sintered pellets was measured from 35 to 330°K and measurements in the neighborhood of the metal-nonmetal transition were done in extreme detail. The transition was found to have the characteristics of a first order phase change broadened by inhomogenity. The latent heat was found to be 1383 J/mole, which is in close agreement with the value obtained from other data using the Clapeyron equation. An entropy change of 5.03 J/mole°K was measured. A change in the Debye temperature is indicated but no conclusive statement can be made due to the extreme sensitivity of the Debye temperature to small experimental error.

Reflectivity measurements were conducted both above

and below the critical temperature and the reflectance was found to decrease discontinuously at the critical temperature at wavelengths in the near infrared. The results of resistivity measurements on a single crystal and a powdered sample are presented.

TABLE OF CONTENTS

LIST OF TABLES

LIST OF FIGURES

I INTRODUCTION

In recent years a wide variety of substances have been found to change from a metal to a nonmetal (either semiconductor or insulator) as a function of temperature and/or pressure. This phenomenon is called the metal-nonmetal (MNM) transition and occurs in such systems as mercury vapor, iodine, disordered semiconductors and glasses, metal ammonia solutions and transition metal compounds. A large number of transition metal compounds exhibit this transition and in this section some of the background information on the characteristics and general problem of the metal MNM transition in transition metal compounds will be presented. This introduction is not intended to be an exhaustive review of the subject, but is meant to provide background information such that the reader will have a basic understanding of the problem. A more complete review of the subject of the metal-nonmetal transition can be found in an article by Mott and Zinamon[1] (1970); and Volume 40 of Reviews of Modern Physics is devoted entirely to the metal-nonmetal transition. Reviews dealing specifically with the transition metal compounds are found in articles by Doniach[2] (1969) and Adler[3] (1968), and the metal-nonmetal transition in the transition metal oxides is discussed by Adler in Volume 21 of Solid State Physics (1968).

A. THE METAL-NONMETAL TRANSITION IN TRANSITION METAL COMPOUNDS

Among the transition metal compounds metal-nonmetal transitions are found in substances such as Ti_2O_3, Ti_3O_5, VO_2, Ti_4O_7, V_2O_3, V_3O_5, V_4O_7, V_6O_{13}, VS, CrS, TiS, NiS and Fe_3O_4. The list is not complete, but is sufficient to demonstrate that the transition is not uncommon. These materials are semiconducting at low temperatures and exhibit a negative temperature coefficient of resistance and become metals (positive temperature coefficient of resistance) at higher temperatures. Over a very narrow temperature range, at a critical temperature, their conductivities jump almost discontinuously, sometimes by as much as a factor of 10^7 as in the case of V_2O_3. Many of the compounds exhibit crystalline distortions, antiferromagnetic transitions, discontinuous volume changes and thermal hysteresis at the critical temperature. The transitions are of first order. On the other hand MnO, NiO, CoO, FeO, FeS_2, Fe_2O_3 and a number of other compounds are good insulators from 0^oK to their melting point and do not undergo a MNM transition, and TiO, CrO_2, TiS and CoS_2 are good metals at all temperatures. It is clear that there exist a wide variety of electrical properties in a group of very similar compounds.

According to the one-electron picture of solids a crystalline substance with an even number of electrons

per unit cell will be an insulator at absolute zero temperature if the maximum energy of the valence band is separated from the minimum energy of the conduction band by a positive energy gap. At temperatures greater than zero, if the energy gap is small, the substance will be a semiconductor because electrons can be thermally activated across the gap into a conduction band. If the energy gap is negative, that is, the bands overlap, or if a partially filled band exists, then the substance will be a metal. Since energy bands in solids are almost temperature independent a strictly one electron model cannot account for the MNM transition.

In order to demonstrate that the electronic properties of some of the transition metal compounds cannot be described by ordinary band theory, consider MnO. MnO has the NaCl structure and is an antiferromagnet. Both above and below the Neel temperature it is an insulator with a resistivity on the order of 10^{15} Ω cm. In the transition metal oxides, the bands in the vicinity of the Fermi energy are composed of the d orbitals of the cations. The 3d band of the cation is split into a sixfold-degenerate (t_{2g}) subband and an upper fourfold-degenerate subband by a strong crystalline field due to the ionic nature of the O^{2-} ions. After satisfying the requirements of chemical bond, each manganese ion has only five 3d electrons. Thus band theory predicts that

MnO should have a partly filled band and should then be metallic.

If no crystalline symmetry change occurs at the transition temperature, a simple mechanism for the metal-nonmetal transition is ordinary band overlap. In a semiconductor if a filled valence band is separated from an empty conduction band with an energy gap that decreases with an increasing temperature and these bands are not of the same symmetry, then as the gap decreases, the resistivity of the sample will decrease exponentially. As the bands cross the resistance would increase linearly as in metallic conductivity. This type of transition would be gradual and no sharp jump in the conductivity would be seen. Mott[4] has suggested that the transition would be sharpened somewhat if exitons were produced near the transition temperature but this would not produce a sharp transition where the resistivity changed several orders of magnitude.

Slater[5] pointed out that in an antiferromagnet an electron encounters a spin dependent potential. The number of molecules in the magnetic permitive cell is doubled in the antiferromagnetic state from that in the paramagnetic state. Thus antiferromagnetism could possibly split a band into two subbands each containing an equal number of states. If one band were full and the other empty below the transition, non-metallic behavior would be predicted. One objection to this model is that

the insulating properties of MnO, NiO and similar compounds do not disappear at the Neel temperature. They do disappear, however, in NiS and V_2O_3.

Many of the compounds which undergo a metal-nonmetal transition also exhibit crystalline distortions at the critical temperature. If a distortion will increase the number of molecules per unit cell as might occur when ion pairs line up along a given crystalline axis, the increase in periodicity could introduce an energy gap. A simple reduction in symmetry can cause splittings due to higher order terms in the crystalline field. This model was treated quantitatively by Adler and Brooks[6]. It is not clear that crystalline distortion, especially of the kind required by their theory occur in all cases of the MNM transition.

In order to explain the purely insulating properties of MnO, NiO, and CoO, electronic correlations were invoked by Mott[4,7]. Consider an array of one electron atoms with one atom per unit cell. According to band theory, this array would be expected to be metallic because it has a half filled band. Suppose now that the lattice parameter is relatively large such that the material has narrow bands. In this case the electronic energy levels will not be very different from the atomic levels and the overlap between orbitals will be small. If an attempt to add a second electron to a site is made, there will be a Coulomb repulsion energy, U, if the

electrons have opposite spin. Thus conduction of electrons in such an array will have an activation energy U. Suppose that the lattice parameter is decreased. Mott argued that the change in resistivity must be discontinuous because if an electron is removed from one atom and placed on another atom in the insulator, the electron and the hole would attract each other by means of a coulomb interaction forming an exciton which does not participate in conduction. This will happen only when screening by other free carriers is small. The screened coulomb potential is given by

$$V = - \frac{e^2}{Kr} e^{-\alpha r}$$

where α is a screening constant. This potential will become too weak to have bound-state solutions at sufficiently large values of α producing a sharp transition in the conductivity. In this manner the insulating properties of MnO and NiO might be explained. MnO is sometimes called a Mott insulator. Indeed, Kohn has shown that a one dimensional array of monovalent atoms can be nonconducting.[8] Experimentally, a Mott transition should manifest itself as a sharp change in the conductivity as a function of pressure.

A model which includes the effect of correlations into band theory was proposed by Hubbard[9,10,11]. He introduced the following Hamiltonian:

$$H = \sum_{ij} T_{ij}\, c_{i\sigma} c_{j\sigma}^{+} + U \sum_{i} n_{i\uparrow} n_{i\downarrow}$$

which is written in the Wannier representation where sigma is a spin and i and j are lattice sites. The Coulomb matrix element for electrons on the same site is geven by

$$U = \langle ii \left| \frac{e^2}{R} \right| ii \rangle$$

and is the energy necessary to place two electrons on the same site. The second term then, counts the number of doubly occupied sites and multiplies the result by U. The first term is a hopping matrix which allows electrons to move from site to site and T_{ij} is an overlap integral. Using this Hamiltonian Hubbard showed that correlation effects in narrowband materials with large values of U can give insulating states.

In the preceeding paragraphs several theroetical models have been presented which attempt to explain the electronic properties of the transition metal compounds. There are several other models, but they sill not be discussed. Generally, the properties of each of the compounds are examined and one or more of the models is invoked to explain why the compound has a metal-nonmetal transition or why it is a metal or an insulator. A chicken or the egg problem exists, however, because many of the substances exhibit a crystalline

distortion, a magnetic transition and a sharp change in the conductivity all at the same temperature. Does the crystalline distortion induce the conductivity change or vice versa? Also, if the metal-nonmetal transition occurs at the same temperature as a crystalline distortion and the antiferromagnetic ordering, does the antiferromagnetism or the crystalline distortion induce the conductivity change? Mott[1] has made a point of stating that he believes it would be wrong to suppose that the same mechanism is responsible for the metal-nonmetal transition in all the transition metal compounds. With these introductory remarks in mind, a review of the experimental situation for NiS will now be presented.

B. THE METAL-NONMETAL TRANSITION IN NiS

The transition metal compounds in general and NiS in particular present a fundamental experimental problem because it is very difficult to make stoichiometric single crystals. Most of the transition metal compounds crystallize over a wide compositional range in the same crystalline structure. The compositional variation is a result of the formation of defects in the structures. The electronic properties of all these compounds can be dominated by impurities and defects and in many cases the published data may not accurately represent the intrinsic properties of the crystal. The fact that deviations from stoichiometry change the electronic properties of NiS drastically has been pointed out by several authors[12,13] and this fact must be borne in mind when interpreting experimental results on the metal non-metal transition in NiS.

In the stoichiometric composition, NiS has been found to exist in three distinct phases conventionally labeled α , β and γ NiS[14]. The type generally produced in chemical reactions is α NiS and it is amorphous. The type of interest in this work is β NiS which has the NiAs structure. It is stable only above 379± 3°C[15] at which temperature the crystal undergoes a $\beta \rightarrow \gamma$ inversion. That is, below 379°C, γ NiS is the stable stoichiometric compound and is of the

rhombohedral structure. The γ type is the form commonly found in nature and is known as the mineral millerite. The most recent and complete study of the Ni - S system and related compounds was done by Kullerud and Yund[15] (1962) who constructed a complete composition vs. temperature phase diagram from 200 to 1030°C. Their results are shown in Figure 1. As can be seen from the diagram β NiS forms a relatively extensive solid solution with excess sulfur, but will not take measurable amounts of excess Ni into its structure. At 400°C NiS in the NiAs structure will exist from about 49.9 to 51.1 at.% S. Stoichiometric β NiS can be forced to retain its high temperature NiAs structure by quenching the crystals in cold water from above 379°C. It was noted by Kullerud and Yund[13] that quenched samples were relatively unstable at room temperature. They found that at 25°C, whether kept in a vacuum or in the atmosphere, the β modification partially converts into millerite after a few months. This indicates that only newly prepared samples should be used in experiments although no indication of the conversion was seen during the x-ray measurements conducted for this thesis.

Experimental work relative to the metal-nonmetal transition was first done by Sparks and Komoto[16]. They conducted powder neutron diffraction studies on hexagonal NiS and found a paramagnetic-antiferromagnetic ordering

at 263°K. Below the Neel temperature, T_N, within a given hexagonal layer, the magnetic moments were found to be ferromagnetically coupled while adjacent layers were antiferromagnetically coupled. The temperature dependence of the lattice parameters was determined by measuring the shifts in two nuclear peak positions which showed that the c/a ratio increased on cooling through the transition with the a and c lattice parameters increasing by .3 and 1% respectively. No indication of a lattice distortion was found and a considerable thermal hysteresis was observed. Thus, the transition was found to possess several characteristics of a first-order transition -- a thermal hysteresis and discontinuities in the volume of the unit cell and the sublattice magnetization. Further work by the same authors[12,15] has shown that the magnetic moment at 4.2K is $1.66 \pm .08\mu_\beta$; that only four degrees below T_N, the moment was $1.5 \pm .1\mu_\beta$ indicating that most of the ordering occurs at or near the transition temperature. Almost no magnetic diffuse scattering[18] was found above the transition, in this case less than $.5\mu_\beta$ indicating that the magnetic moment associated with the Ni atoms above T_N is small.

The neutron diffraction data indicated that there might be interesting behavior in the resistivity near T_N. These measurements were carried out by Sparks and

Komoto[19] on compressed sintered samples and revealed an abrupt metal-semiconductor transition at the magnetic ordering temperature which occured at 264 ± 1°K. A resistance ratio, that is, $\rho(T < T_N)/\rho(T = 0^oC)$, of 100 was reported with a discontinuous jump by a factor of about 40 at the critical temperature. Their results are shown in Figure 2. Above the Neel temperature the resistivity was found to be a linear function of temperature and possess a positive temperature coefficient thus indicating metallic conduction. A plot of $\log\left(\rho(T)/\rho(T = 0^oC)\right)$ versus 1/T was found to be composed of two straight lines connected by a curved region similar to that which is observed for impurity semiconductors. Near the critical temperature the activation energy was found to be .12 ev while at lower temperatures, less than .01 ev.

The temperature and pressure dependence of the resistance was measured by Anzai and Ozawa[20] who found a sharp increase in the resistance at 230°K in polycrystalline ingots with a resistance ratio up to 20 and an activation energy near the transition of .01 ev. Although the resistivity increased abruptly at 230°K, the transition extended over a relatively wide temperature range: from 230 to 250°K. A study of the pressure dependence of the transition temperature showed that T_N decreases linearly with increasing pressure and that

$dT_N/dP = -(6.0 \pm 0.3)$ deg/kbar. This result has been recently verified by McWhan et al.[21] The magnetic susceptibility of powdered samples of NiS was measured by Sparks and Komoto[12] (Figure 3). Above and below the transition the susceptibility was found to be virtually temperature independent with a discontious change of 15% at T_N. This anomalously small increase was later explained by Horwood et al.[22,23,24], who showed that the susceptibility was anisotropic; that the susceptibility parallel to the c axis increased while that perpendicular to the c axis decreased. The results of these susceptibility measurements are shown in Figure 4. Other magnetic susceptibility measurements were done by Anzai and Ozawa[20] principally to confirm that the metal-semiconductor transition occured at the same temperature as the magnetic transition in their samples. The magnetic transition in these samples was not sharp. Tsubokawa[25] performed magnetic susceptibility measurements on powdered samples and torque measurements on single crystal samples before Sparks and Komoto had determined that NiS underwent a metal-semiconductor transition. He determined that NiS became antiferromagnetic at a critical temperature of 150°K and from the torque measurements on single crystals determined that the spins were directed along the c axis which was later corroborated by Sparks and Komoto[15].

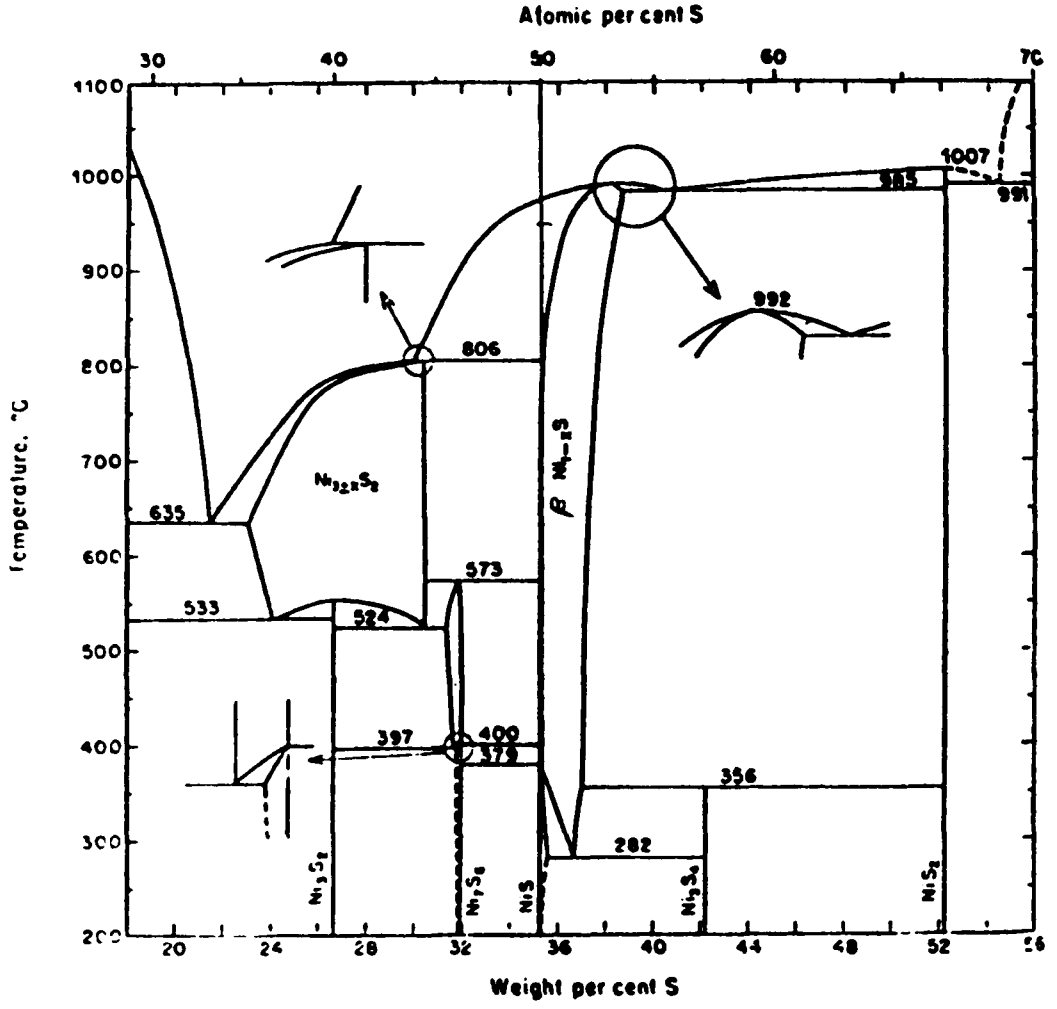

Figure 1

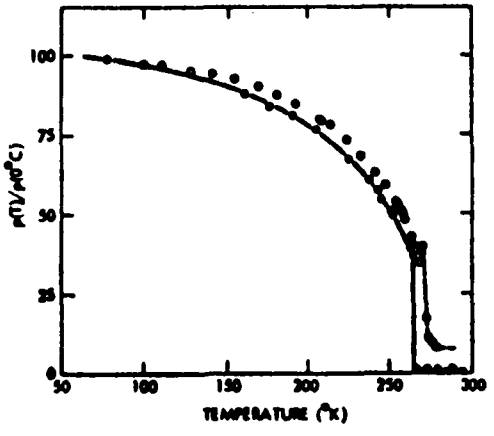

Figure 2

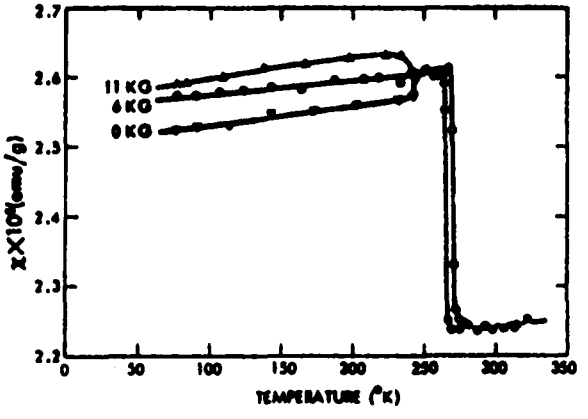

Figure 3

Smith and Sparks[26] used neutron diffraction to study effects of pressures up to 8 kbar at temperatures both above and below T_N. The results have shown that the compressibility of the lattice is small and essentially independent of temperature. They suggest that there is a migration of Ni atoms from their octahedral positions to their tetrahedral interstitial sites with increasing pressure, but that at 5 kbars the process is reversed and there is a tendency toward perfect ordering of the NiAs lattice. Also at 5 kbars, the Ni moment increases toward its maximum allowed value. These data have been refuted by Anzai and Ozawa[27] who studied the pressure dependence of the resistivity in the same pressure region. No anomalous behavior in the resistivity was found at 5 kbars suggesting that the disorder found by Smith and Sparks was not present in the samples used by Anzai and Ozawa. They did, however, see a change in the resistivity at 3.5 kbars which extended over a relatively wide pressure range of 3 kbars and at a temperature of 219°K. The resistivity decreased gradually with increasing pressure. This effect was considered to correspond to the antiferromagnetic-paramagnetic transition.

A measurement of the specific heat near the transition temperature was first done by Tsubokawa[25] on samples with a Neel temperature of about 150°K and for which the

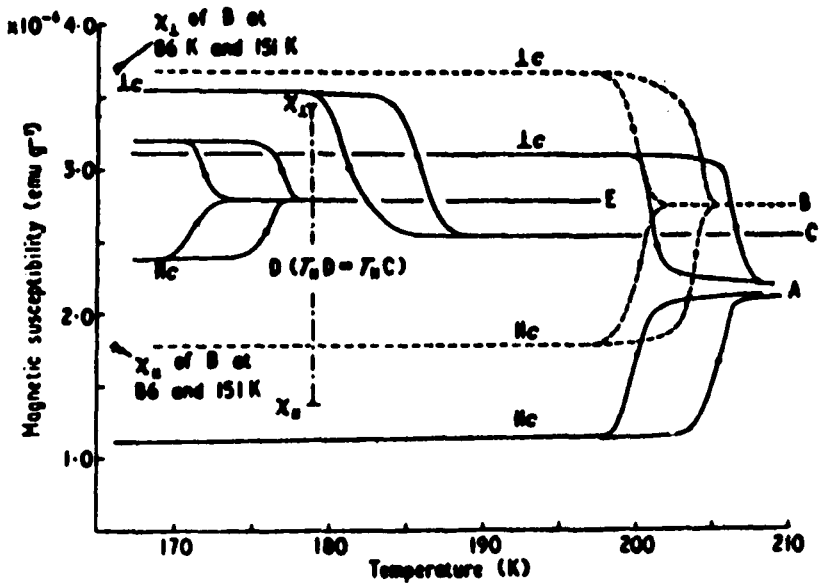

Figure 4

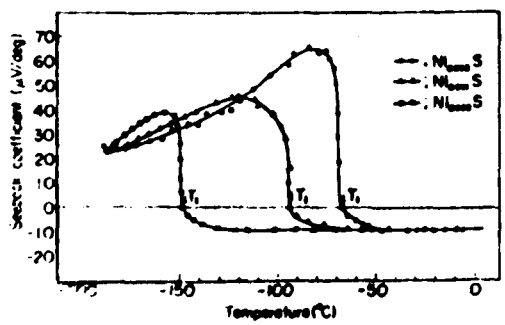

Figure 5

heat absorption due to the anomaly at T_N was estimated to be 50 J/mole. Raccah and Goodenough[28] used differential thermal analysis to show that the transition was first-order and endothermic.

Alsen[29] was the first to determine that the crystal structure of NiS is of the NiAs type. He determined the lattice parameters to be 3.42 and 5.30 Å for a and c respectively. These results were confirmed by Levi and Baroni[30] by both electron and x-ray diffraction. Lafitte[31] studied the variation of the lattice parameters as a function of composition and found that both a and c decreased in the sulfur rich samples. Lattice parameters for stoichiometric NiS were given as:

$$a = 3.4392\text{Å} \qquad c = 5.3484\text{Å}$$

Thermoelectric power measurements were performed as a function of Ni-S composition by Ohtani and Kosuge[32]. (Figure 5). The most notable result of these measurements is that the sign of the carriers changes from negative to positive at the transition temperature as the temperature is decreased indicating that the dominant current carriers are holes below T_N. The sign of the Seebeck coefficient changed at T_N for three different samples of three different sulfur concentrations, thus indicating that the transition mechanism appears to be common in all nonstoichiometric samples because there is no essential difference in the conduction behavior among

the samples.

Ohtani[33] measured the Hall coefficient, the mobility and the carrier concentration below the transition as a function of temperature in polycrystalline samples of varying sulfur concentration. The data were interpreted in terms of the one carrier model. In agreement with measurements of the thermoelectric power by Ohtani[32], the samples were clearly hole conductive and the number of carriers increased with an increase in sulfur content. For each sample studied the carrier concentration increased markedly at the transition temperature as the temperature was increased. A relatively low mobility below T_N, on the order of $3 cm^2/volt\text{-}sec$, was observed for all samples which implies narrow band conduction.

Single crystal resistivity and Hall measurements were performed by Horwood *et al.*[22,23] who also adopted the one carrier model to interpret the data. The carrier concentrations in the semiconducting and metallic phases were found to be on the order of 10^{18} and 5×10^{19} cm^{-3}, respectively. In contrast, Ohtani[33] found a carrier concentration of about 5×10^{20} cm^{-3} in the semiconducting state. Immediately below T_N, the activation energy of the conductivity was 0.17ev Adler's theory[34] was used to calculate the 3d band width which was found to be 0.4ev. From this result and the results of their observed mobilities, 1,000 $cm^2V^{-1}sec^{-1}$, the authors

concluded that the dominant mode of conduction below T_N was by holes in a wide band which overlaps the Ni 3d band. This was taken to be the sulfur 3p band. Ohtani and Horwood are in agreement, then, only in their conclusions regarding the type of carrier observed. Results of the single crystal resistivity and Hall measurements of Horwood *et al.*[24] are shown in Figures 6 and 7.

In a very abbreviated form, the above is a summary of much of the experimental work done on NiS regarding the metal-nonmetal transition. If a generality can be made about the data it is that the variability of the samples can be extremely high. A compilation of some of the different transition temperatures observed by the various experimenters is given in Table I. The trans-

Reference	T_N(°K)	Remarks
Tsubokawa(25)	150	magnetic measurements
Townsend(24)	172	magnetic susceptibility
Ohanti(32)	205	$Ni_{.995}S$, thermoelectric power
Horwood(27)	206	resistivity
Anzai(27)	230	resistivity
Sparks(16)	263	neutron diffraction
Sparks(12)	264	a review article
Smith(26)	265	pressure measurements

TABLE I Some reported transition temperatures of NiS.

ition temperature for NiS ranges fron about 150 to 265°K and no two groups have ever reported the same critical temperature. Resistance ratios vary from about 20 to

100 in polycrystalline samples.

Sparks and Komoto[12] determined how the transition temperature varies as a function of relative concentrations of Ni and S. They found that the transition temperature is a very sensitive function of the sulfur content and that T_N decreases rapidly as the quantity of sulfur increases (Figure 8). Nickel sulfide has a transition temperature of about 265°K while $Ni_{.98}S_{1.02}$ transforms at 150°K. The observed variability probably reflects the difficulties which are encountered in preparing stoichiometric samples.

Another experimental problem associated with NiS samples is that when passing through the transition temperature they shatter into thousands of small granules. This is probably caused by the discontinuous volume change at the critical temperature. If the sample is not at an exactly uniform temperature some portions will transform at different times than others causing the crystal to crack. Likewise, the same result will occur if the composition is not exactly homogeneous since different compositions have different critical temperatures.

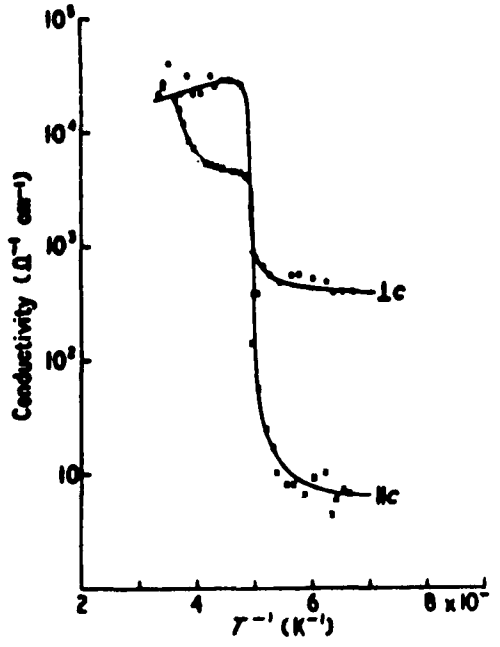

Figure 6

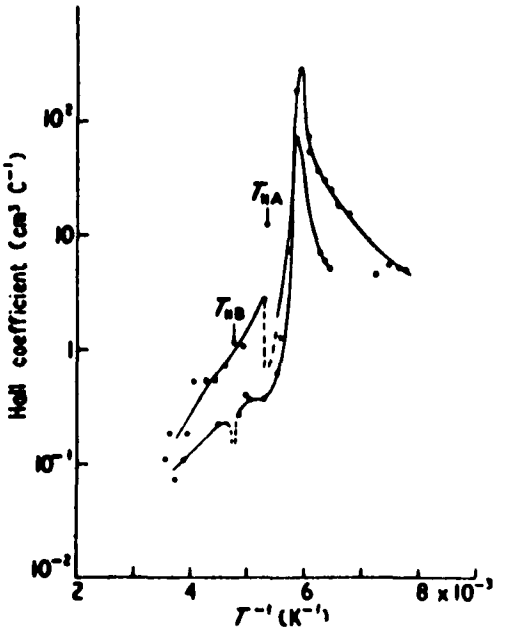

Figure 7

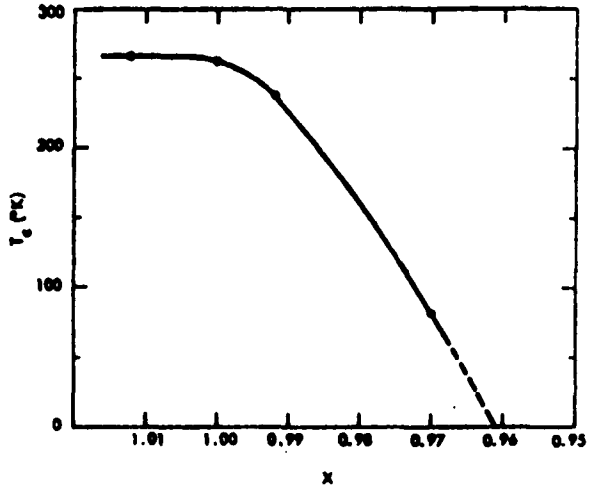

Figure 8

II CRYSTAL PREPARATION AND HANDLING

Since neither single crystal nor powdered samples of the hexagonal phase of Nis were available commercially and no information regarding crystal preparation of this form of NiS could be found in the literature, the first year of research was devoted to developing a method of producing relativly homogeneous crystals and powders. In addition, methods of etching and chemically polishing samples had to be found such that polished surfaces were suitable for optical measurements. To determine the uniformity of composition of the NiS ingots, a standard chemical method for quantitativly determining the amount of Ni in a small sample had to be developed so that the composition of a sample could be determined to within a tenth of a percent. This section contains a report of the various attempts made to produce NiS, a method of preparing NiS ingots of relativly uniform composition, chemical methods of polishing and etching NiS crystals, and a method of determining the Ni content in a sample gravimetrically.

A. ATTEMPTS AT PRODUCING NiS POWDERS AND CRYSTALS

Several methods of producing NiS were attempted. Because a relativly pure stock of chemicals could be obtained, a chemical method of producing stoichiometric NiS was tried first. Generally, the proceedure involves reacting a nickel salt in an aqueous solution with a soluable sulfide. These type reactions produce the black amorphous α NiS precipitate. For example,

$$NiSO_4 + Na_2S \rightarrow NiS\downarrow + Na_2SO_4$$

or,

$$NiSO_4 + H_2S \rightarrow NiS\downarrow + H_2SO_4$$

The precipitate is then filtered and well washed with distilled water. The principal difficulty with this method is that the precipitate, when still wet and exposed to air, reacts with air and produces a yellow-green, sulfur rich compound.

A more promising method of producing the powder was then investigated. First, Ni metal was dissolved in acetic acid and to reduce the time necessary to complete the reaction, the mixture of acetic acid and Ni was kept warm. After the solution was a deep green, all of the Ni residue was filtered out and H_2S gas was bubbled through the remaining nickel acetate-acetic acid solution. This forms a black precipitate. The

reactions are:

$$Ni + 2HC_2H_3O_2 \rightarrow Ni(C_2H_3O_2)_2 + H_2$$

and

$$Ni(C_2H_3O_2)_2 + H_2S \rightarrow NiS + 2HC_2H_3O_2$$

The precipitate was found to be amorphous by x-ray diffraction but did not react with air when wet as did the previous amorphous powder. The difference is not understood. Also noted in this reaction was that an occasional coating of crystalline NiS was deposited on the surface of the beaker. The amorphous NiS was thououghly washed with distilled water, alcohol, acetone, ether and then dried. The residue was then placed in a clean quartz tube, evacuated, sealed and placed in an oven at 500°C for two days. X-ray diffraction patterns of this powder showed a plentitude of lines many of which could not be identified, but some of which corresponded to those of NiS in the NiAs structure.

Chemical methods were then abandoned because exactly stoichiometric powders of crystalline NiS in the hexagonal phase could not be produced from the amorphous powders.

A crude attempt at zone leveling was tried. Ni metal and S were placed in a quartz tube which was then evacuated and sealed. The mixture was then melted in a

furnace and cooled. A radio frequency induction heater was used to melt a narrow zone in the NiS. It was found that the NiS disassociated, the sulfur condensing on the ends of the tube leaving a very non-stoichiometric residue. The sulfur could not be remelted by the induction heater because it is not a conductor.

In a modification of this process, the zone refiner was placed in an oven. Instead of an induction heater, a resistance heater wound on quartz tubing was used to melt a narrow zone. The temperature of the oven was maintained at 900°C and the current in the resistance heater was maintained such that a narrow molten zone appeared in the ingot. This zone was repeatedly passed back and forth over the ingot. The resulting ingot contained relativly large crystals, but on chemical analysis, the composition proved to vary from 49.6 to 52.6 at.% Ni which was unacceptable.

B. A METHOD FOR PREPARATION OF INGOTS OF NiS

Ingots of NiS were prepared from high-purity Ni and S powders purchased from Johnson, Matthey and Co., Limited and the American Smelting and Refining Company, respectively. The quoted impurity content in each case is less than 10 ppm. The Ni is first reduced in a H_2 atmosphere by spreading the powder on the bottom of a clean pyrex tube which is placed in a horizontal furnace.

The furnace is then tilted and hydrogen gas is introduced on the high side while the low side is ignited to prevent explosions. The temperature is then increased and held at 500°C for one hour after which it is then lowered to room temperature. This process tends to keep the NiS from sticking to the quartz tube when cooling the ingot because the surface of the ingot is clean. Ingots made from unreduced Ni powder have slick, bluish surfaces which seem to stick to quartz. Since Ni does not readily react with oxygen, this process probably does not reduce the NiO to Ni as much as it removes volatile impurities.

Weighed portions of Ni and S are then placed in a quartz tube about one inch in diameter, evacuated to about 10^{-5} torr with a diffusion pump and sealed. Evacuation is facilitated by gently and carefully heating only the Ni powder with a Bundsen burner. The Ni is always introduced in the tube before the S and thus is always at the closed end of the tube. When the desired pressure is reached, the quartz tube is tipped off after which the Ni and S is thoroughly mixed by shaking the tube. The tube is then placed in a horizontal position in an oven at 120°C for one week in order to allow a partial chemical reaction of the Ni and S to occur. This reaction is exothermic and will result in an explosion if allowed to proceed too rapidly.

The partially reacted Ni and S is then placed in a horizontal tubular furnace and the temperature gradually increased to 400°C where it is allowed to bake several days and the chemical reaction is completed. The NiS is then melted and the furnace tilted at an angle of about 10° from the horizontal introducing a temperature gradient after which the temperature is gradually lowered through the melting point. The furnace is then placed in a horizontal position and the ingot is annealed at 950°C for one week, 900°C one week and at 750°C for two weeks. At the two higher annealing temperatures the system is a mixture of solid βNiS and liquid. The temperature is then slowly lowered to 400°C at which point the quartz tube and ingot are removed from the furnace and placed in cool water to quench the NiS in the high temperature phase.

An indication of the overall composition of the ingot can be obtained because the transition temperature is a sensitive function of the composition. Representative samples of the ingot are therefore placed in alcohol whose temperature is -10 to -15°C which is slightly below the transition temperature. Those test samples which are stoichiometric will crack into small pieces when they transform into the semiconducting state. This procedure has been used to produce ingots weighing up to 80 g. containing large single crystals.

C. POLISHING AND ETCHING OF NIS CRYSTALS

CHEMICAL POLISHING:

A method of chemically polishing single crystals of NiS was developed in preparation for optical measurements. Cleaved surfaces are ideally best for optical measurements, particularly in the ultraviolet because the surface is less strained that when prepared by other methods. In order of descending surface quality, these methods are: cleavage, electropolishing, chemical polishing and mechanical polishing. It was possible to cleave several of the single srystal samples perpendicular to the c-axis, but since this is the only direction the crystal cleaves, other orientations must be cut and polished by other methods. Attempts at electropolishing were unsuccessful. A detailed description of a method for chemically polishing NiS crystals which produced the best surfaces follows:

The sample to be polished is first oriented by an x-ray back-reflection Laue photograph and cut by spark erosion. The surface to be prepared is then planed with the spark cutter until smooth. It is important that the slowest planing speed be used in the final stages of planing because this produces shallower surface damage than faster speeds. Experience has shown that the final chemically polished surface is always

smoother when the surface was planed slowly.

A mixture of 49 parts HCl, 49 parts HNO_3 and 2 parts glacial acetic acid is mixed and allowed to stand a few minutes. It is not certain that the acetic acid is necessary, but it does no harm. The sample is placed in the bottom of a beaker in about 50 ml of the acid mixture. The beaker is then warmed to about 50°C and maintained relatively near that temperature throughout the polishing. The chemical reaction produces water, free sulfur, nitrogen oxide and nickel compounds. NO is a colorless gas, but is quickly oxidized in air to NO_2 which is a reddish-brown gas. The gas produced at the surface of the sample makes bubbles which tend to remove free sulfur produced at the surface. The reaction is vigorous. Allow it to proceed from one to four minutes or until the surface appears polished. If the sample is permitted to come into contact with air while the surface is acidic, discoloration will occur, therefore the following procedure for removing the sulfur and acid was developed. When the sample has finished polishing pour most of the acid out of the beaker not allowing the sample to break the surface. Replace most of the remaining acid with carbon disulfide which when agitated will dissolve most of the sulfur. Replace the carbon disulfide with reagent grade acetone; then replace the acetone with water.

The acetone allows the carbon disulfide and water to mix. The surface must then be cleaned again with carbon disulfide, therefore replace the water with acetone and the acetone with carbon disulfide. After the remaining sulfur is completely dissolved, reverse the procedure again such that the sample is standing in pure water. Allow the sample to remain in water overnight changing the water occasionally to remove any residual acids. Note that throughout this process, the sample has not been allowed to come in contact with air until all acids have been removed, and that reagent grade chemicals and distilled, deionized water were used. Also, be certain that carbon disulfide does not come into contact with hot surfaces or flames since the vapors are explosive.

Most success was had with planes parallel to the c-axis. Surfaces obtained were smooth enough that a reflection of the numbers on an IBM computer card could be clearly read when the card was held one inch from the surface. If the card-sample distance is greater the image begins to distort. Clean crystals do not tarnish and no precautions were taken to keep polished samples in an oxygen free environment.

If polycrystalline samples are polished, an uneven surface will be obtained since different crystalline orientations polish at different rates.

ETCHING NiS:

The procedure of chemical polishing previously described can be used to clean the surface of a crystal or to remove surface damage due to spark erosion in preparation for back reflection x-ray photographs. Since different crystalline orientations polish at different rates, the procedure can be used to determine grain boundaries in polycrystalline samples.

Another method of determining grain boundaries was found: If a sample is placed in warm dilute sulphuric acid, the reaction which occurs slowly, is

$$H_2SO_4 + NiS \rightarrow NiSO_4 + H_2S$$

Near the surface of the sample, the reverse reaction also occurs:

$$H_2S + NiSO_4 \rightarrow NiS\downarrow \text{(black precipitate)} + H_2SO_4$$

The NiS produced in this reaction is a fine, black, amorphous powder which settles on the surface of the sample clearly revealing the grain boundaries. Also, the rate of reaction is a function of crystalline orientation.

MECHANICAL POLISHING:

Several crystals were mechanically polished although results from these samples have not been presented. The method is standard: A pitch lap was made for each abrasive to be used, the coarsest powders were used

first. A typical series of powders is 80,100,400,600,800 and then rouge or barnsite. The numbers indicate the mesh through which the powder has been sieved. A 400 mesh powder, for example, has no particles larger than 36 microns. More detailed instructions can be obtained elsewhere, see for example, Volume 6A of Methods of Experimental Physics[35]. The important point is that NiS crystals polished in this manner leave the bulk crystal unstrained as indicated by x-ray diffraction. The surface however, is not of sufficiently good quality to permit optical measurements.

D. GRAVIMETRIC DETERMINATION OF Ni

Accurate determination of the quantity of trace elements in samples are standard, but if the element is a large percentage of the total sample, quantitative determinations on the order of .1% or less are difficult. A chemical procedure of determining the quantity of Ni in a NiS sample was developed. Except for the method of dissolving the NiS, which proved to be relatively difficult, most of the procedure is standard and standard laboratory procedures are followed. One major drawback is that large samples on the order of .4 to .6g. of NiS must be used. To minimize errors at least three separate determinations on the same sample must be made. This means that the mass of the NiS sample

to be analyzed must be at least on the order of 2g. Standard deviations of .02 at % Ni have been obtained. The procedure is as follows:

1. Crush sample in mortar and pestal until the particles are millimeter size or smaller.
2. Weigh the sample. This is done by placing portions of the NiS in standard weighing bottles. First the sample plus the bottle is weighed, then the sample is poured into a 600 ml. beaker containing 15 ml. of concentrated HNO_3. The bottle and the remaining sample are then weighed. A Heusser scale was used which has a sensitivity of 10 micrograms.
3. Keep the HNO_3-NiS mixture warm until the reaction stops. A white residue remains.
4. Add approximately 30 ml. of HCl which will dissolve the remaining white residue. Heat, gradually increasing the temperature until only moist solids remain.
5. Dilute to 200 ml. with water and heat almost to boiling.
6. Add NH_4OH until the solution is alkaline, that is, when it changes from green to blue. Add HCl until the solution becomes green again.
7. Add one ml. of dimethylglyoxime solution for each

2 mg. of anticipated Ni. A solution of dimethylglyoxime is prepared by dissolving one gram of $C_4H_8O_2N_2$ per 100 ml. of ethyl alcohol.

8. Add NH_4OH slowly until the solution is amonical. A red precipitate will form. This is $Ni(C_4H_4O_2N_2)_2$. Thoroughly stir and gently heat. Allow the mixture to digest at least 30 min.

9. Filter in standard tared filter crucibles, and wash with cold water. Dry to constant weight. All of the Ni is contained in the precipitate and can be weighed to determine the Ni content in starting material.

III X-RAY MEASUREMENTS

Most MNM compounds undergo a crystalline distortion at the critical temperature. No previous experimental work on NiS has indicated in a concrete manner, that a distortion does not occur at the MNM transition. Sparks and Komoto[16] studied the first five peaks of a powder, neutron diffraction pattern in order to determine the type of magnetic ordering in the semiconducting state, but the data are not sufficient to conclusively state that no distortion occurs at the ordering temperature. Thus, x-ray powder diffraction studies were undertaken. Powder work was decided upon because NiS crystals shatter when passing through the transition and because a single crystal diffractometer with a low temperature attachment was not available.

A. THEORETICAL BACKGROUND

In order to determine the electron density of a crystal, and thus the crystalline structure, the positions and intensities of the diffraction maxima must be measured. The intensity of a peak associated with a set of planes in the crystal with miller indices hkl is related to the structure factor F_{hkl}, as follows:

$$E_{hkl} = KL_{hkl}P_{hkl}|F_{hkl}|^2$$

where K is a scale factor, and Lp is the product of the Lorenz and polarization factors respectively. L and p take into account variations of the measured intensity due to the particular experimental arrangement and due to polarization of the beam on diffraction. The combined Lorentz-polarization factor Lp has the form

$$Lp = \frac{1 + \cos^2 2\theta}{\sin^2\theta\cos\theta}$$

The electron density in a crystal is given by

$$\rho(x,y,z) = \frac{1}{V} \sum F_{hkl} e^{i2\pi(hx + ky + lz)}$$

where V is the volume of the cell; x, y, z give the position in the cell; F_{hkl} is the structure factor. The Patterson function is defined by

$$A(u,v,w) = \frac{1}{V^2} \sum |F_{hkl}|^2 e^{i2\pi(hu + kv + lw)}$$

The electron density has peaks at atom locations. The coordinates of the r^{th} peak in the Patterson function are related to the coordinates of the i^{th} and j^{th} peaks in the electron density by

$$u_r = x_j - x_i$$

$$v_r = y_j - y_i$$

$$w_r = z_j - z_i$$

Therefore, for every pair of peaks in the electron density corresponds to a specific peak in the Patterson function.

The Patterson function is the most direct synthesis of the original data because it is a function of $|F|^2$ which is directly measured in the experiment. The F's must be calculated in order to determine $\rho(x,y,z)$.

3. SAMPLE PREPARATION

Samples were produced in the manner already described except that the x-ray samples were annealed at 980°C for 96 hours and 750°C for three days. This high-temperature anneal homogenized the ingot producing a uniform distribution of Ni and S throughout the ingot. The temperature was then gradually reduced to 400°C from which temperature it was quenched in room temperature water. Portions of the ingot were arbitrarily selected from which powders were made by grinding the pieces in a mixer-mill and sieving them through a 400 mesh screen which ensured that the particle size was less than 37μ. The resulting powder was then placed in a clean quartz tube, evacuated to a pressure on the order of 10^{-6} torr and sealed. This was then annealed for 5 hours at 500°C and 6 hours at 450°C. Annealing at higher temperatures seems to produce either larger crystallites or sintered powders. The overall composition of the powder was

checked by chemical analysis and found to be (50.0 ± 0.02)% at Ni.

Preferred orientation of a powder can occur if the sample has a preferred direction of cleavage as is found in NiS. It is possible for small platelets to be made when powdering a crystal such that one crystalline axis is perpendicular to a flat surface of a platelet. If a powder of these platelets is compressed, the platelets will not be randomly oriented. Random orientation can be maximized by powdering the crystal thoroughly and by careful insertion of the sample into the sample holder. A check for preferred orientation in a portion of the sample used was accomplished by taking a transmission powder x-ray photograph. This was done by milling a depression in a thin piece of bakelite. Bakelite was chosen because of its rigidity and transparancy to x-rays. A sample of the sieved powder used in the x-ray measurements was placed in the depression. All efforts were exerted to introduce preferred orientation into the sample. A monochromatic x-ray beam was passed through the sample and allowed to expose the film placed on the opposite side. A schematic diagram of the arrangement is shown in Figure 9. The resulting photograph showed uniform ring intensities indicating that the powder was randomly distributed in orientation.

The x-ray intensity data were taken with Ni-filtered

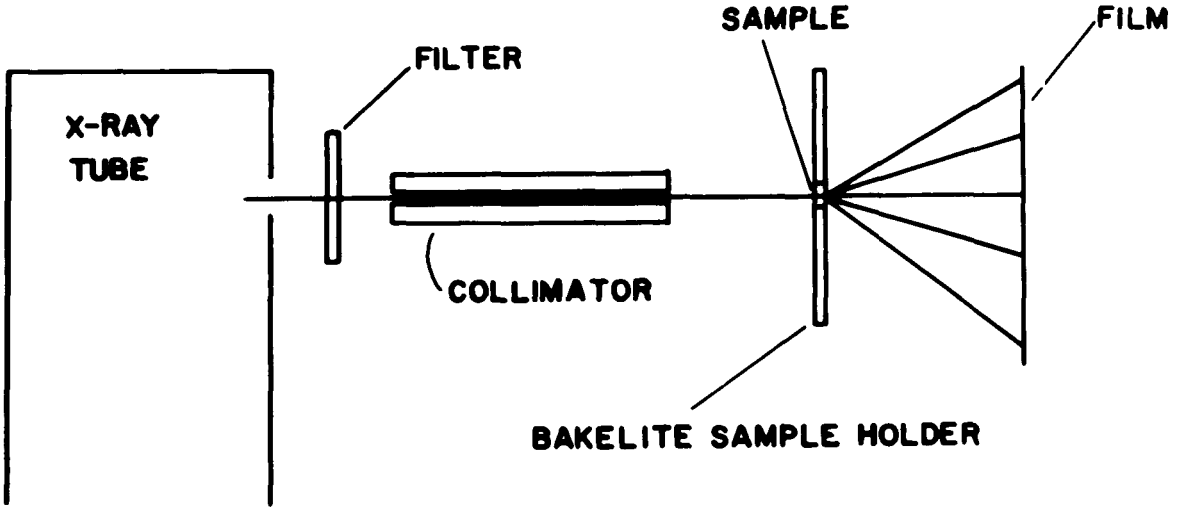
SAMPLE
FILM
FILTER
X-RAY
TUBE
COLLIMATOR
BAKELITE SAMPLE HOLDER

Figure 9

CuKα radiation on a General Electric diffractometer equipped with a cryogenic sample mount. The peak widths (full width at half-maximum) varied from 0.25° at 30 ° to 0.45° at 150° where the angles are given in 2θ. At low values of 2θ the Kα and Kβ peaks were not resolved; whereas, they were at higher angles. These are normal values expected of an x-ray machine with good resolution. Intensity measurements were carried out on three different samples at 300°K and on two of these samples at 77°K. A weighted average of the results at each temperature was used in the final structure analysis. The intensity of each peak was measured by scanning the entire peak at 0.2 deg/min and measuring the total count for the scan. This procedure gives the integrated intensity of the peak plus the background. The background was determined by making 100 sec counts at each degree or half-degree 2θ for several degrees 2θ on each side of the peak. The background was then extrapolated under the peak by fitting a line to the points and was then subtracted from the total count obtained by scanning the peak leaving only the intensity due to the diffraction peaks. Larger peaks were scanned once or twice; the smaller ones two or three times in order to get better statistics. Peak positions were measured for each peak directly from the chart.

In order to observe the phase transition, a sample

holder was designed such that the temperature of the sample could be measured and controlled. This was accomplished by allowing only a small heat leak from the sample to the liquid nitrogen cold reservoir. A heater wound near the sample was used to adjust the temperature. No other temperature regulation was employed, but with this arrangement the sample temperature could be maintained constant ($\pm$ 0.1^{o}K) for a period of an hour. This provided ample time to observe qualitatively, any changes in the diffraction peaks at a given temperature near the transition. The sample temperature was measured with a copper-constantan thermocouple referenced at 0.0^{o}C; the e.m.f. was measured with a potentiometer. A diagram of the dewar and sample holder is shown in Figure 10.

Ni powder (99.999%) was used as a standard to find the correct values of the lattice parameters and as a check on the measurements of the intensities. Ni was chosen because most of its diffraction peaks don't overlap the NiS peaks. About 20% Ni powder, by weight was mixed with the NiS powder. A run was then made containing both sets of peaks. To correct the lattice parameters, a plot is made of the deviation of the peak position of the Ni lines from the correct positions as given in the literature versus the angle 2θ. These points generally lie on a straight line and thus this graph can be used to correct the positions of the NiS

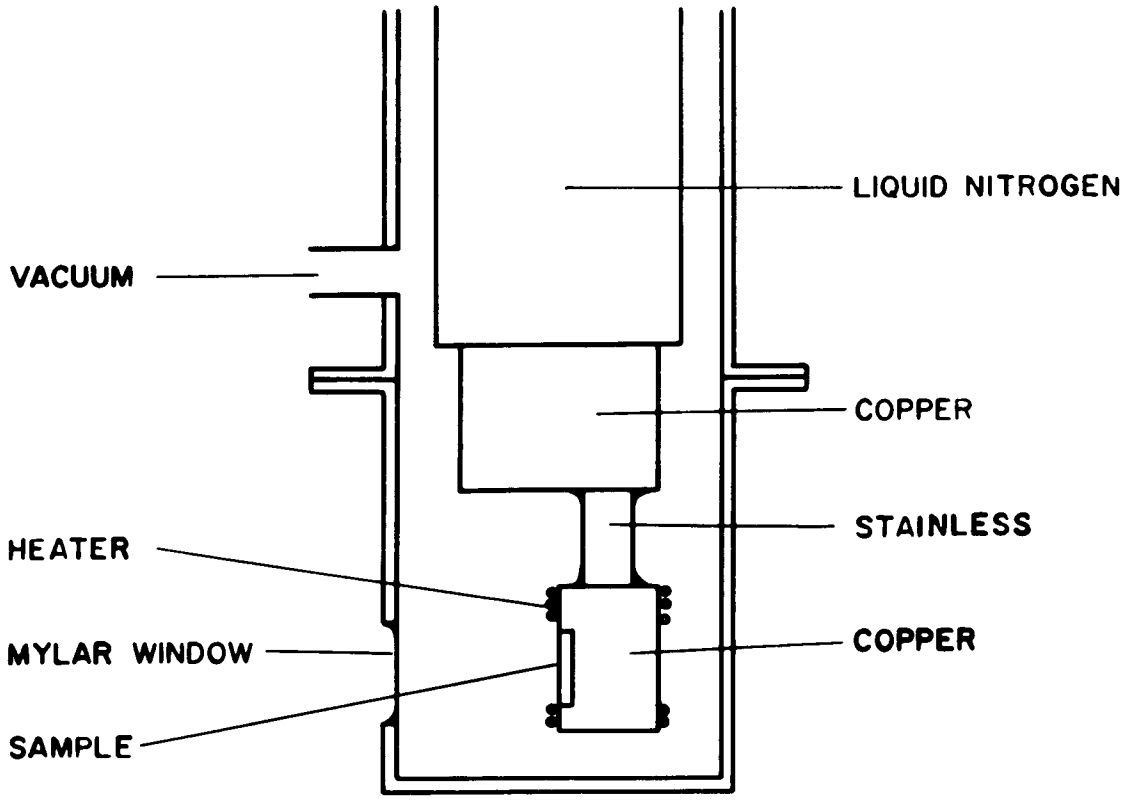
LIQUID NITROGEN
VACUUM
COPPER
STAINLESS
HEATER
MYLAR WINDOW
COPPER
SAMPLE

Figure 10

diffraction peaks. Table 2 shows the measured intensities of the Ni lines and the accepted values found in the literature. Ni powder was used in only one of the three samples since addition of the Ni powder decreases the intensity of the NiS peaks causing poor counting statistics. Data for calculation of the lattice parameters were taken from the sample with the Ni standard.

miller indices	observed I	accepted I
111	100 ±.5	100
200	42 ± 1	42
220	19 ± 2	21
311	19 ± 2	20
222	5 ± 3	7
331	14 ± 1	14

TABLE 2 Observed and accepted values of the intensity of Ni diffraction peaks.

C. RESULTS AND DISCUSSION

When the temperature of the NiS was gradually reduced new peaks appeared in the diffraction pattern at the metal-nonmetal transition temperature due to the appearance of the semiconductor phase. The angular separation of the low temperature and high temperature peaks was generally within 1^{o} 2θ. As the temperature decreased, the low temperature peaks gained in intensity at the expense of the high temperature peaks. A plot of the intensity ratio for the 102 reflection (Figure 11)

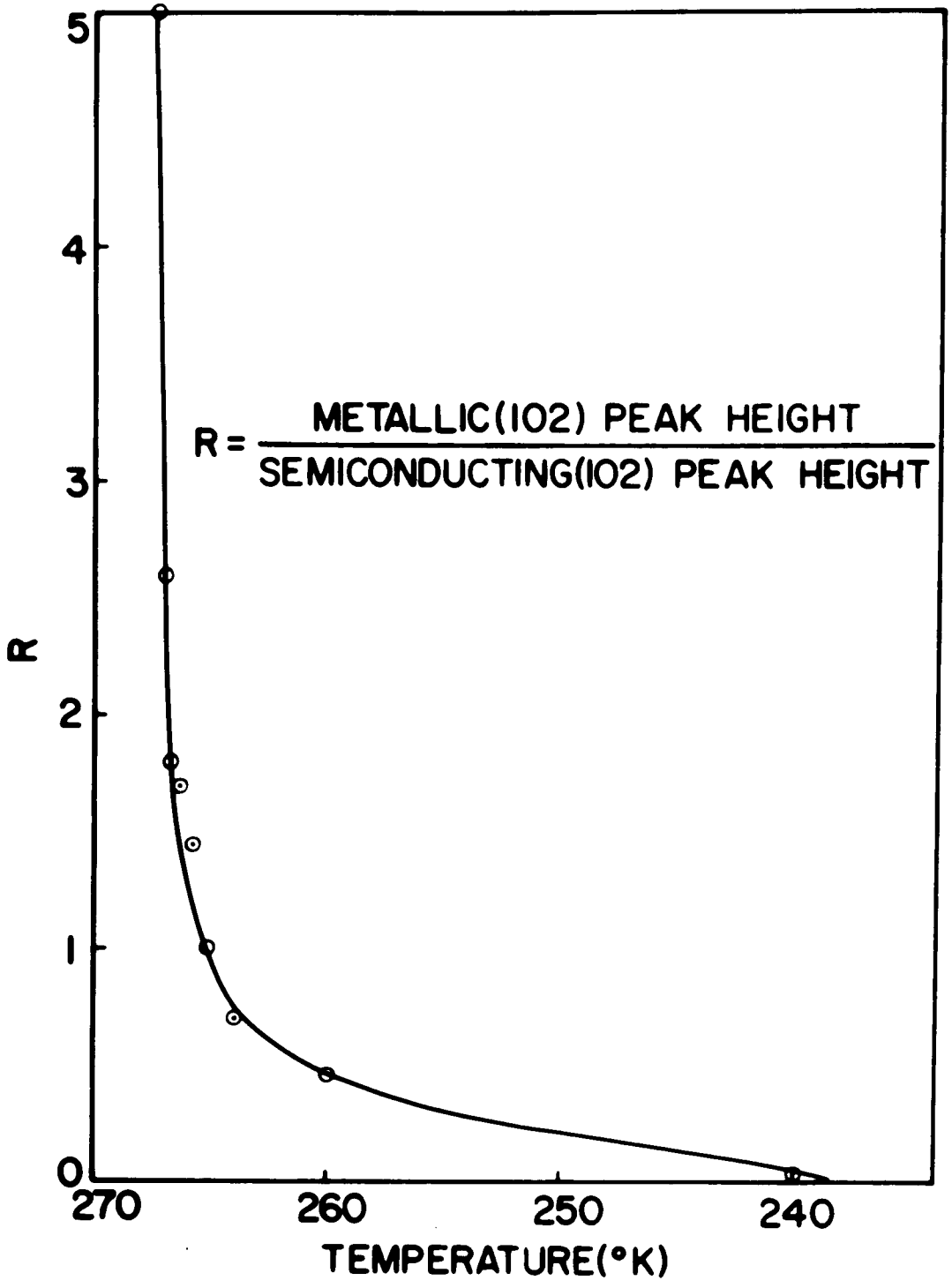
5
4
3
2
1
0
R
R = METALLIC(102) PEAK HEIGHT / SEMICONDUCTING(102) PEAK HEIGHT
270
260
250
240
TEMPERATURE(°K)

Figure 11

shows that the phase change is essentially complete within 7°K of the critical temperature. No trace of the high temperature phase was detected at 77°K. Apparently both structures exist simultaneously just below the transition because of slight inhomogenity of the sample.

Initial results showed that the diffraction pattern could be indexed at both 300 and 77°K to a hexagonal lattice. At room temperature, NiS has the NiAs structure shown in Figure 12. In this structure, the large nonmetal anions form a hexagonal closepacked lattice, while the smaller metal cations compose a simple hexagonal lattice by occupying the octahedral interstitial sites of the hcp lattice. The tetrahedral sites are vacant. In the unit cell, the cations are at (0,0,0) and (0,0,$\frac{1}{2}$) while the anions are located at (1/3,2/3,z) and (2/3,1/3,z± $\frac{1}{2}$).

Lattice parameters were calculated from a complete set of diffraction maxima by minimizing the quantity R defined by

$$R = \sum_j \frac{\theta_{cj} - \theta_{oj}}{\sigma(2\theta)}^2$$

where j is an observation, θ_{oj} is an observed angle, and θ_{cj} is a calculated angle. The angle θ_c is calculated by choosing a set of lattice parameters a and c and finding

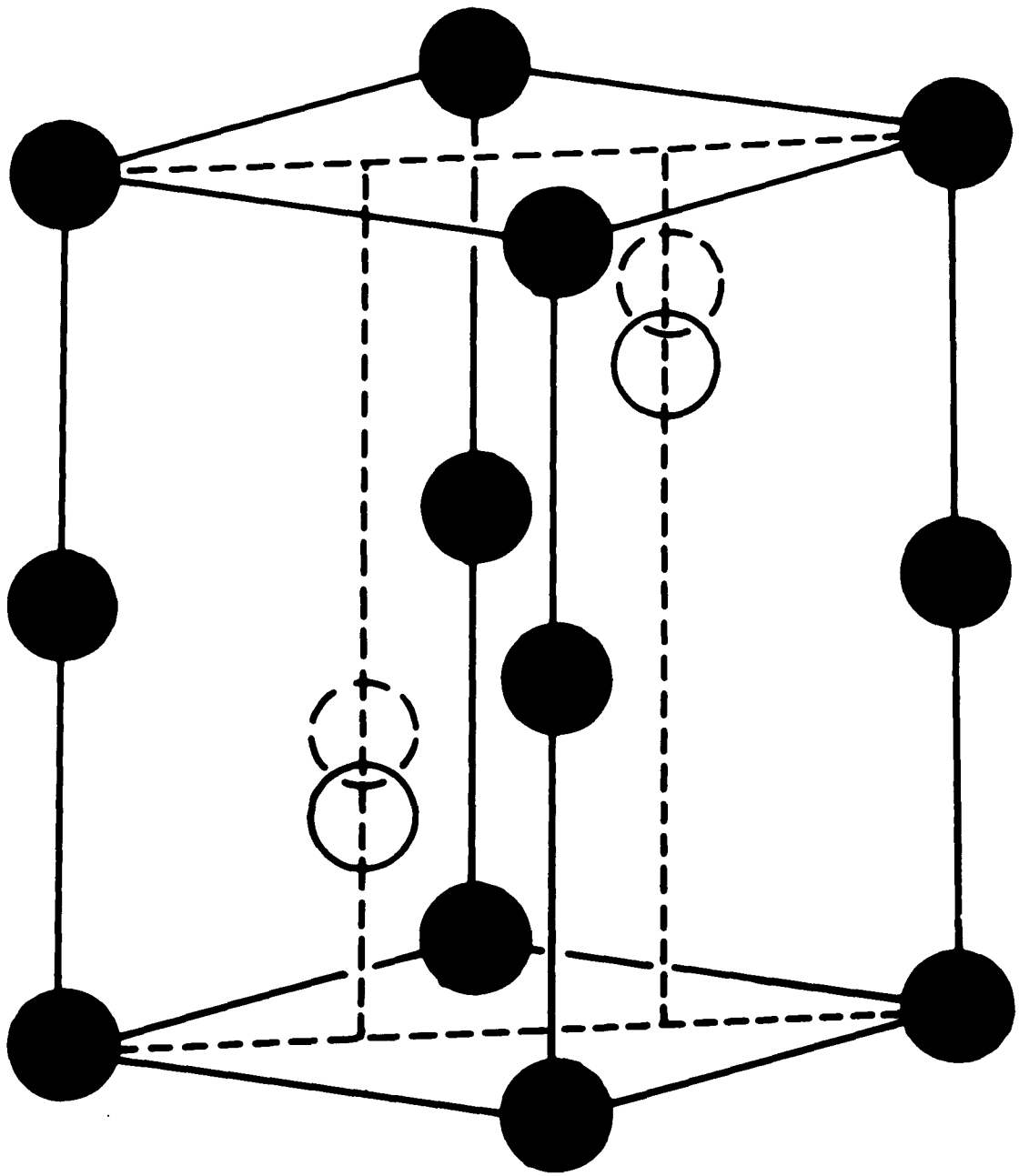

Figure 12

$d_{hkl}(a,c)$ where, for a hexagonal lattice,

$$d_{hkl}(a,c) = \left(\frac{4}{3a^2}(h^2 + hk + k^2) + \frac{l^2}{c^2}\right)^{-\frac{1}{2}}$$

and is the interplaner spacing. Then

$$\theta_c = \sin^{-1}(\lambda/2d_{hkl}(a,c)).$$

The set of lattice parameters which minimizes R is the set which best fits the observed data.

The calculated lattice parameters are in good agreement with those of Lafitte[31], but the length of the c axis differs slightly from that measured by Sparks and Komoto[14]. at 300°K, a and c were found to be 3.4395 and 5.3514Å respectively while at 77°K they were 3.4456 and 5.405Å.

Tables 3 and 4 give the observed intensities and the observed and calculated structure factors for the samples at 300 and 77°K. The intensity data were used to compute the Patterson (vector) maps at both temperatures with resolutions of 0.1Å. The resulting maxima corresponding to Ni-S vectors were found to be spherical at 300°K, but slightly elongated in the direction of the c axis at 77°K. This result is indicative of a shift of sulfur atoms with respect to the nickel atoms below the transition temperature.

The NiAs structure type is consistent with two possible space groups. The centrosymmetric model, space

Table 3

Intensities and structure factors for hexagonal NiS at 300°K.

h	k	l	Intensity (Counts)	Standard Deviation	Observed Structure Factor	Calculated Structure Factor
0	1	0	4189	54	31.35	31.98
0	0	2	276	23	15.66	16.13
1	0	1	2697	46	20.67	19.22
1	0	2	5994	64	42.02	43.02
1	1	0	3199	50	51.82	50.35
1	0	3	363	28	14.25	15.18
0	2	0	301	28	18.97	19.96
1	1	2	133	25	9.24	8.32
0	2	1	323	30	14.55	14.55
0	0	4	319	32	38.41	35.17
2	0	2	1132	40	30.54	30.57
0	1	4	163	32	12.40	7.43
2	0	3	93	32	9.97	14.02
2	1	0	101	34	10.45	11.84
2	1	1	200	42	10.54	13.53
1	1	4	861	45	31.51	28.68
1	2	2	998	48	24.07	23.47
0	1	5	88	35	10.12	14.02
0	3	0	390	41	30.08	30.76
2	1	3	160	41	9.45	13.06
0	2	5	104	29	9.52	13.06
2	2	0	453	34	27.42	25.62
1	0	6	323	35	16.11	13.09
1	3	1	246	36	8.47	11.74
3	0	4	956	57	20.45	21.00

Table 4

Intensities and structure factors for hexagonal NiS at 77°K.

h	k	l	Intensity (Counts)	Standard Deviation	Observed Structure Factor	Calculated Structure Factor
0	1	0	4320	50	31.57	32.28
0	0	2	392	21	18.38	19.68
1	0	1	2818	41	20.90	19.47
1	0	2	6531	61	43.25	44.15
1	1	0	3571	63	54.28	51.96
1	0	3	369	23	14.14	15.35
0	2	0	348	24	20.24	20.74
1	1	2	152	22	9.78	11.56
0	2	1	323	23	14.42	15.21
0	0	4	286	27	41.60	35.58
2	0	2	1418	46	33.83	32.25
0	1	4	272	28	15.78	12.24
2	0	3	149	28	12.43	14.65
2	1	0	155	27	12.83	12.64
2	1	1	260	28	11.93	14.62
1	1	4	890	47	31.76	29.67
1	2	2	1132	38	25.46	25.46
0	1	5	147	35	13.00	14.17
0	3	0	488	36	33.42	33.82
0	2	4	104	30	10.95	8.20
2	1	3	192	32	10.30	14.12
0	2	5	86	44	8.74	13.65
2	1	4	172	34	8.53	5.94
2	2	0	522	65	29.39	29.10
1	3	1	315	54	9.61	13.56
3	0	4	1157	77	23.14	22.95

group $P6_3/mmc(D_{6h}^4)$, restricts the nickel atoms to the positions (0,0,0) and $(0,0,\frac{1}{2})$ and the sulfur atoms to the positions (1/3,2/3,1/4) and (2/3,1/3,3/4). The noncentrosymmetric model, space group $P6_3mc(C_{6v}^4)$, the Ni atoms are restricted to the same positions, but the sulfur atoms are in the positions (1/3,2/3,z) and $(2/3,1/3,z+\frac{1}{2})$ where z may effectively assume any value.

A least squares procedure was used to fit the data from both temperatures to both symmetries. In all four models the function minimized was $\sum w(\Delta F)^2$ where the sum is taken over all diffraction maxima, w is the weight of each observation derived from counting statistics, and ΔF is the difference between the observed and the calculated structure factors. Each calculated structure factor is modulated by a temperature factor $\exp(-\frac{1}{4}s\cdot B\cdot s)$, where s is the reciprocal lattice vector of length $2\sin\theta$ and B is the anisotropic thermal displacement tenson Only the B_{11} and B_{33} components are independent since the remaining four elements of this symmetric tensor are related by space=group symmetry[37] as follows:

$$B_{11}=B_{22}=2B_{12},\ B_{13}=B_{23}=0.$$

The crystallographically independent unit in each space group effectively contains only one Ni and one S. Thus five parameters including two thermal parameters for Ni and two for S as well as a data scaling factor

were adjusted in the centrosymmetric models. The atomic scattering factors used were those of Ibers[39]. The final weighted residual factors

$$R = (\sum w(\Delta F)^2 / \sum w|F_o|^2)$$

for all four refinement models are shown in Table 5.

Temp (°K)	Space group	Number of parameters refined	z	R
300	$P6_3/mmc$	5	0.25 (constrained)	0.047
300	$P6_3mc$	6	0.237 ± 0.016	0.047
77	$P6_3/mmc$	5	0.25 (constrained)	0.052
77	$P6_3mc$	6	0.275 ± 0.007	0.049

TABLE 5. R values for structure refinements for different temperatures and symmetries.

At 300°K, the R value for the constrained and unconstrained models are identical. In addition, the position of S differs from 0.250 in the noncentrosymmetric model by less than one estimated standard deviation. It must therefore be concluded that the crystal structure of NiS in the metallic state is centrosymmetric. However, at 77°K, the R value decreases when the centrosymmetric constraint on the sulfur position is released. The R factor ratio test of Hamilton[40] indicates that this decrease is significant at the 90% confidence

level. Further, z varies significantly (more than 3σ) from 0.250, and the estimated standard deviation is small and reasonable. These results, together with the evidence from the Patterson syntheses, lead us to conclude that NiS in the semiconducting state is noncentrosymmetric.

The values of the thermal displacement tensor components shown in Table 6 are not physically meaningful since the sulfur tensors are marginally nonpositive definite and correspond to negative rms displacements. Nevertheless, our conclusions concerning the atomic positions and the change in crystal structure are not mitigated by these results. Rather, these results indicate that a slight disordering of the nickel and sulfur atoms may exist in this sample at both high and low temperatures, although the extent of interchange cannot be established.

Further support for a slightly disordered structure and evidence of the over-all correctness of these two crystal structures, is furnished by the weighted electron density difference synthesis. Neither the centrosymmetric high-temperature structure nor the noncentrosymmetric low-temperature structure displayed residual electron density peaks above 0.7 electrons Å^{-3} except at the tetrahedral interstitial sites. At these positions, prominent residual peaks of 1.8

Table 6

Lattice parameters, temperature coefficients, and positions of S atoms at 300°K and 77°K. Standard deviations are shown in parentheses.

Temperature	Lattice Parameters (Å)		Components of Thermal Displacement Tensor				Position of S Atoms
°K	a	c	B_{11}(Ni)	B_{33}(Ni)	B_{11}(S)	B_{33}(S)	z
300	3.4395(2)	5.3514(7)	.054(16)	.038(5)	-.004(13)	-.004(5)	.250
77	3.4456(8)	5.405(1)	.044(15)	.031(6)	-.015(15)	-.004(7)	.275(7)

electrons Å^{-3}, corresponding to approximately 0.09% Ni, were observed. These observations support the conclusion of Sparks and Komoto[12] that no abrupt change in the disorder occurs over the transition.

The change in the NiS crystal structure which occurs over the MS transition is subtle but significant. Above 266°K, both the S and Ni atoms are in nearest-neighbor environments of octahedral symmetry. At the transition temperature, a concerted S atom shift of 0.134 Å toward the hexagonal nickel basal planes places the S and Ni atoms in local crystal fields of C_{3v} symmetry. The six Ni-S distances change from 2.394 Å at 300°K to 2.483 and 2.331 Å at 77°K, while the unit-cell volume shows a 1.3% increase on lowering the temperature from 300 to 77°K.

D. OTHER RECENT X-RAY WORK ON NiS

Another x-ray diffraction study of NiS was recently done by McWhan *et al.*[21] on a cleaved single crystal of NiS. They measured intensities for the Friedel pairs[41] of (00l) and (hh0) and saw no evidence for the breakdown of Friedel's law in the low temperature phase. Friedel's law states that the intensities of the reflections (hkl) and ($\bar{h}\bar{k}\bar{l}$) are equal. For an acentric crystal it has been shown[41] that if one atom of the crystal has an absorption edge just on the long wave length side of the radiation used for diffraction, then $|F_{hkl}|^2$ and $|F_{\bar{h}\bar{k}\bar{l}}|^2$ are not equal. This is known as the breakdown of Friedel's law. The intensities of eleven peaks were measured seven of which could be used to determine the positions of the sulfur atoms. A least-squares refinement was done where four parameters including a scale factor, the position of the sulfur atom and two thermal parameters were adjusted such that the calculated structure factors best fit the eleven measured structure factors. Their refinement gave the position of the sulfur atoms to be $z = .252 \pm .002$ in the low temperature phase. Unit weights were used for each reflection and an emperical absorption correction based on room temperature data was used.

An evaluation of the results of this experiment is difficult, however, because important information has been omitted from the published data. In the first phase,

no indication as to the accuracy of the raw experimental data has been presented. A small standard deviation in the calculated position of the S atom may not be meaningful since only eleven data points were used in a least-squares refinement (only seven of which are useful in locating the position of the sulfur atom along the z axis) and four parameters were adjusted in the fit. Secondly, the transition temperature of the samples used in the x-ray and pressure experiments has been given as 200-235°K which indicates that the crystal used was not stoichiometric. They indicate that the sample contained excess Ni and the only place this could fit in the lattice is in the tetrahedral sites around the sulfurs. This in itself would inhibit the S motion. No indication of lattice parameter in the low temperature phase is given nor was the temperature at which the measurements were made. One can only conclude from these omissions that serious doubt exists about the measurements being actually made on the semiconducting phase. Furthermore, since the properties of the crystal are sensitive to the composition[3,24,32], the structure change in a crystal with a transition temperature of 200°K, and which does not crack, may not be as marked as one with a transition temperature of 266°K and shatters at the transition. Thirdly, the wave length of the x-radiation is not given. If the x-radiation used were that of Cu or Mo (the two most common x-ray tubes)

the difference in the intensities of the (hkl) and ($\bar{h}\bar{k}\bar{l}$) reflections would be on the order of 5%. Thus, if the accuracy of the data are on the order of 2 to 3% (an average value), a difference in the intensities of the Friedel pairs might not have been observed. In order to see a significant difference in the intensities of the Friedel pairs, Zn K radiation would have to be used which is strongly absorbed by Ni.

McWhan et al.[21] claim that powder data presented in this section of this thesis is very sensitive to the weighting scheme used and show that if a unit weighting scheme is used, z=.258±.013. When the calculated weights are used, however, the standard deviation becomes .007 indicating a much better fit and that the derived weighting scheme is probably better. The authors use a unit weighting scheme and do not test their own data to determine whether their results are also sensitive to the weighting scheme employed. A Patterson map for the powder data was calculated from the experimental structure factors which shows distortions in the semiconducting phase but none in the metallic phase. No weights are employed in calculating the Patterson function suggesting that there are real changes in the powder data at low temperatures. Finally, the authors took data on only one crystal. If the crystal were twinned, or became twinned upon passing through the transition, no breakdown of Friedel's law would be observed.

In conclusion, the x-ray data presented by McWhan *et al*. is questionable and more information on their experimental procedure is necessary before a proper evaluation can be made. What has been presented however is no more conclusive than the powder data presented in this thesis.

IV SPECIFIC HEAT MEASUREMENTS

One of the important factors in the MNM transition is that it is a first order phase transition. Although previous measurements on NiS had shown there to be a volume discontinuity at the transition, no measurements had been performed which determined the existance of a latent heat, entropy change or any other thermodynamic properties. Theoretical models which predict the MNM transition must agree with these measurements and furthermore, a knowledge of the values obtained from these measurements could aid in the development of a model.

A. PREPARATION OF SAMPLES

NiS powder was prepared by taking an ingot of NiS and placing it in alcohol at approximately -10^{o}C. Since the transition temperature is a sensitive function of the composition, those portions of the ingot which are of the stoichiometric composition will transform into the semiconducting phase. Since crystals of NiS break up into very small pieces, on the order of fractions of millimeters, it is possible to separate that portion of the ingot which has transformed into the semiconducting state from the remainder and thus the stoichiometric from the nonstoichiometric NiS. These

small fragments were powdered in a mixer-mill and pressed under 40 tons of pressure into 13mm diameter pellets, about 13mm in length. The pellets were then placed in a clean quartz tube, evacuated to 10^{-6}torr and sealed. In order to attain this pressure, the pellet and the quartz tube must be outgassed by occasionally applying a gentle heat with an acetylene torch. The pressure, while sealing the tube, remained on the order of 10^{-6} torr. The evacuated quartz tube and pellet were then placed in a horizontal furnace and sintered by holding the temperature at 725°C for three days. The temperature was then slowly lowered to 400°C after which the tube and pellet were dropped into room temperature water to quench the sample and prevent it from transforming into the rhombohedral phase.

Two cylindrical holes were then spark eroded into the pellet, one .075 inches in diameter and the other .035 inches. The larger hole was cut through the center of the cylinder and the smaller about 1/4 inch from the center and 1/4 inch deep. Both were cut parallel to the cylindrical axis of the pellet. A copper constantan thermocouple was glued with GE 7030 varnish in the smaller hole and a heater in the center hole.

The heater was made by machining a piece of Al into a hollow cylinder 3/8 inches long. The outer diameter was .056 inches and the inner .040 inches. On

this cylinder was wound four layers of .002"constantan wire which had a total resistance of 750 ohms. This heater had a final diameter of .075 inches and was glued into the center of the pellet with GE 7030 varnish. Aluminum was chosen as the material used as the coil form for the heater because it is readily available, easily machineable and absorbs a small quantity of heat per unit volume compared with other available materials.

Even though sintered samples don't crack into small, individual pieces when passing through the transition, it was found that the properties of the surface of the sample did change after having passed through the critical temperature. The surface seemed to become rougher, that is, radiative coupling to the walls was greater and was probably due to cracking. To alleviate this problem, the surface was covered with gold leaf glued on with GE 7030 varnish which had been well diluted with a mixture of equal parts of alcohol and toluol. The total mass of the addenda which includes the heater wound on an aluminum cylinder, the gold leaf and the varnish weighed .0837 grams. This was on the order of one per cent of the mass of the sample.

B. APPARATUS AND TEMPERATURE CONTROL

A vacuum calorimeter was used to measure the specific heat of NiS, a diagram of which is given in Figure 13. The

Figure 13

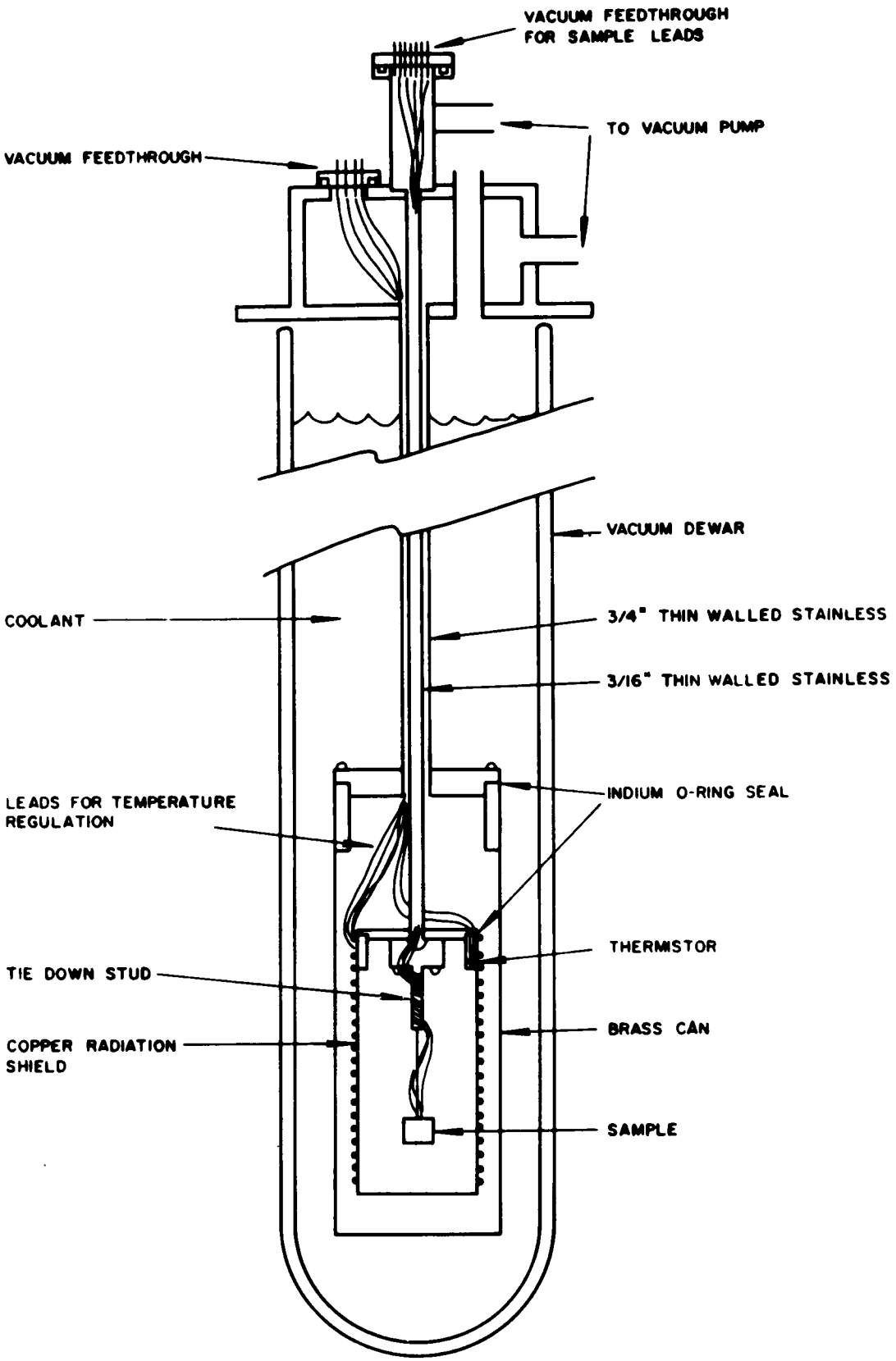
VACUUM FEEDTHROUGH FOR SAMPLE LEADS
TO VACUUM PUMP
VACUUM FEEDTHROUGH
VACUUM DEWAR
COOLANT
3/4" THIN WALLED STAINLESS
3/16" THIN WALLED STAINLESS
INDIUM O-RING SEAL
LEADS FOR TEMPERATURE REGULATION
THERMISTOR
TIE DOWN STUD
BRASS CAN
COPPER RADIATION SHIELD
SAMPLE

inner can is a radiation shield and was machined from copper. A heater of constantan wire was wound nonmagnetically on the outside of this can. A copper stud was firmly fixed to the inside of the lid. This stud served as a support for the sample which was suspended by a nylon thread and as a tie block for the wires connected to the sample. All wires connected to the sample were wound several times around this stud and glued with varnish. This assured that the wires, before going to the sample, would be at the same temperature as the radiation shield. The outer can was made of brass.

The calorimeter was immersed in a bath of liquid helium, liquid nitrogen, or a mixture of ethyl alcohol and dry ice. The alcohol and dry ice mixture maintains a temperature of $-72^{o}C$. In order to reduce temperature gradients in the calorimeter, the bath temperature was chosen to be near the sample temperature. All copper wires connected to the sample were B & S guage 46.

The temperature of the sample relative to the radiation shield was measured with a differential thermocouple. A Kiethley 150A microvoltmeter was used as a meter-amplifier, the output of which was connected to a proportional temperature regulator. The proportional temperature regulator controlled the current in the heater wound on the radiation shield. Thus the tem-

perature of the radiation shield could be controlled relative to the sample. The zero suppress on the Kiethley 150A, a d.c. bias, can be used to maintain temperature differences other than zero. Thus, if the sample heater is turned on, the temperature of the radiation shield will remain equal to that of the sample maintaining the calorimeter adiabatic. In another mode of operation, the zero suppress of the Kiethley 150A is adjusted such that a nonzero temperature difference is maintained. In this manner, the temperature of the sample can be either raised of lowered by radiation exchange with the walls of the calorimeter. A diagram of this circuit is given in Figures 14 and 15. Another temperature regulator was used to maintain the vacuum jacket at a constant temperature for long periods of time. This is also a proportional regulator and senses the temperature by means of a thermistor imbedded in the radiation shield. The circuit diagram is shown in Figure 16.

C. MEASUREMENT OF SPECIFIC HEAT

Data were taken on two samples. Quantities actually measured were the power P, the increment of temperature ΔT, and the interval of time Δt, over which the temperature was measured. As a constant power is supplied to the sample, the temperature of the

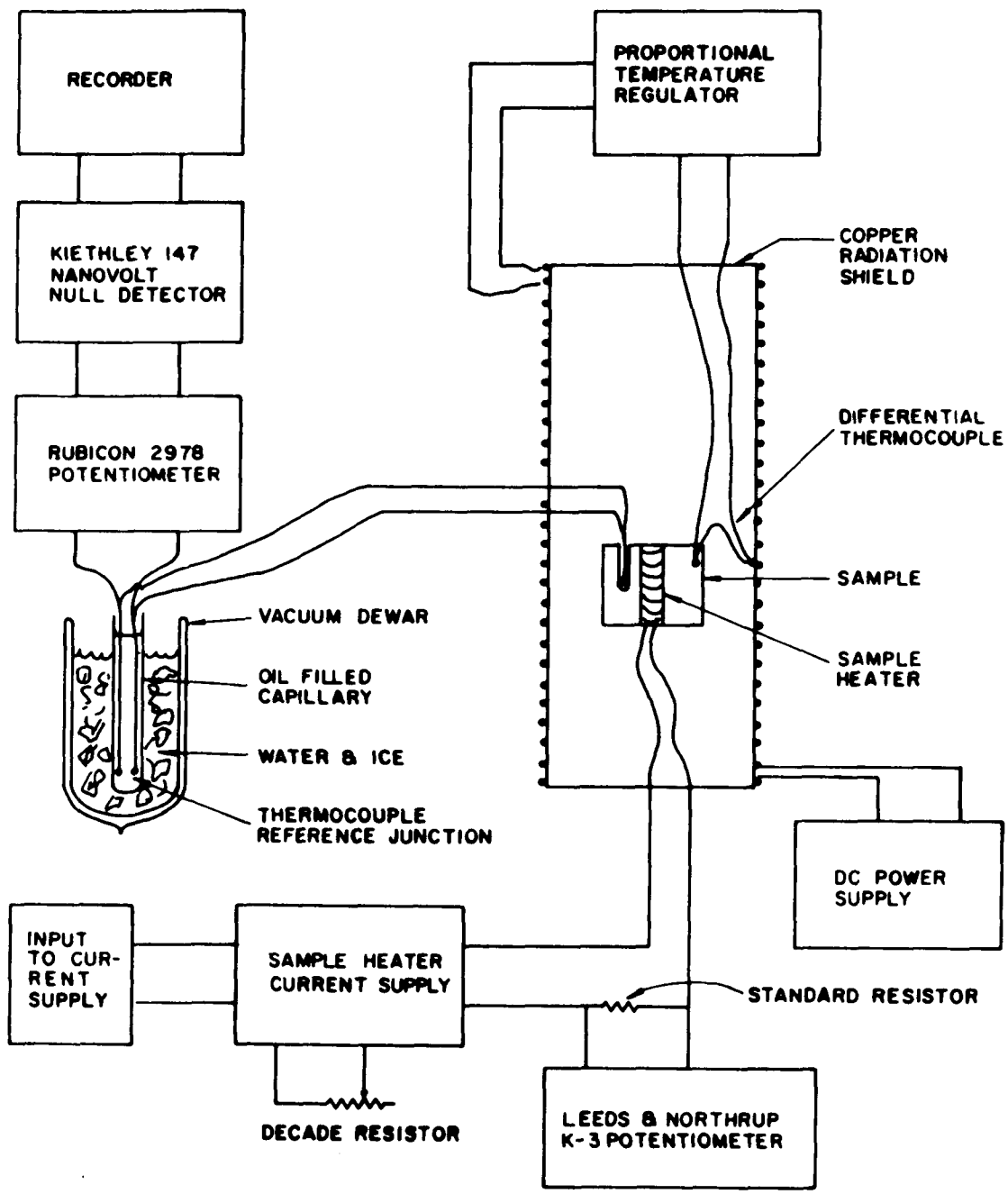
RECORDER
KIETHLEY 147
NANOVOLT
NULL DETECTOR
RUBICON 2978
POTENTIOMETER
PROPORTIONAL
TEMPERATURE
REGULATOR
COPPER
RADIATION
SHIELD
DIFFERENTIAL
THERMOCOUPLE
SAMPLE
SAMPLE
HEATER
VACUUM DEWAR
OIL FILLED
CAPILLARY
WATER & ICE
THERMOCOUPLE
REFERENCE JUNCTION
DC POWER
SUPPLY
INPUT
TO CUR-
RENT
SUPPLY
SAMPLE HEATER
CURRENT SUPPLY
STANDARD RESISTOR
DECADE RESISTOR
LEEDS & NORTHRUP
K-3 POTENTIOMETER

Figure 14

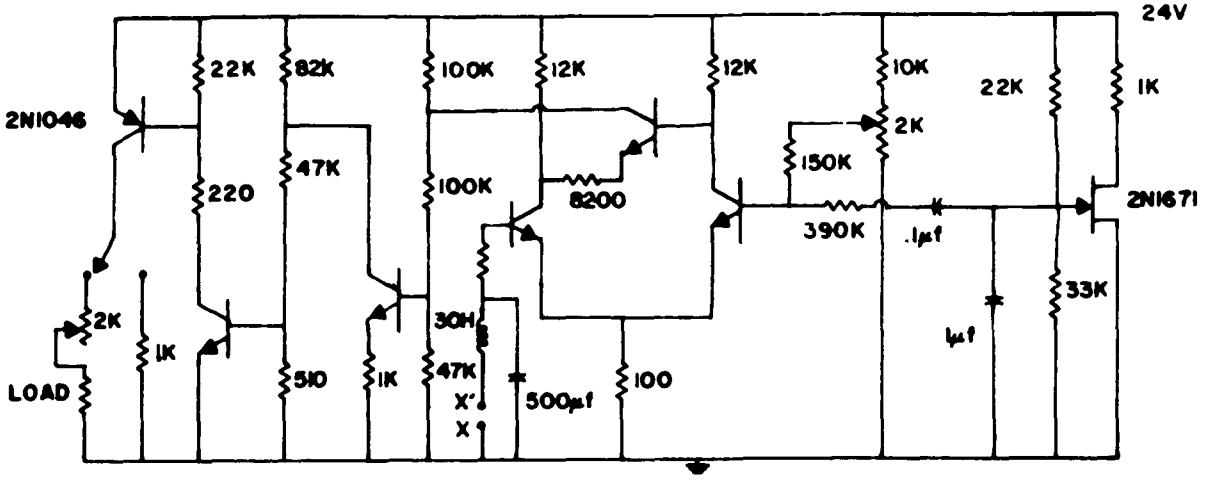
24V
22K
82K
100K
12K
12K
10K
22K
1K
2N1046
2K
150K
220
47K
100K
8200
390K
.1μf
2N1671
2K
1K
30H
33K
LOAD
510
1K
47K
500μf
100
X'
X
1μf

Figure 15

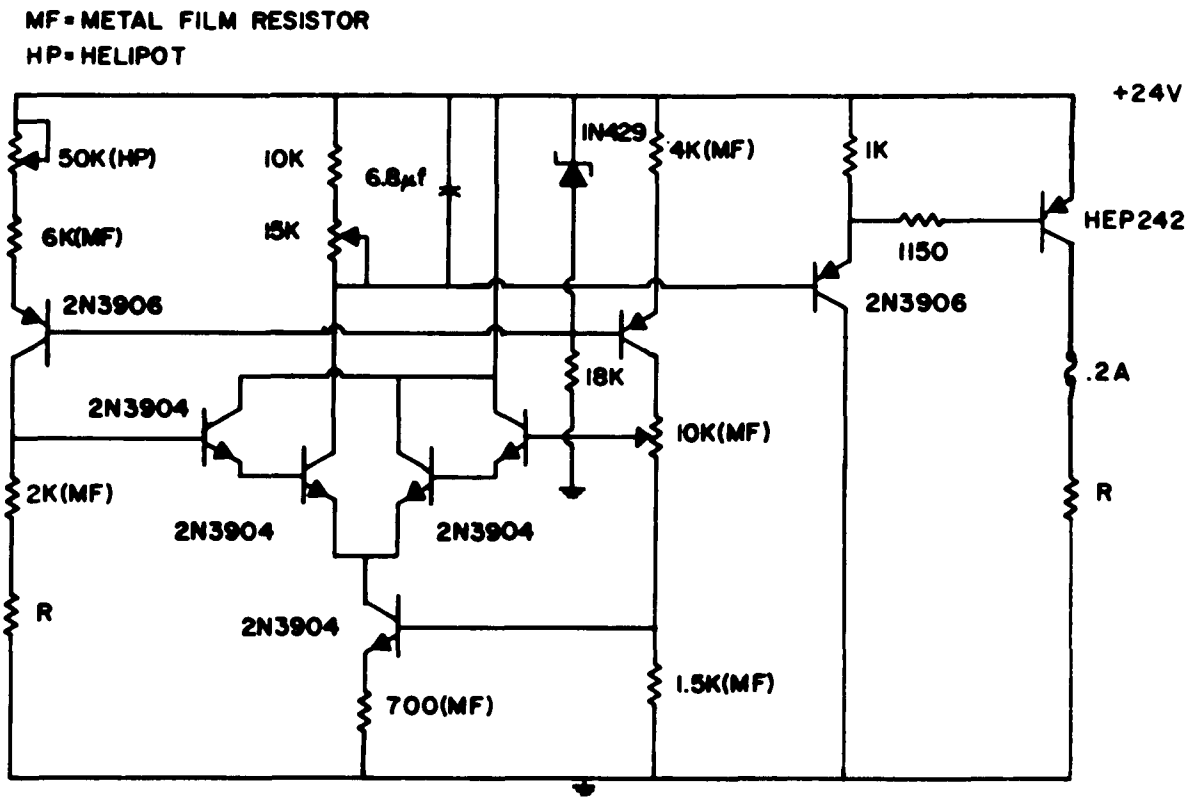
MF = METAL FILM RESISTOR
HP = HELIPOT
+24V
50K(HP)
10K
6.8μf
1N429
4K(MF)
1K
HEP242
6K(MF)
15K
1150
2N3906
2N3906
.2A
18K
2N3904
10K(MF)
2K(MF)
R
2N3904
2N3904
R
2N3904
1.5K(MF)
700(MF)

Figure 16

sample and time are continuously recorded. The specific heat is then given by:

$$C_p = \frac{P \Delta t}{m \Delta T}$$

where m is the mass of the sample and C_p is the specific heat.

The absolute temperature of the sample was measured with a copper-constantan thermocouple composed of .0015 inch diameter copper wire and .010 inch diameter constantan. Calibration of the thermocouple was checked at the freezing points of water and mercury and the boiling point of nitrogen. The deviations of the measured temperature from the standard tables were 0.00, .02, and 1.0°C for water, mercury and liquid nitrogen respectively. The e.m.f. of the thermocouple was measured with a six dial potentiometer (Rubicon 2768--0.1 V resolution) which was used to offset the major portion of the thermocouple voltage. The off balance voltage was amplified with a Kiethley 147 nanovolt null detector and recorded continuously on a strip chart recorder. The overall noise level of the measuring system was 0.01 V short term (1 sec) and 0.05 V long term drift. This corresponds to a temperature resolution for the copper-constantan thermocouple used of 0.25mK short term and 1.25mK long term drift in the neighborhood of the transition. The calibration of

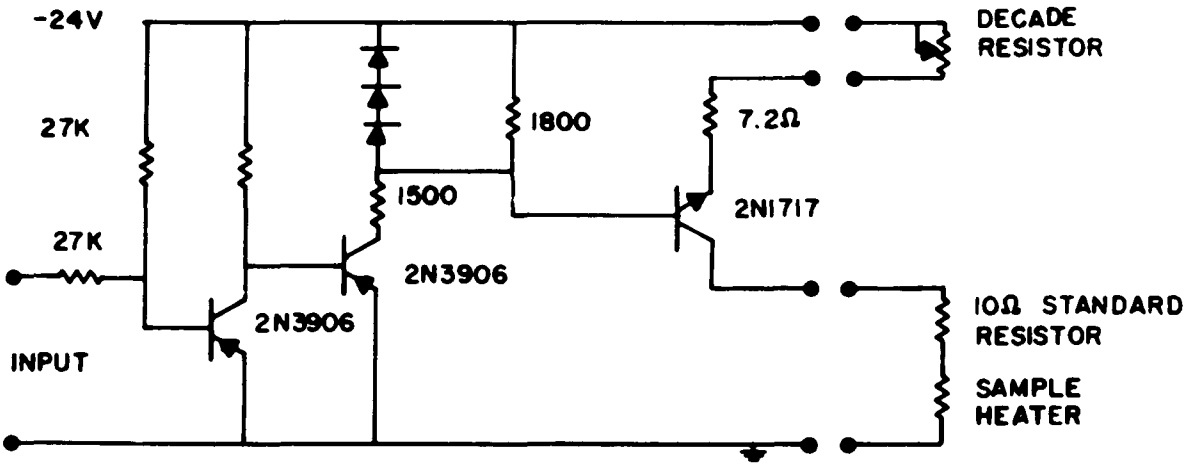
-24V
27K
27K
INPUT
2N3906
2N3906
1500
1800
7.2Ω
2N1717
DECADE
RESISTOR
10Ω STANDARD
RESISTOR
SAMPLE
HEATER

Figure 17

the entire system was checked by measuring the specific heat of pure copper over the range of temperature near the transition. The measured values were within 1% of the published values. The thermocouple was referenced at the melting point of ice.

The resistance of the sample heater was measured as a function of temperature during or after the specific heat measurement. A least squares fit to the data was made such that the constants in the equation $R(T) = a + bT + cT^2$ were known. Current to the sample was supplied by means of a constant current circuit shown in Figure 17 which could supply either a single heat pulse or a constant current to the sample heater depending upon the signal provided at the input of the circuit. Desired current values were obtained by adjusting the decade resistor. The magnitude of the current was found by measuring the voltage across the standard resistor in series with the sample heater with a Leeds and Northrup K-3 potentiometer.

The time increment, Δt, was measured directly from the stripchart recorder. Data were recorded at a fast enough rate that good time resolution could be achieved.

Thus, continuous heating curves were recorded and used to compute the specific heat from 35 to 330°K. Data were taken from the chart paper at approximately 0.008°K intervals near the transition and at wider

intervals at points away from the transition. Temperature resolution near the transition was better because the magnitude of the specific heat near the critical temperature is larger, causing the rate of heating or cooling to become slower, thus permitting a better equilibrium and temperature resolution.

Because the mass of the addenda was on the order of one percent of the mass of the sample and mainly composed of aluminum, it was assumed that the specific heat of the addenda was equal to that of aluminum. The specific heat of the sample was then corrected taking into account the change of the heat capacity of aluminum with temperature. No radiation correction was necessary on the heating curves because the temperature of the sample and the radiation shield were equal.

Only in the neighborhood of the specific heat anomaly were continuous measurements of the specific heat made while cooling the sample. This was done by maintaining the radiation shield at a lower, measured temperature than the sample, thus extracting heat from the sample by radiation exchange. The maximum difference in the endpoint temperatures over which the cooling run was made was 18.0^{o}K. Measurements of the specific heat at the endpoint temperatures were made in the conventional manner for calibration purposes. Thus, the radiated power necessary to give the correct value of

the specific heat at the end point temperatures is known, and an extropolation of the power can be made between these points. Provided the temperature difference in the end point temperatures is relatively small, a linear extrapolation of the power can be made. In this temperature range, with an end point temperature difference of $18^{o}K$, T^{4} differs from linearity by a maximum of .75%. This is probably a good estimate of the maximum error introduced in the radiated power by making a linear extrapolation of the power across the range of temperature over which the cooling run was made.

Since preliminary resistivity and heat capacity measurements indicated that the equilibrium times for NiS near the MNM transition are extremely long, several heating and cooling rates were used to check for non-equilibrium effects. A run was performed in which both the heating and cooling rates were at the limits of stability for the calorimeter and three weeks were required to heat or cool the sample over a ten degree range near the transition. These results did not differ within experimental error from those obtained when the heat input or output was adjusted to cover the same temperature range in 36 hours. Faster rates, of order 1h for the same temperature range, produced noticeable changes in the heating and cooling curves. All of the data reported here were obtained from a sample which hadn't

previously been cycled through the transition and during the run was cycled at an average rate of approximately 0.03^{o}K per h near the transition.

Specific heat measurements using heat pulses were also carried out. In this case

$$C_p = \frac{1}{m} \frac{\Delta Q}{\Delta T}$$

where ΔQ is the increment of heat supplied by the heat pulse and ΔT is the temperature rise of the sample resulting from the heat pulse. The results were exactly the same as those obtained by the continuous heating method except near the critical temperature. This method has several drawbacks. These are: (a) collection of data is extremely slow, (b) in the neighborhood of the critical temperature where equilibrium times are very long, interpretation of the plot of the heat rise of the sample verses time is very difficult, (c) no data can be taken while cooling the sample through the transition, (d) for short heat pulses, measurement of the power supplied to the sample is difficult, (e) temperature resolution is very poor thus providing few data points in the neighborhood of the critical temperature. No data taken by the heat pulse method is presented here because the data were not sufficiently good.

D. RESULTS AND DISCUSSION

For an isobaric process $\Delta Q = \Delta H$, where ΔQ is an

increment of heat and ΔH an increment of enthalpy. Therefore what has actually been measured is the enthalpy as a function of temperature and

$$C_p = \frac{1}{m} \left(\frac{\partial H}{\partial T} \right)_p$$

The enthalpy, or heat, supplied by the sample heater or removed by radiation exchange has been plotted as a function of temperature in Figure 18 for the first of the two samples. It can been seen from this curve that during a cooling run the sample supercools approximately $2.5^{\circ}K$ and that there is considerable hysteresis associated with the transition. The amount of supercooling and hysteresis was increased with much faster cooling rates but is not measurably decreased with slower rates. If fast heating rates are used, a small but measurable amount of superheating is also observed. Because of the supercooling during the cooling run, the transition temperature cannot be determined exactly. This was taken to be the maximum temperature reached by the sample after supercooling for the cooling run, and is $268.97^{\circ}K$ This temperature is within $1.7^{\circ}K$ of the transition temperature obtained from the ratio of the enthalpy to the entropy change across the transition.

The specific heat at constant pressure, C_p, was

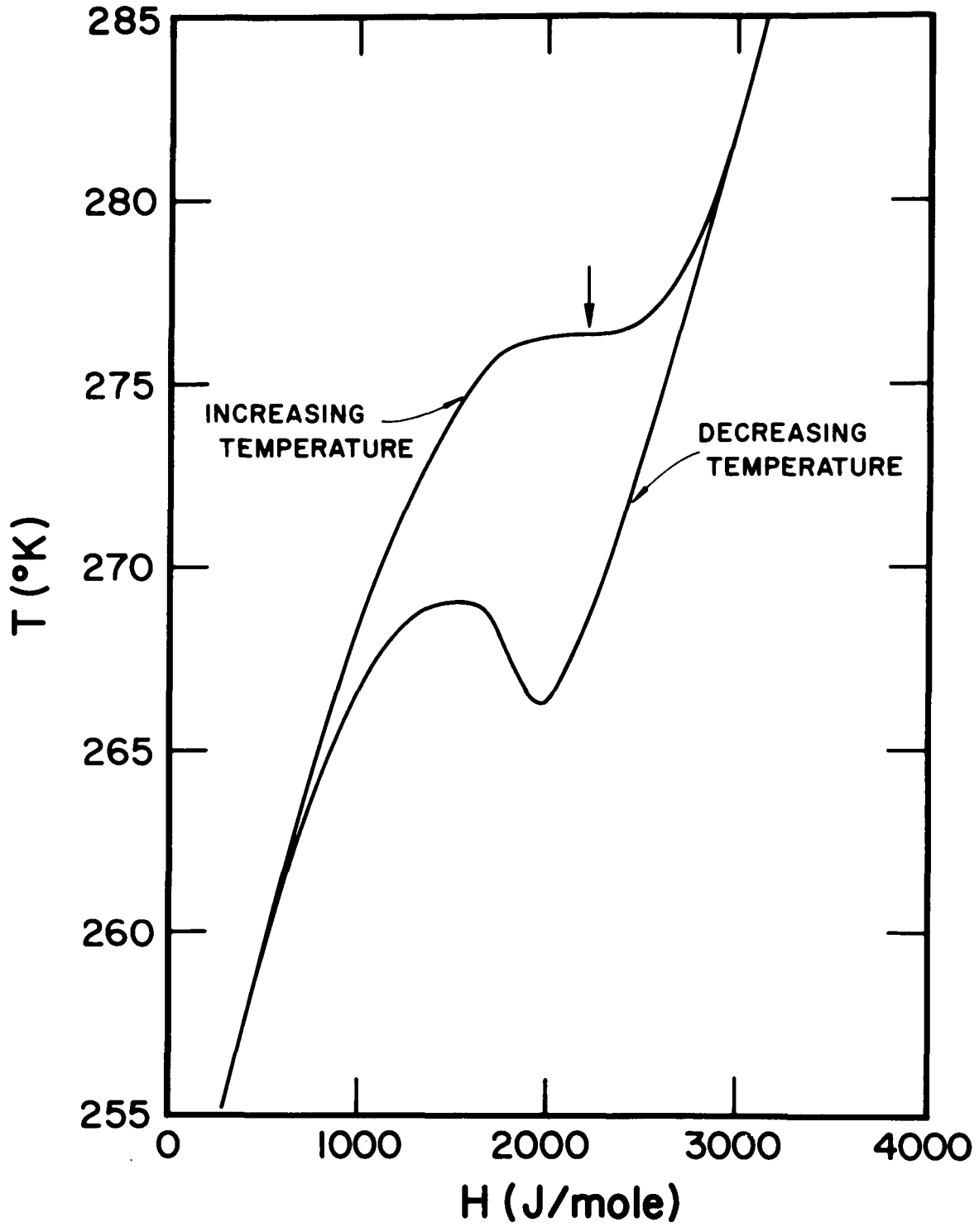
285
280
275
270
265
260
255
T (°K)
INCREASING
TEMPERATURE
DECREASING
TEMPERATURE
0
1000
2000
3000
4000
H (J/mole)

Figure 18

calculated from the slope of the enthalpy curve, and for the second sample, this data is shown in Figure 19. The lattice contribution to the specific heat was subtracted from the peak by extrapolating the data to the transition temperature from both sides of the peak. The data in the temperature ranges immediately above and below the specific heat anomaly are linear in temperature within experimental error. From 219 to 253°K, $C_p(T) = 27.431 + 0.078462T$ with a standard deviation of $\sigma = 0.13$. From 278 to 330°K, $C_p(T) = 31.0165 + 0.067876T$ with $\sigma = 0.07$. The data from 278 to 330°K were taken before lowering the temperature through the transition and was combined with data taken from 288 to 300°K taken after having cycled the sample through the transition. In Figure 20 the values of C_p near the transition for the first sample with the lattice contribution subtracted for both heating and cooling runs is shown. The data shown for the cooling run are only a portion of the positive parts of the specific heat. Supercooling and subsequent selfheating of the sample occurs, giving negative values in addition to double valued positive specific heats. It can be seen that the cooling curve exhibits sharp discontinuities in C_p due to supercooling. On the heating run such is not the case and there are no infinities associated with the heating curve. A subsidiary peak occurs approximately 0.3°K

Figure 19

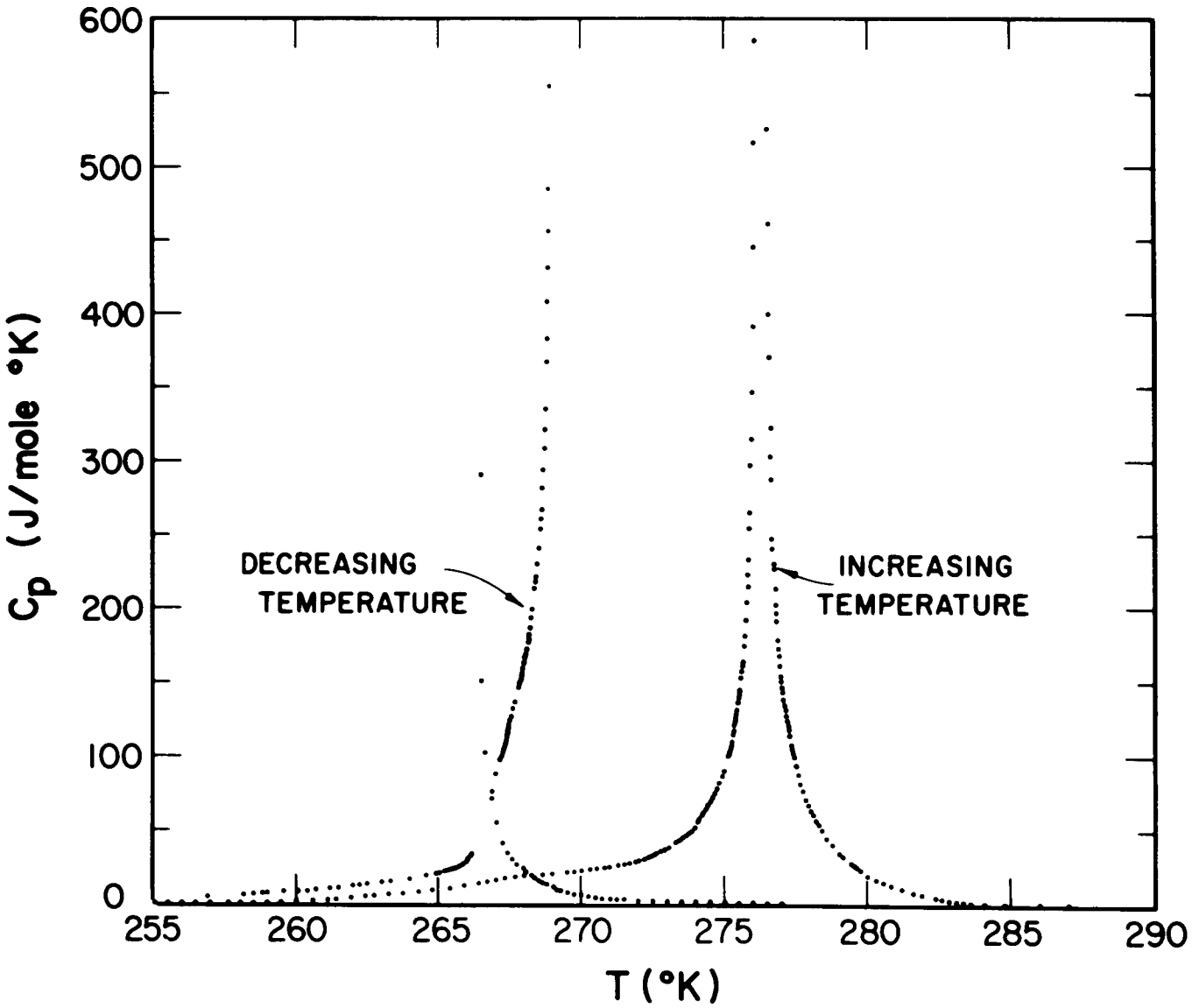
600
500
400
300
200
100
0
C_p (J/mole °K)
DECREASING TEMPERATURE
INCREASING TEMPERATURE
255
260
265
270
275
280
285
290
T (°K)

Figure 20

below the main peak on the heating curve. Detail of the heating curve near the critical temperature is shown in Figure 21.

Both the enthalpy (ΔH) and the entropy (ΔS) changes were computed from the data. For the increasing temperature curve, the enthalpy change was found to be 1383 J/mole or 0.0143 eV per Ni atom and the entropy change 5.03 J/mole-deg. This entropy change corresponds to $\Delta S = 0.88R\ln 2$. This result is in agreement with the latent heat computed from the Clapeyron equation which yields 1400 J/mole based on the data of Smith and Sparks[26] and Anzai and Ozawa[27] with a transition temperature of 276.4°K.

Thus, the metal-nonmetal transition displays the characteristics of a first order transition. Broadening of the peak is probably due to inhomogenity of the sample. The measured entropy change of $\Delta S = 0.88R\ln 2$ is in good agreement with the conclusion of Sparks and Komoto[16] who measured the sublattice magnetization to be within 90% of its saturation value 4°K below the transition. These two results suggest that one electron per Ni atom is involved in the ordering process and that the entropy change is due entirely to the electrons. It should be emphasized that this conclusion is based on the assumption that at the transition the spins merely disorder. If, on the other hand, the localized spins

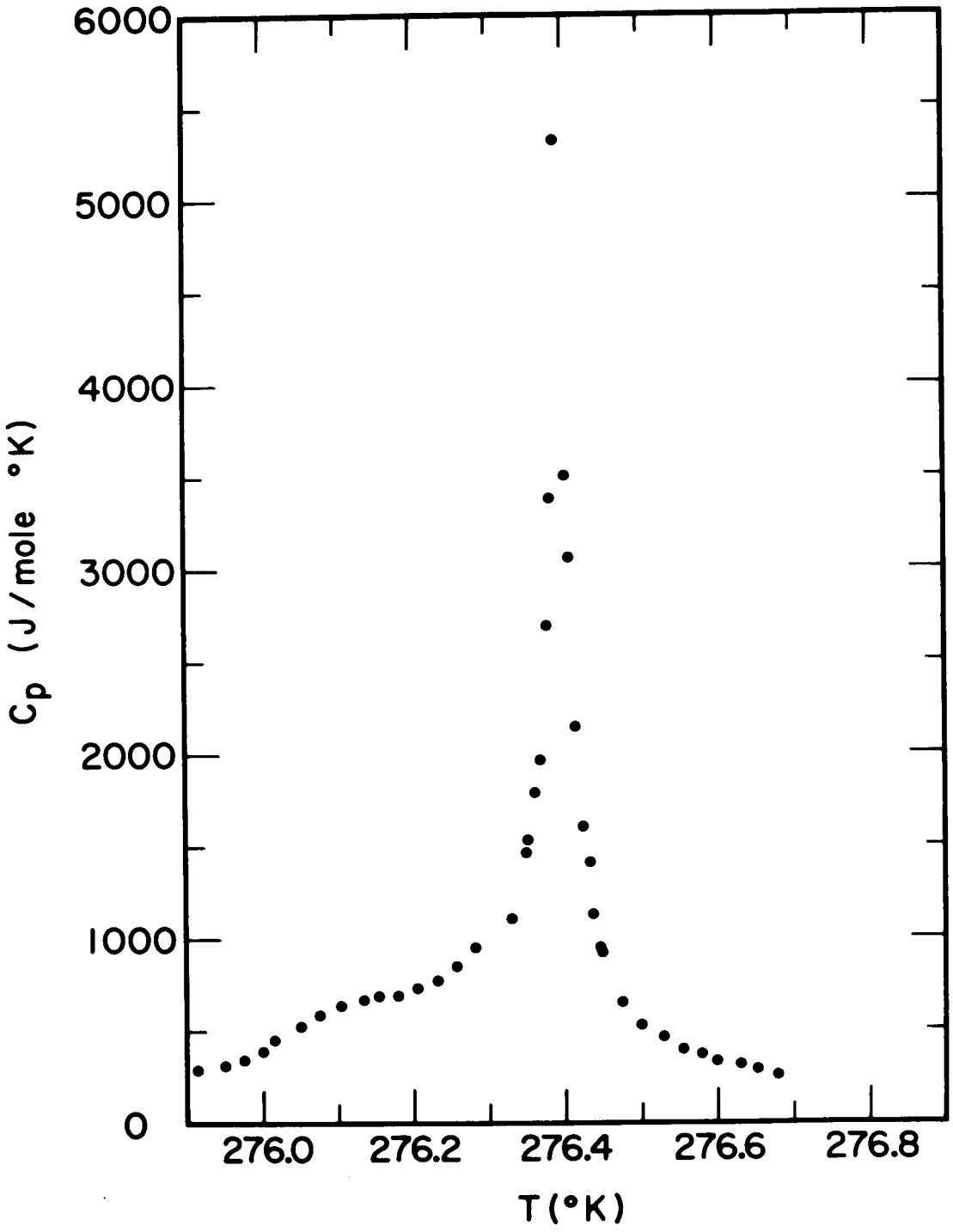
6000
5000
4000
3000
2000
1000
0
C_p (J/mole °K)
276.0
276.2
276.4
276.6
276.8
T(°K)

Figure 21

become part of the conduction band at the transition, the value of $\Delta S = 0.88R\ln 2$ must be reinterpreted.

There is a possible change in the Debye temperature at the transition because the specific heat increases by 0.61 J/mole-deg when the specific heat data are extrapolated to the transition temperature from both sides of the transition.

In order to calculate the Debye temperature, the specific heat at contant volume, C_v, must be known. Since the volume expansivity, β, the molar volume, v, and the isothermal compressibility, k, are not known as a function of temperature, the Nernst-Lindemann equation is used. This is a relation between the specific heats at constant pressure and volume. Specifically,

$$C_p - C_v = AC_p^2T,$$

where $A = v\beta^2/kC_p^2$ which has been found to be approximately constant for most substances when evaluated at one temperature. The only available data for v, β and k are at 77 and 300°K due to Smith and Sparks[26] and Sparks and Komoto[16]. Having found C_v, the Debye temperature can be found. This was done for NiS using the two extrapolated values of C_p at the critical temperature. The results are $\theta_i(T \lesssim T_c) = 276^oK$ and $\theta_o(T \gtrsim T_c) = 183^oK$ where the uncertainty, $\sigma = 80^oK$ for both measurements.

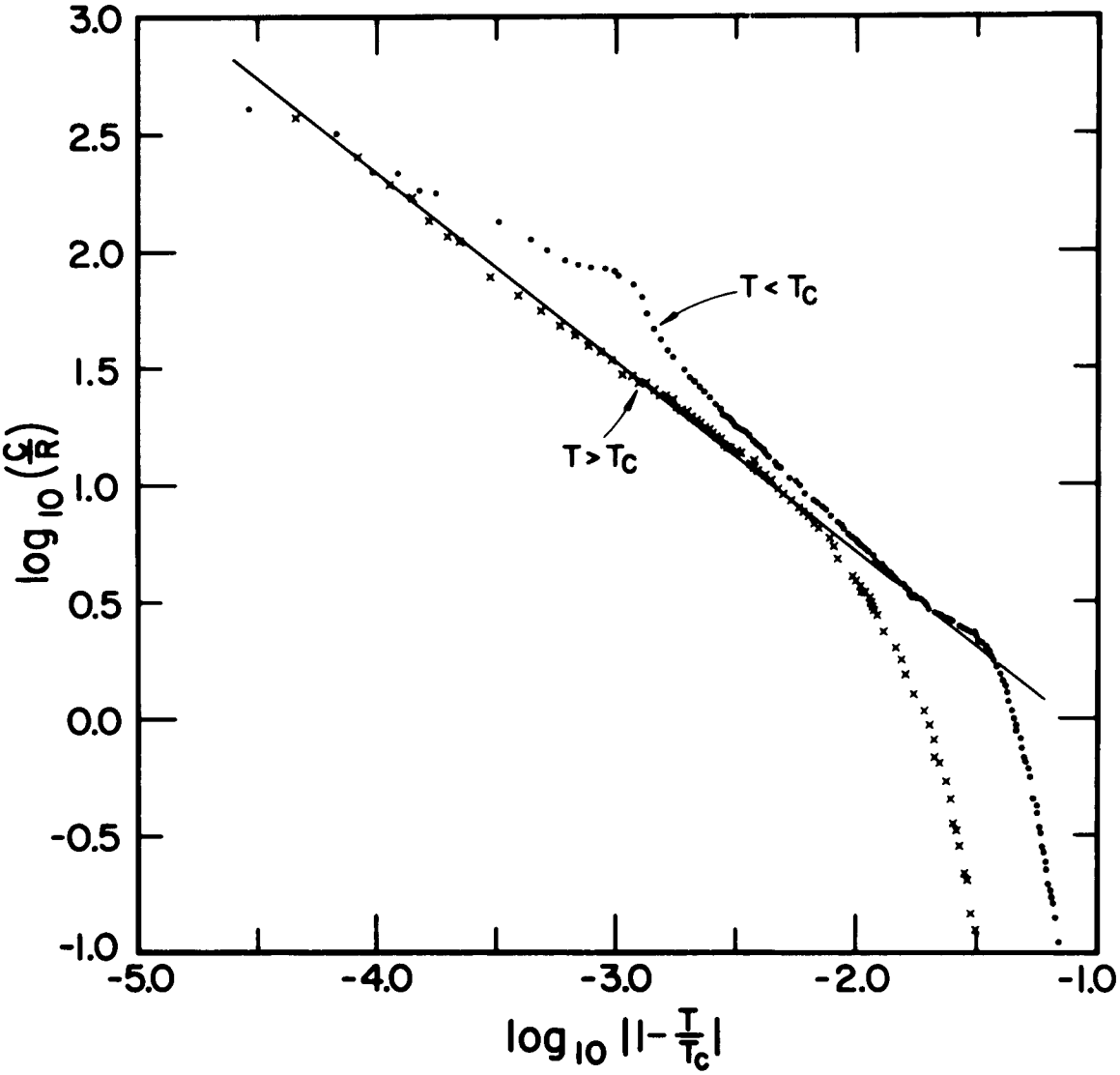
3.0
2.5
2.0
1.5
1.0
0.5
0.0
-0.5
-1.0
-5.0
-4.0
-3.0
-2.0
-1.0
T < Tc
T > Tc
log10 (C/R)
log10 |1-T/Tc|

Figure 22

The uncertainty was estimated by estimating a maximum of ± 1.0° error in C_p and maximum possible error in estimating the compressibility from the paper of Smith and Sparks[26]. The volume expansivity was assumed to introduce no error. Thus, no conclusive statement concerning the Debye temperature can be made because of the extreme sensitivity of the Debye temperature to experimental errors in this temperature range.

An attempt to fit the data to a scaling law applicable to second order transitions was made. Figure 22 shows the results of this fit for the data both above and below T_c. The function which was fit for this data was $C_p \propto (1 - T/T_c)^{-\alpha}$. It can be seen that the fit for the data on the high temperature side of the peak is quite good over a large range. The additional peak observed on the low side of the peak causes the data to deviate from a straight line, however it fits on the same line as the high temperature data on either side of the subsidiary peak. The value of α obtained from the fit is 0.81 on the high side of the transition.

A complete listing of the specific heat data can be found in the Appendix.

V RESISTIVITY MEASUREMENTS

Resistivity measurements were carried out on several samples during the course of this work. All were done in a similar manner. The vacuum calorimeter described in detail in the section on specific heat measurements was adapted. See Figure 13. Since the resistance in the metallic state is very small, a four probe technique was employed where the current was introduced on two leads and the voltage across the remaining two leads was measured with a potentiometer. Only direct current measurements were made. Temperature control was similar to that used during the specific heat measurements. Leads were usually attached by spot welding copper wires to the samples with a Hughs constant voltage spot welder. All measurements were made with the current in the forward and reverse directions to minimize effects due to thermal e.m.f.s.

A. Single Crystal Resistivity

The first sample was a single crystal 2 x .8 x 13 mm where current flow was perpendicular to the c axis. The sample was attached to a solid copper block with thermally conducting, electrically insulating varnish. The block was then attached to the bottom of the tie down stud of the calorimeter. The sample was therefore thermally connected to the radiation shield. The sample temperature was reduced by reducing the temperature of the radiation

shield. Current flow was perpendicular to the c axis and resistance was measured while the temperature was gradually reduced. Close to but prior to reaching the critical temperature the sample was allowed to sit over night. The next morning, the resistance of the sample had increased by a factor of three which was not understood at the time. Measurements on later samples show that very long time constants exist in the neighborhood of the transition. The resistivity of the sample at room temperature was measured to be 4.2×10^{-5} ohm cm, and the resistance of this sample was approximately 2.4 m ohm between the voltage leads which were about 9 mm apart. A plot of $\rho(T)/\rho(T=0^{o}C)$ verses temperature is given in Fig. 23 which definitely shows a discontinuity in $\rho(T)$. While descending through the critical temperature several small peaks occured which can probably be attributed to cracking of the sample. The resistance ratio, $\rho(max)/\rho(T=0^{o}C)$, is about 200, but the contribution due to cracking of the crystal is difficult to determine. When the crystal was removed from the calorimeter, it was still intact, but the slightest disturbance caused it to crumble into small pieces.

B. Resistivity Measurements on Specific Heat Sample

After completing the specific heat measurements described in another section, the sintered pellet on which

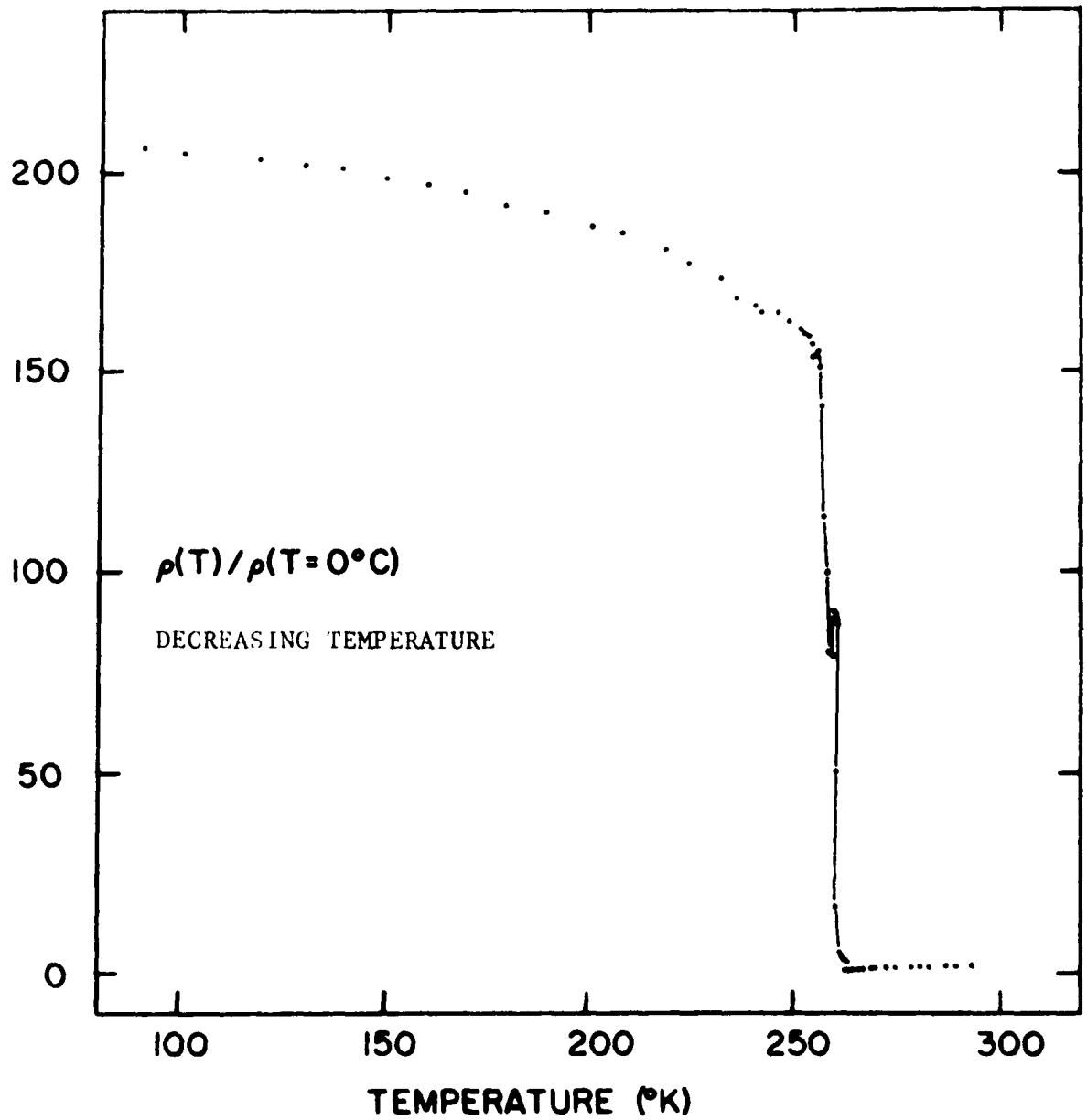
200
150
100
50
0
ρ(T) / ρ(T = 0°C)
DECREASING TEMPERATURE
100
150
200
250
300
TEMPERATURE (°K)

Figure 23

the latent heat was measured was removed from the calorimeter. All addenda were removed by dissolving the G.E. varnish in alcohol. Leads for resistivity measurements were attached to the side of the pellet, and the pellet was then replaced in the calorimeter by suspending it with a nylon thread as if specific heat measurements were to be conducted. The differential thermocouple between the sample and the radiation shield was connected such that the temperature of the radiation shield could be regulated relative to the sample temperature. The temperature was lowered by maintaining the temperature of the radiation shield at a lower temperature than the sample. The results of this resistivity measurement are shown in Fig. 24. Notice that the resistance of the sample increased while the sample supercooled and during the self heating period, and that the sample supercooled about 2.55°K which is slightly larger than the supercooling measured in the specific heat run. The minimum temperature achieved in supercooling was 264.7°K or 2.7°K lower than measured while measuring the specific heat. This discrepancy can probably be attributed to the fact that the rate of temperature descent was on the order of five times faster in the resistivity run.

A heating run was conducted on this sample which displayed the hysterisis seen in the specific heat run. In the neighborhood of the transition, the heating rate was

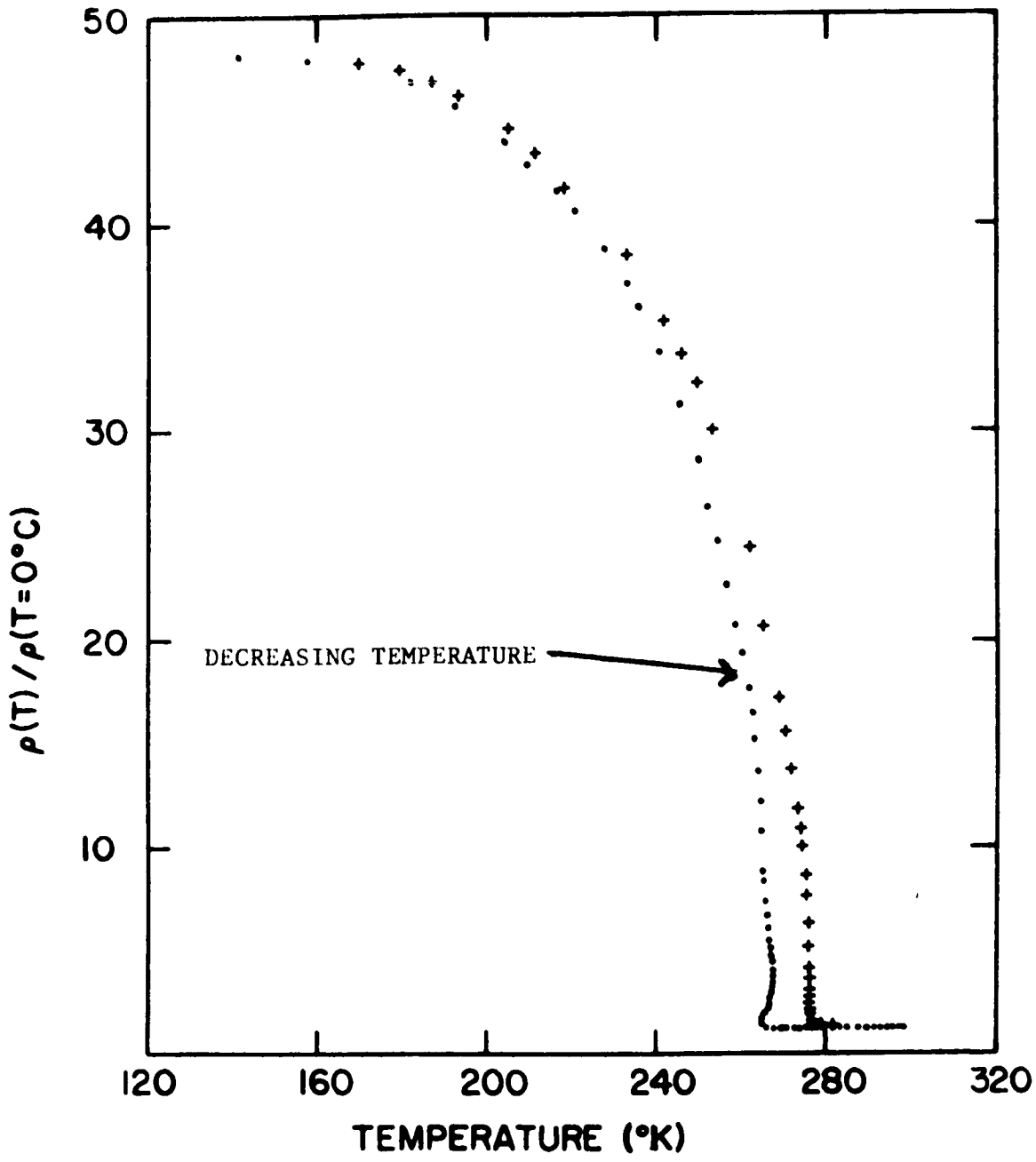
50
40
30
20
10
ρ(T) / ρ(T=0°C)
DECREASING TEMPERATURE
120
160
200
240
280
320
TEMPERATURE (°K)

Figure 24

very fast--on the order of 0.6 deg/hour between 274 and 276°K. The sample was observed to superheat 0.1°K which is probably the result of nonequilibrium effects due to rapid heating of the sample.

The resistance ratio for this sample is on the order of 50 which is about half that seen by Sparks and Komoto[19] on a similar sample. Notice, however, that the residual resistance has increased by 10% during the second cycle through the critical temperature. Since only specific heat was measured on the first cycle the residual resistivity due to this cycle is not known but could easily be a factor of two which would increase the resistance ratio to the value seen by Sparks or Komoto. The residual resistivity seen by Sparks and Komoto[19] increased by an estimated factor of about nine on cycling through the transition the first time.

This measurement displayed no abrupt change in the resistivity as observed in the resistivity of Sparks and Komoto[19] but changed continuously as a function of temperature. Since the resistance does change rapidly at T_c this is perhaps the result of better temperature resolution in the present measurement, or, if the sample were attached to a heat sink, self heating of the sample would not be seen causing a large resistance change at one temperature while the ordering was occuring.

An isothermal ($\pm$0.005°K) measurement near the critical

temperature of the resistance of the sample showed a continuous resistance change for a period of 100 h near the transition temperature. A plot of the resistance, ρ, vs time in this case fits a functional form of

$$\frac{\rho_\infty - \rho}{\rho_o} = 2.3\, e - \frac{t-t_o}{\tau}$$

with τ=49h. Here ρ_∞ is the final state resistivity and ρ_o is the resistivity at time $t=t_o$. Thus, the equilibrium times near the transition are extremely long. To ensure complete equilibrium, measurements of the properties of NiS near the transition would require hours at a conatant temperature.

VI OPTICAL MEASUREMENTS

Reflectance measurements were conducted to determine the reflectivity of NiS in the metallic state, to obtain data with which to fit parameters occuring in an energy band calculation and to determine how the reflectance changes when the sample passes through the critical temperature.

Since resistivity measurements indicated that the band gap in the semiconducting state was on the order of .3 ev, optical measurements in the visible and infrared regions of the spectrum were planned. A McPherson model 218 monochromator and a model 817 double beam reflectance attachment were available for measurements in the visible and near ultraviolet. Since no instrument at LSU existed for making variable temperature optical measurements in the infrared, a complete system had to be designed and constructed. A partially constructed helium dewar to which a variable temperature tail section could be adapted and a Perkin-Elmer model 12B infrared monochrometer were at my disposal. Two detectors, a bolometer and a lead sulfide detector were available which could be used in conjunction with a PAR model 124 lock-in amplifier. The source for the monochromator, the variable temperature tail section of the dewar and a reflectometer were designed and constructed.

A. APPARATUS AND MEASUREMENT OF REFLECTANCE IN THE INFRARED

The model 12B infrared monochromator was originally part of an infrared spectrometer assembly and had been removed from the assembly with a band saw. It is a single pass instrument designed for use in a single beam mode and to be used with a NaCl prism. A schematic diagram of the monochromator and light source is shown in Figure 25. The light source was arranged such that the f-number of the source matched the f-number of the monochromator and such that the image of the source was focused on the slit S1. This ensures that the beam which passes through the slit S1 does not overlap the edges of mirror M3. A Nernst glower was used as a source. The glower and associated mirrors were housed in a separate light tight box which was attached to the monochromator such that the entire source assembly could be easily removed. The portion of the beam which passes through S1 is collimated by M3, an off-axis paraboloid mirror. The beam passes through and is refracted by the prism and reflected by the Littrow mirror, M4, back through the prism to M3. The paraboloid then focuses the energy on the exit slit S2 by means of mirror M5. Mirror M6 was installed to direct the beam out of the side of the monochromator to the reflectometer.

Since the monochromator was not alligned, much time

Figure 25

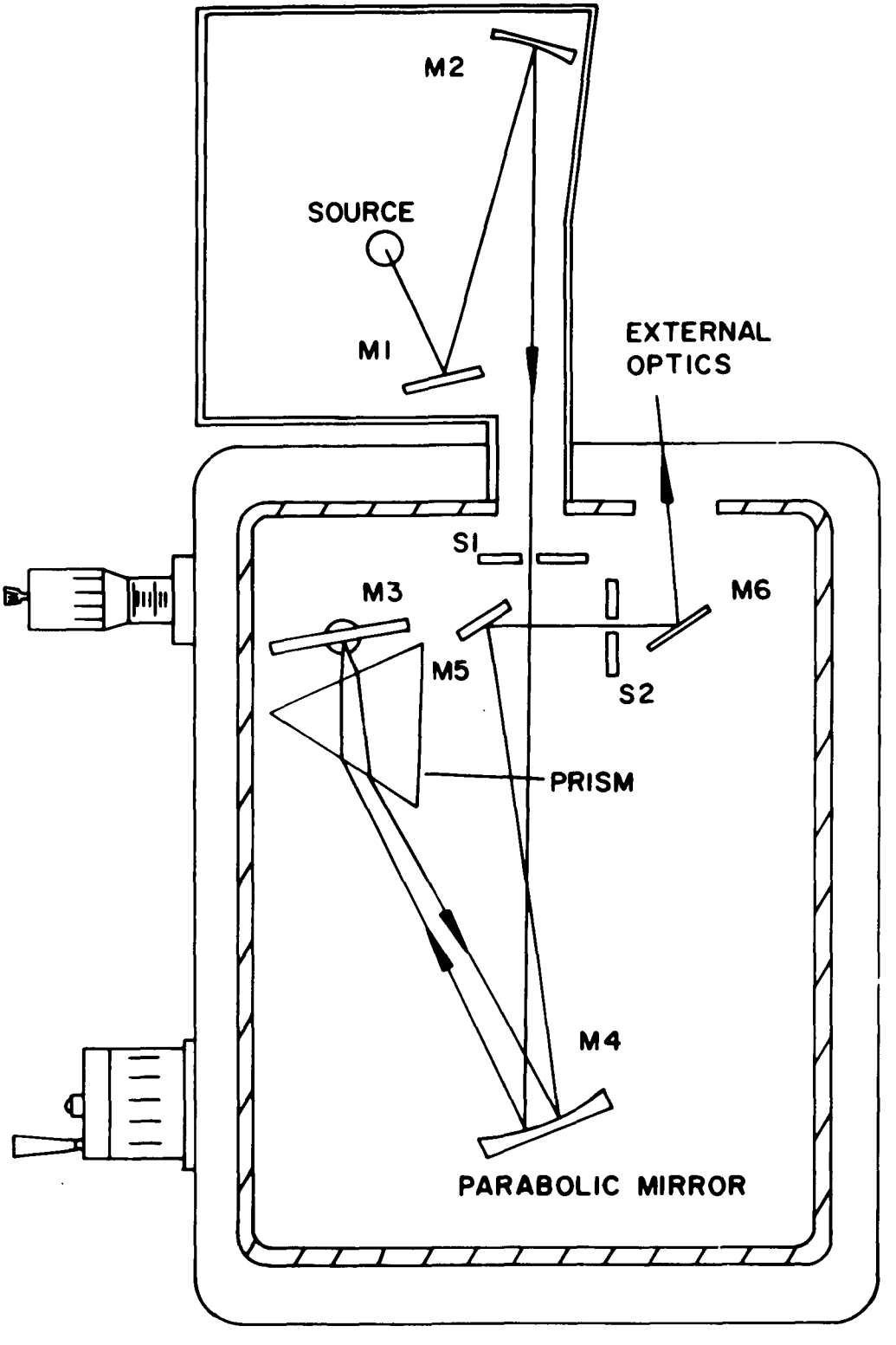
M2
SOURCE
M1
EXTERNAL
OPTICS
S1
M3
M6
M5
S2
PRISM
M4
PARABOLIC MIRROR

was spent getting the instrument in working order. A mercury discharge lamp was used as a line source for allignment and calibration purposes in the visible and near infrared. At .7ev a resolution of 1.7mev was obtained with the sodium chloride prism and slit width of 1.5mm. Better resolution could not be obtained because the slits were found not to be in vertical allignment. Resolution better than this is not needed for reflectance measurements in metals since very sharp structure is not anticipated.

Calibration of the instrument was accomplished by utilizing a mercury vapor discharge lamp housed in a quartz envelope. The positions of each of the discharge peaks was recorded as a function of the number of turns on the prism drive. The positions of the carbon dioxide absorption bands were located by filling the monochromator with CO_2, and in the far-infrared, the wavelength of the absorption bands of a polystyrene strip were measured. The polystyrene strip is supplied by Beckman as a standard for calibrating infrared spectrophotometers. These calibration points were used to determine the constants in the following standard equation[42] used for calibrating infrared spectometers:

$$T = T_o + Az^2 + \frac{B}{Z_2^2 - Z^2}$$

where T is the number of turns of the prism drive and Z is the wavenumber given in inverse contimeters. A,B,T_o and Z_2 are constants to be determined by the least squares fit. This fit was accomplished by utilizing the General Foods Multiple Regression Program, MRP-49, available at the LSU Computer Center.

In designing a reflectometer a first consideration is that the image must be focused on the sample and the detector because both tend to be small. The image on the sample must be sharp in order that the subsequent image on the detector will be adequate. With this in mind, a 90^o off axis torroidal mirror of focal length 10cm already available was utilized as a first mirror to reflect the monochromator beam to the sample. When using a torroidal mirror, the best image is obtained when used at exactly the angle for which it was designed and with a magnification of one. Some experimentation showed that a slight reduction in image size to about 3/4 of the object size could be achieved with little distortion. In addition, it was found that the object size for this particular mirror could be no larger than about 4mm on a side. The slits of the monochromator, normally about 1/2 inch high, were reduced to 4mm by masking the top and bottom with sheet aluminum. Thus, a good image of the slit, about 3mm high, was focused on the sample.

Because of the relatively short focal length of the

torroidal mirror, the beam had to be brought out of the monochromator near the entrance slit in order to provide room for the dewar which housed the sample and for the second mirror which collected reflected light from the sample. This was accomplished by mirror M6 shown in Figure 26 which includes the final design of the reflectometer attachment. M6 reflects the beam to the torroidal mirror, M7, which subsequently reflects if to the sample. Before the beam reaches the sample it is chopped by a chopping mirror. In one position of this chopping mirror, the beam passes directly to the sample from which it is reflected to mirror M8, a spherical mirror which then reflects the energy to the detector. When the chopping mirror is rotated, the beam takes a different path: it is reflected by the chopping mirror to a spherical mirror, M9 which subsequently reflects the beam to the detector.

The reflectometer was designed such that the path lengths of both beams were approximately equal and so that the angle between the incident and reflected beam on the sample was less than 20^{o}. In order to maintain good images, off axis reflections from spherical mirrors were on the order of 25^{o} or less.

All of the spherical mirrors were originally concave lenses. A coating of aluminum was evaporated on the front surface of all the mirrors simultaneously, including

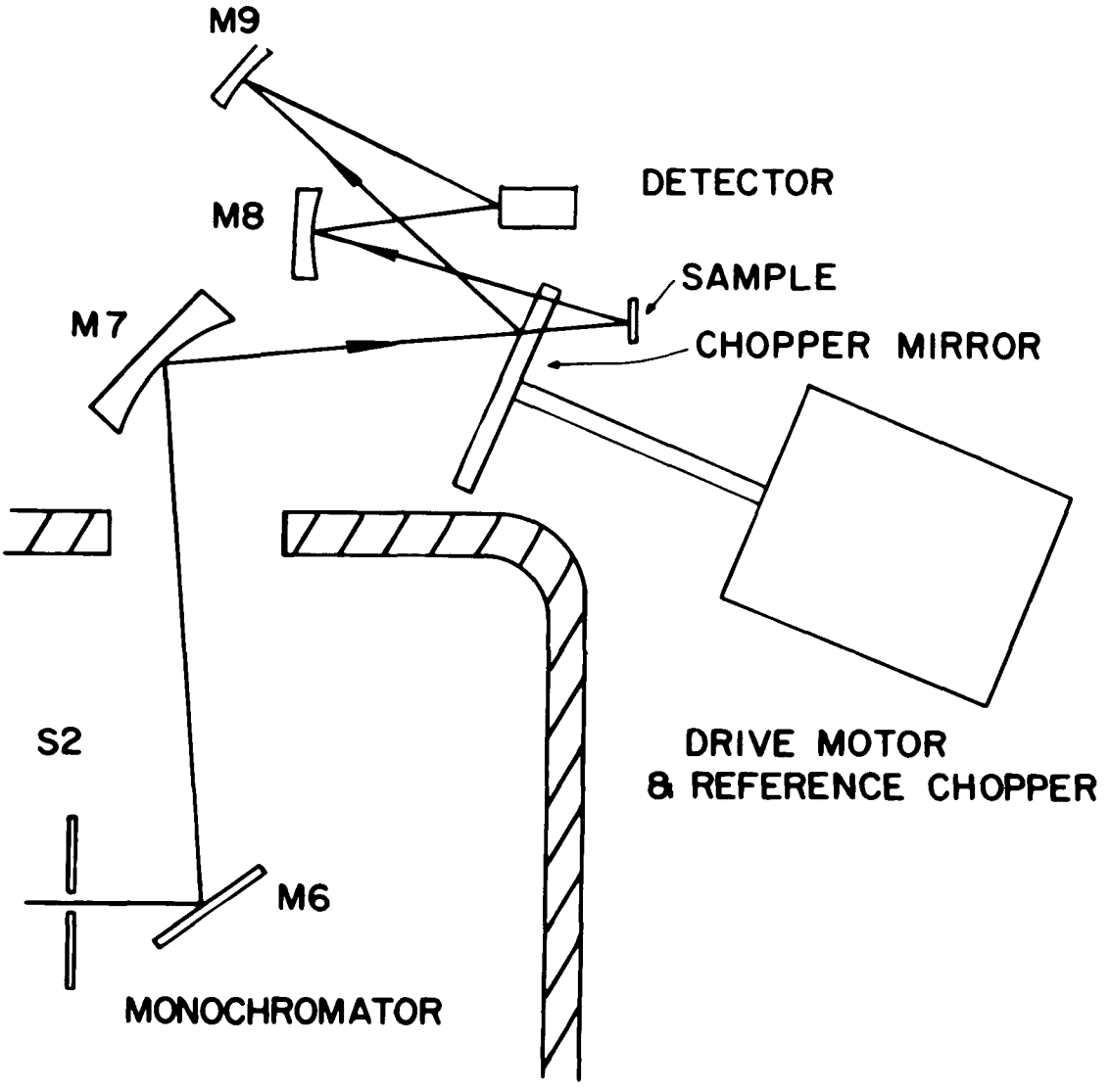
M9
DETECTOR
M8
SAMPLE
M7
CHOPPER MIRROR
S2
DRIVE MOTOR
& REFERENCE CHOPPER
M6
MONOCHROMATOR

Figure 26

the chopper mirror. The coating was thick enough such that no visible light would pass. Front surface aluminum mirrors must be used because they are achromatic and of high reflectivity throughout the infrared region of interest. In fact, the reflectivity of aluminum films at wavelengths greater than 1.5 microns is greater than 95% [43].

The light chopper which divides the beam into the sample and reference channels was constructed by cutting the chopper out of 1/8 inch sheet aluminum. Microscope slides, cut to fit on each of the blades, were attached to the chopper with a low vapor pressure epoxy. Aluminum was then evaporated on the glass surfaces. A second chopper wheel was cut which was exactly the same shape as the first and mounted on the same shaft. This wheel was used as the reference signal chopper and housed in a light tight box along with a synchronous motor to drive the wheels. A photodiode lamp arrangement was used to produce the reference signal for the lock-in amplifier.

A partially finished stainless steel helium dewar was available to which a variable temperature tail could be attached to be used as a sample holder. The dewar was completed and leak tested. The copper sample holder was constructed such that a thermal resistance was placed between the sample and the coolant. Two heaters of contantan wire were wound near the sample. Current to

one heater was supplied by a d.c. power supply and the second was used for the temperature regulation current supplied by a proportional temperature regulator described earlier in the section on specific heat measurements. The temperature of the sample holder for the temperature regulator was sensed by a thermistor and the absolute temperature of the sample was measured with a copper-constantan thermocouple. All wires were brought out of the vacuum chamber of the dewar by means of a vacuum feed through. A diagram of the sample holder and dewar is shown in Figure 27. The vacuum jacket of the tail section was modified such that an one inch diameter window could be mounted in front of the sample to enable light to pass in to the sample and be reflected out of the dewar. A KCl window was used for this purpose because it has a 90% flat transmittance over the entire range of wave lengths measured. NaCl could have been used, but KCl is less soluable in water than NaCl thus permitting a longer window life.

3. INFRARED MEASUREMENTS

In measuring the reflectance of NiS in the infrared two detectors were employed: a PbS detector to be used from about 1 to 2 microns and a bolometer from 2 to 10 microns. The output of the detector was measured by a PAR model 124 lock-in amplifier. The reference signal to

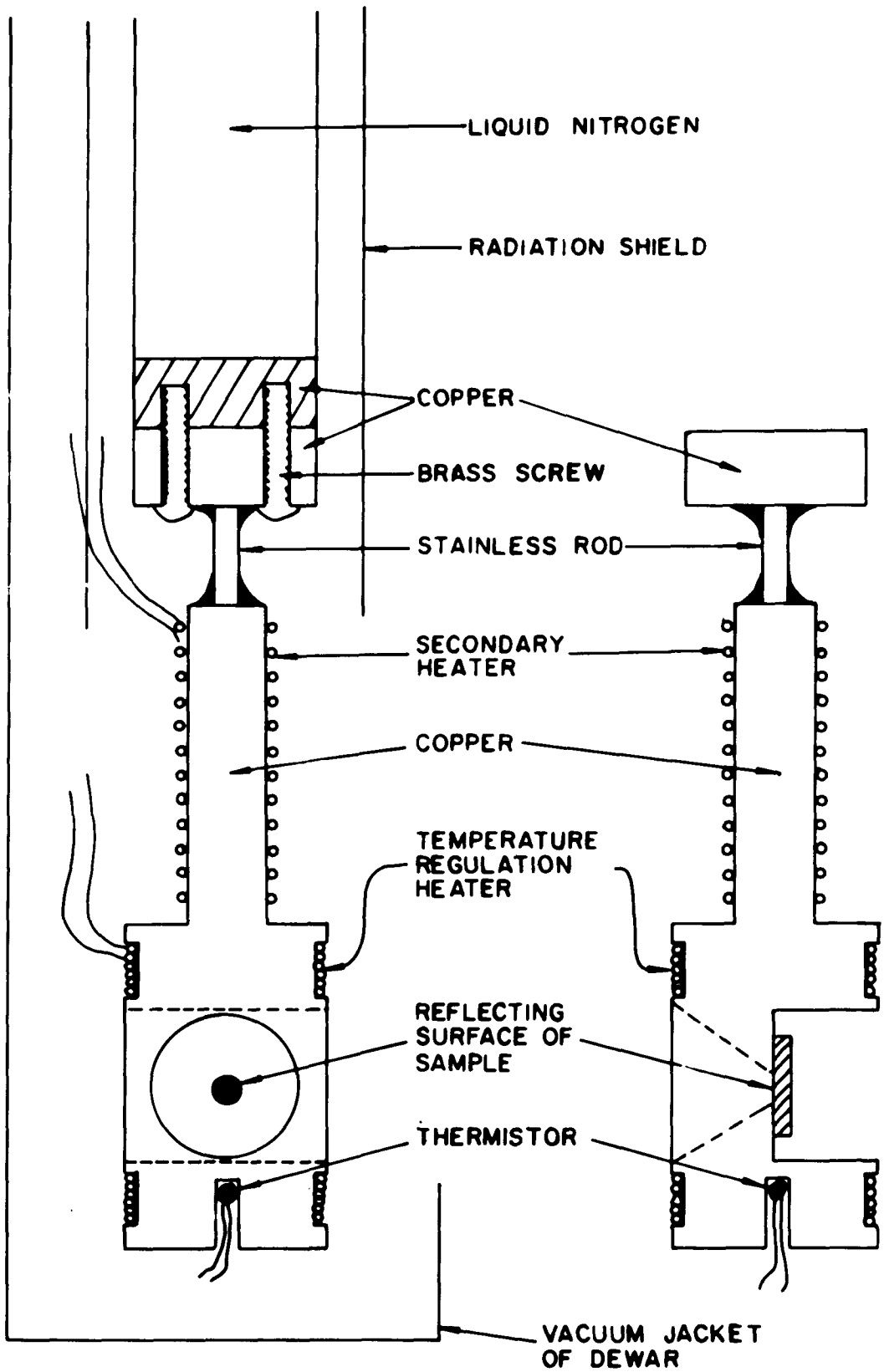
LIQUID NITROGEN
RADIATION SHIELD
COPPER
BRASS SCREW
STAINLESS ROD
SECONDARY HEATER
COPPER
TEMPERATURE REGULATION HEATER
REFLECTING SURFACE OF SAMPLE
THERMISTOR
VACUUM JACKET OF DEWAR

Figure 27

the amplifier was supplied the chopper wheel arrangement already described. The Nernst glower was turned on and allowed to warm up for a period of time no shorter than about three hours to minimize drift in the output of the lamp. The light beam in the sample channel was then physically blocked such that only the reference channel would strike the detector. A narrow portion of the spectrum was scanned by turning on the prism drive motor and the amplitude of the output signal was recorded on an X-Y recorder. The reference channel was then blocked and the output from the sample channel was recorded. The background radiation level was measured by turning the wavelength drive to a portion of the spectrum where the detector was not sensitive, as in the case of the PbS detector, or to where no radiation whould strike the detector because the window in front of the detector is opaque in that region. The background levels from both channels were measured and subtracted from the signal level in the sample and reference channels. The reflectivity was than found by dividing the remaining signal in the sample channel by that in the reference channel. This division eliminates variations in the output intensity of the lamp which are a function of wavelength. Each sample at each temperature was measured three times and the results averaged. A check was made on the lamp to determine how the output of lamp and measuring system

varied with time by measuring the signal at one wavelength for a period of about 10 minutes, the time required to scan the reference and sample channels during a measurement. Less than 1% deviation in the output signal was found.

Since the sample and reference channels are not identical because of the KCl window in the sample channel and possible differences in path lengths between the channels, a standard mirror was placed in the sample mount. The reflectance of the mirror was measured in the spectral region where the PbS detector is sensitive. Since the absolute reflectance of the mirror is known accurately, the magnitude of the reflectance of the sample could be corrected accordingly. A similar correction was to be made to the reflectance in the remaining region of the spectrum where measurements with the bolometer were made, but the bolometer went bad and could not be easily replaced. The magnitude of the reflectance in the far infrared was then adjusted such that the reflectances, as measured by the bolometer and the PbS detectors, would match where these sensitivities overlapped at about 2 microns. Thus no correction would be made in the far infrared for structure due to slight path length differences in the channels resulting in slight differences in absorption in the two channels. The width of this structure, however, would be much less

than the total wavelength range measured with the bolometer.

C. APPARATUS AND MEASUREMENT OF REFLECTANCE IN THE VISIBLE AND NEAR ULTRAVIOLET

A McPherson model 218 monochromator in conjunction with a model 817 double beam attachment was used to measure the reflectance of NiS in the visible and near ultraviolet. Tungsten light sources in the visible or a hydrogen discharge lamp in the ultraviolet were used as sources. A photomultiplier with a S-20 spectral response was employed. This photomultiplier has a maximum sensitivity at 4100Å. A sodium salicilate window is used which scintilates at all wavelengths shorter than 4100Å and is transparent to longer wavelengths. This permits a photomultiplier to be used throughout the visible and ultraviolet regions of the spectrum. A major drawback of this instrument is that very large samples, on the order of 3/4 inch in diameter must be used because the diameter of the beam is very large. Two single crystal samples were grown to accomodate this instrument and chemically polished according to the methods previously described. These measurements were made at room temperature in the single beam mode of the instrument. A portion of the spectrum was scanned while the output of the photomultiplier was recorded. The sample was then removed from the beam and the intensity of the source was

measured over the same region. Since there was no significant background energy in these measurements, the magnitudes of the two traces could be directly divided to obtain the reflectivity of the sample. The duration of a trace was short enough such that fluctuations in the lamp intensity were negligible.

D. RESULTS AND DISCUSSION

In the infrared, the reflectivity of two samples was measured which were chemically polished according to the procedure outlined earlier in this text. One sample was cut such that the reflecting surface was perpendicular to the c axis and the second such that the c axis was parallel to the reflecting surface. Each of the samples was measured at three temperatures: room temperature, about three degrees below the critical temperature, and the lowest temperature attainable by the apparatus without the addition of liquid helium. The transition temperature was determined by measuring the reflectance at a single wavelength as the temperature of the sample was gradually lowered by turning off the temperature regulator and decreasing the current in the second heater wound near the sample. During this process, the temperature was monitored by reading the thermal em.f. of the thermocouple. When the transition was reached, a sharp decrease in the reflectance was seen on each of the

samples. A trace of this curve is shown in Figure 28 showing a descent through the transition and a subsequent return. These traces were made at a wavelength of two microns. Notice that the reflectance anticipates the transition in the ascending curve by decreasing slightly before increasing sharply. Also the ultimate quantity of light reflected above the critical temperature after cycling through the transition has decreased which is probibly due to cracking or strain in the sample.

Figure 29 shows the reflectance of NiS from .1 to 3.5ev. These data were taken at 300°K on a sample where the c axis was perpendicular to the reflecting surface. The reflectance at three different temperatures for two samples, one with the c axis perpendicular and the other parallel to the sample surfaces are shown in Figures 30 and 31 respectivly. The absolute magnitude of the measured reflectance is estimated to be correct to within about 8%. In all of the measurements the beam was unpolarized so that the reflectance of the sample where the c axis was parallel to the surface contains components from both orientations. Since the surface of this orientation polished much more smoothly than the other, the magnitude of the reflectance is higher because there is less diffuse scattering from the surface. For both orientations, the reflectance

discontinuously at the critical temperature by about 15 to 20% at lower energies with the largest change occuring at the lowest measured energy. At energies less than 0.3ev, the reflectivity decreases even more as the temperature is decreased indicating a possible temperature dependent gap in the semiconducting state. The reflectance at 300°K is lower than in metals such as Ni, Cu,[44] or Al[43] however the d.c. conductivity of metallic NiS is not as high as it is in these examples. Below the critical temperature at low energies, the reflectance remains on the order of 50 to 60% down to the lowest measured energy (0.1ev). In this respect the reflectivity is not unlike that found in semiconductors such as InSb[45] Ge[46] or Si[47]. The changes in reflectivity seen at the critical temperature are similar to those seen in VO_2[48]. Raccah and Goodenough et al.[28] measured the reflectance at room temperature on a polycrystalline sample of NiS the results of which are qualitativly the same as presented here.

A listing of the data for the reflectance measurements is given in the Appendix.

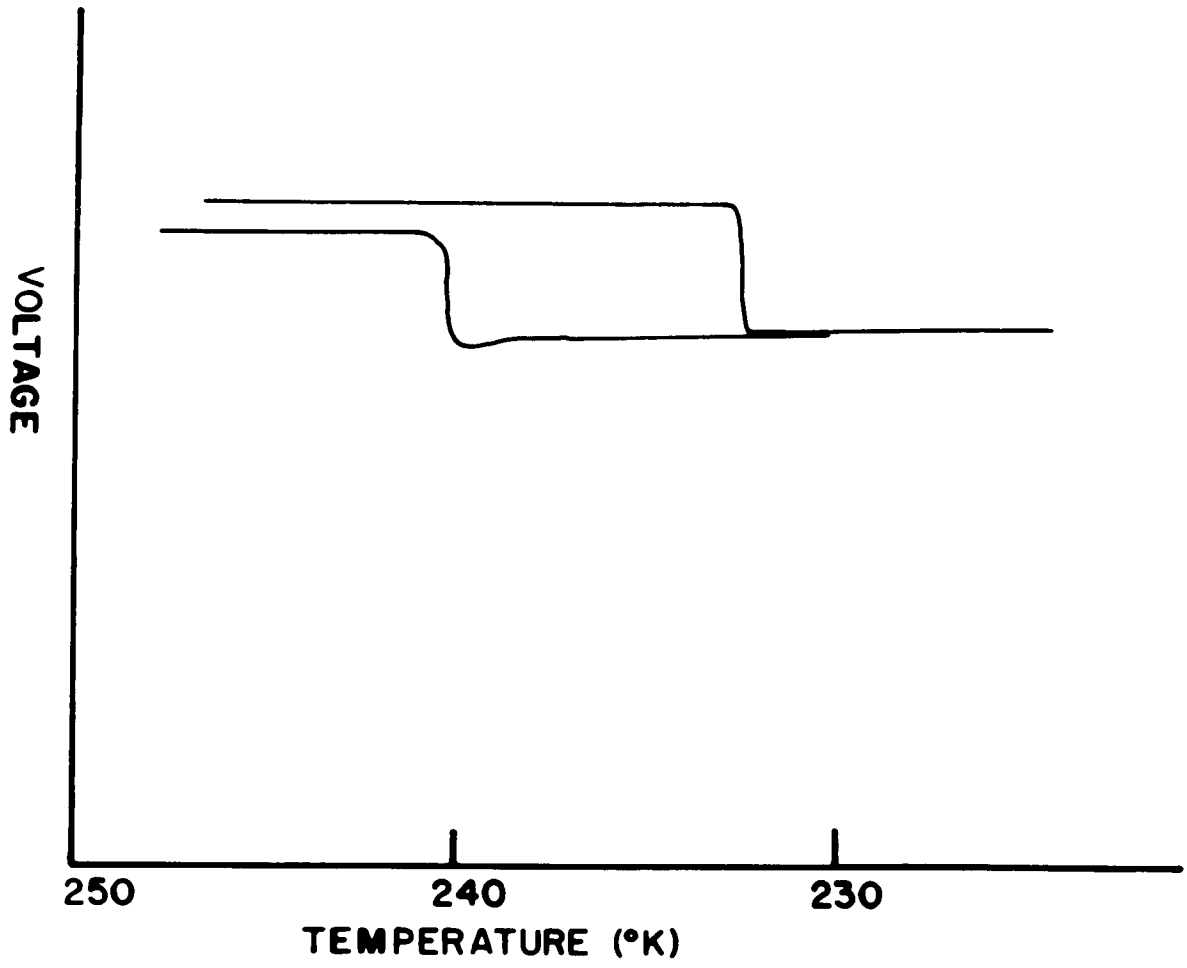

Figure 28

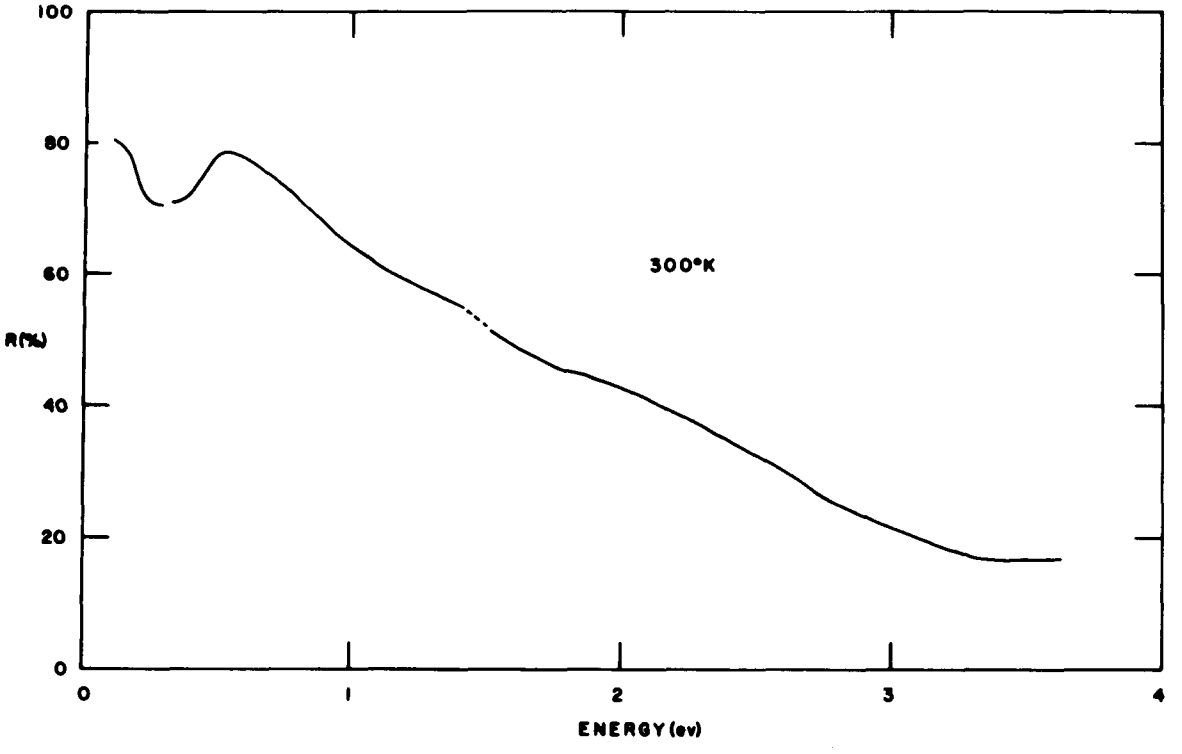

Figure 29

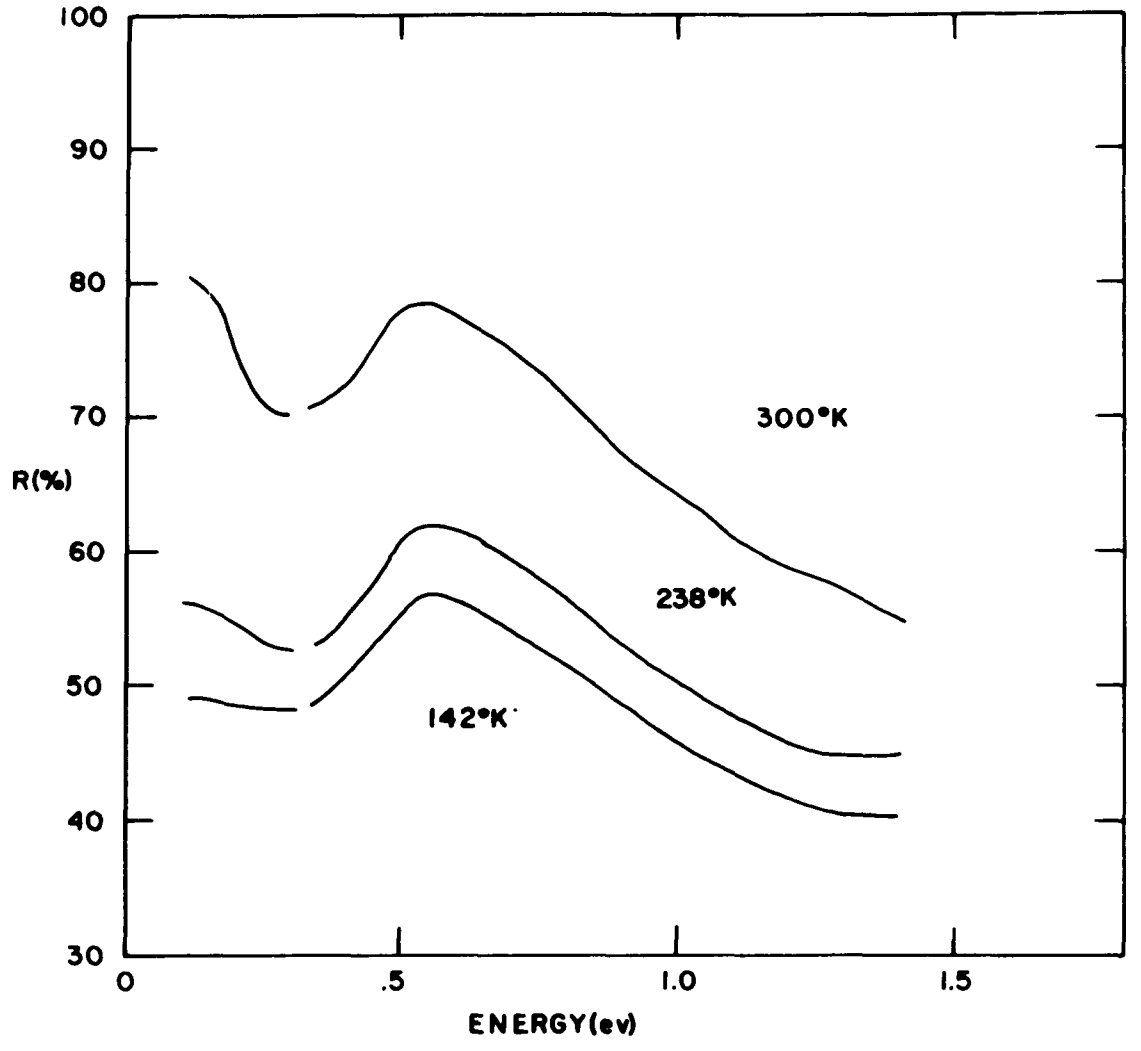

Figure 30

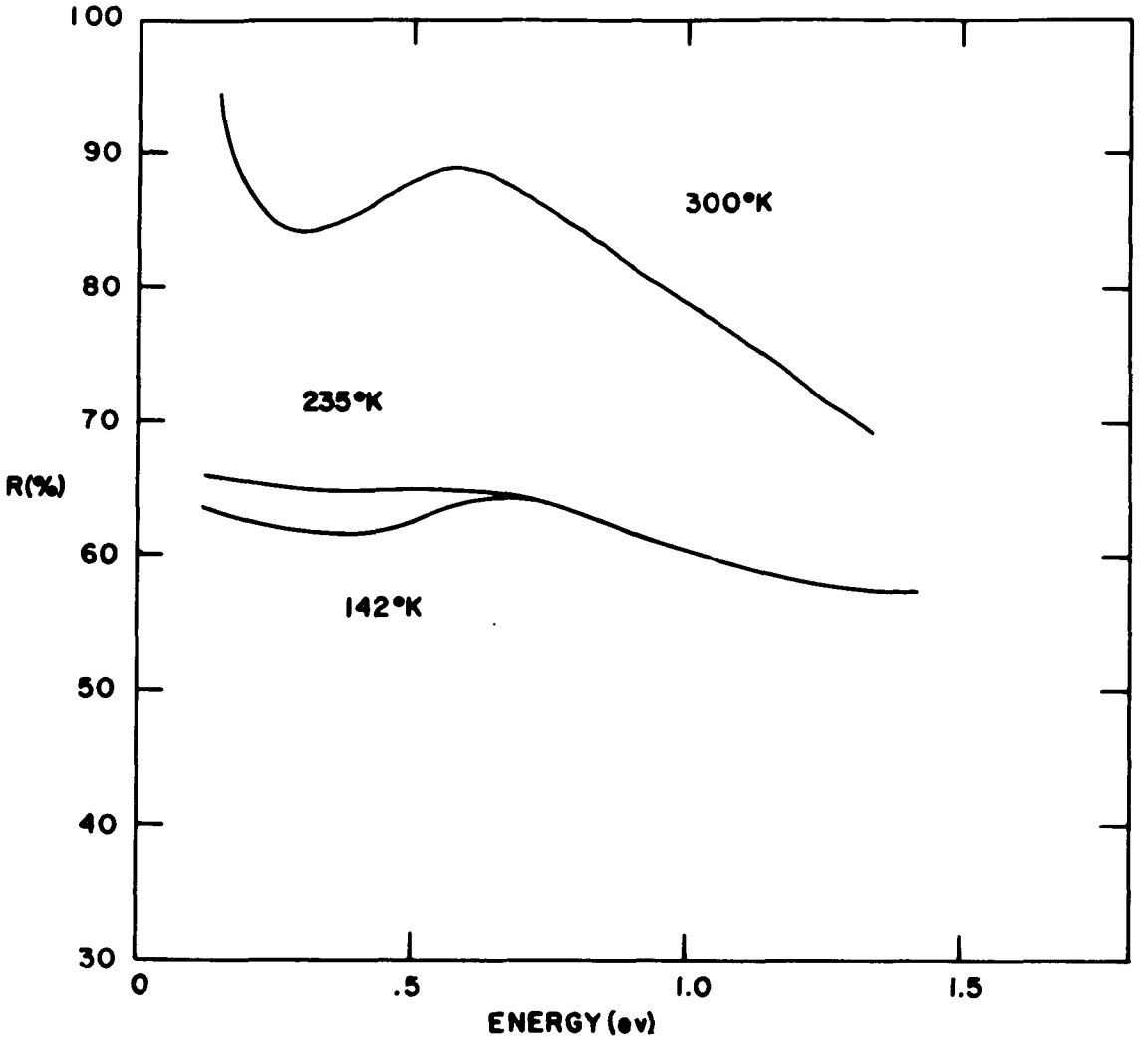

Figure 31

VII. RECENT WORK AND CONCLUSIONS

Recently, Koehler et al.[13] developed a technique of growing stoichiometric single crystals of known composition which have very narrow transitions (1-3°K) at any temperature from 0 to 264°K. The initial ingots were made by the same technique described in this thesis and a modified Bridgeman technique was used to grow very large single crystal ingots. These crystals were of nonuniform composition so an annealing process was used to homogenize them. The composition of their crystals was determined with an electron microprobe. These workers reaffirmed the relationship between the transition temperature and the composition (Figure 8) first observed by Sparks and Komoto[12] and found that cracking of single crystals can be minimized by using very small (1-2mm), very homogeneous crystals. In addition to the work on the Ni-S system, a study of how the additions of oxygen, chromium, iron and zinc in the system affected the MNM transition was performed. It was found that oxygen and iron were accepted in the lattice that these two elements broaden the transition (on the order of 30°K for .1 weight % oxygen) but that they don't significantly alter the transition temperature. In addition, they found that chromium and zinc enter the material in separate phases by forming CrS_3 and ZnS.

It was concluded that the only factor that significantly affects the transition temperature in NiS is stoichiometry.

A pressure-temperature phase diagram of NiS was measured by McWhan et al.[21] who were able to suppress the antiferromagnetic phase by applying pressure and measured the resistivity of the metallic phase down to liquid helium temperatures. Antiferromagnetism in their samples disappeared at pressures in excess of 20 kbar at 4.2°K. Their samples ordered from 200-235°K, but it is not clear from the paper whether this range is the width of the transition or the range of temperature over which different samples ordered. The resistance of the samples was measured to determine the critical temperatures for the phase diagram, but these results were complicated somewhat by the fact that from 5-10% of the sample was converted to the millerite phase during the high pressure measurements.

Recently White and Mott[49] proposed a theoretical interpretation of the experimental data on NiS in the literature. They suggest that the antiferromagnetic state in NiS is an itinerant electron state rather than a localized moment state. This is coupled with the further assumption that the low temperature phase is not semiconducting, but rather semimetallic. In their

model the conductivity parallel to the c axis is reduced at the transition by the anisotropic increase in the lattice parameters and the antiferromagnetic ordering. They further suggest that the observed MNM transition at 265°K may not be a Neel temperature where the spins disorder, but rather a temperature at which the moments disappear completely with the Neel temperature being on the order of 1000°K. It was assumed in their model that the system could be described by a Hubbard Hamiltonian and they suggest that the long range antiferromagnetic state disappears because of screening out of the Hubbard intraatomic electron-electron interaction, U, by the sulfur 3p band. They propose that as the temperature increases, the interaction, U, becomes sufficiently small to cause a first order transition.

Many of the ideas of White and Mott[49] are conjecture so they cannot quantitatively be compared to experimental results. It would seem, however, that the character of the resistivity below the critical temperature indicates that the low temperature phase is semiconducting, that is, the resistivity increases sharply with a decrease in temperature (Figure 24) over a wide range of temperatures while in a semimetal the resistance would decrease gradually as the temperature decreased unless there is a shifting of the bands

as a function of temperature.

In a recent calculation Kimball[50] points out that many MNM compounds have two types of electronic states which participate in conduction. In order to achieve a MNM transition as a function of temperature he has considered a two band Hamiltonian which includes a Heisenberg interaction, J, between localized electrons. In his calculation one band is free electron like (s or p) and the other is localized and antiferromagnetically ordered (d or f). The Kimball model predicts a discontinuous disappearance of the sublattice magnetization as the temperature is increased with possible hysteresis and an increase in the number of conduction electrons by a factor which depends on J at the critical temperature. The transition will occur while the magnetic electrons are still largely ordered. Qualitatively, then, this theory fits the experimental picture for NiS.

If the transition temperature is indicative of the composition of the crystal as has been strongly suggested by Koehler[13] then no transport measurements which are reported in the literature have been done on stoichiometric single crystals. Measurements on non-stoichiometric samples indicate that samples with

similar transitions can have very different properties which is probably the result of impurities and defects. For example, the ratio of carrier mobilities in the semiconducting state as measured by two different groups[24,33] is on the order of 330. All of the data has been interpreted in terms of a one carrier model which no doubt is inadequate, thus the absolute magnitudes of the transport data cannot be taken too literally. Also, thermoelectric power data[32] indicates that in the metallic state, the predominant carriers are electrons. However, the Hall constant[24] is positive. These two results suggest that the conductivity in the metallic state is relatively complicated.

The x-ray diffraction work presented in this thesis suggests that there is a distortion of the lattice at the critical temperature. The data has been interpreted to suggest that the symmetry of the unit cell is found to change from $P6_3/mmc$ in the metallic phase to $P6_3mc$ in the semiconducting phase. Kimball[50] has shown that this distortion would not be capable of producing a M'M transition because the energy bands at the A point in the reciprocal lattice are double degenerate[51] and symmetry considerations show that the degeneracy would not be lifted by the symmetry change. The optical data has not been fully analyzed and will not be discussed in this conclusion.

Specific heat measurements have shown that the change in the entropy and specific heat at the critical temperature are 5.03 J/mole-deg and 1383 J/mole respectively. Also an increase in the lattice contribution to the specific heat of about .6 J/mole-deg was measured. By fitting the data on either side of the specific heat anomaly and extrapolating it to the transition temperature, a change in the Debye temperature at the critical temperature of $\theta_D(T \leq T_c) = 276^\circ K$ and $\theta_D(T \geq T_c) = 183^\circ K$ was determined. An uncertainty of $\pm 80^\circ K$ on the absolute magnitude of Debye temperatures was calculated assuming maximum possible errors of all pertinent quantities in the calculation. The largest error in this calculation is introduced through the uncertainty in the absolute magnitude of the specific heat which was taken to be $\pm 1\%$. This uncertainty was determined from the calibration runs on pure copper. The random error in any one run, however, is only on the order of 0.3%. Thus a change in the Debye temperature can be measured more accurately than the absolute magnitude for any single measurement. Although the measurements are not conclusive, the results indicate that there is a possible change in θ_D at the critical temperature. A change in θ_D could be due to either a change in the phonon spectrum at the critical temperature perhaps due to the number of conduction electrons changing discontinuously

at T_c. It is not clear that these two possibilities can be treated independently and the measured effect may be due to one, both, or the interaction between the two.

Suppose, in the metallic state, that the properties of the conduction electrons can be approximated by a free electron gas. The magnetic susceptibility of the gas is then given by

$$\chi = \mu_\beta^2 N(E_f)$$

where μ_β is a Bohr magneton and $N(E_f)$ is the density of states at the Fermi energy. Since measurements of the susceptibility yield about 2.0×10^{-6} e.m.u./g[24,13,12] and assuming that there are no diamagnetic contributions to χ, the density of states is calculated to be about $22.5/cm^3$-ev. The entropy and specific heat of a free electron gas are of the same magnitude and are given by

$$S = C_v = \frac{2}{3}\pi^2 N(E_f)\, k_B^2\, T$$

At the critical temperature of 276°K then, the entropy of the conduction electrons inferred from the magnetic susceptibility is about 7.3 J/mole°K. In the metallic state the conduction electrons are disordered and have no magnetic moments while in the nonmetallic state they are antiferromagnetically ordered and the crystal becomes a semiconductor. The entropy of the free electron gas might then be on the same order of magnitude as the

change in entropy of the electronic system at the critical temperature and would overestimate the actual change because the entropy of the electrons in the semiconducting state is not zero. The entropy change calculated from γ corresponds to a latent heat, $\Delta H = T_c \Delta S$, of about 2000 J/mole which is larger than, but on the order of the magnitude of the values measured experimentally. This suggests that much of the observed entropy change is electronic in origin, but this result must be interpreted with caution, however, since the density of states inferred from the magnetic susceptibility is usually far larger than that obtained from entropy measurements at low temperatures[52]. The density of states is probably overestimated because the electron gas in the metallic state is not really "free" and electronic correlations must be considered.

Both the entropy of the conduction electrons and their contribution to the specific heat would normally be expected to be approximately equal or at least on the same order of magnitude. Thus if the observed entropy change at the transition is due only to the appearance of free carriers then the specific heat at the critical temperature would be expected to increase in the metallic state by an amount approximately equal to the entropy change. Experimentally this is not the case. The entropy change is 5.03 J/mole-deg whereas the

increase in the specific heat is about .6 J/mole-degree. This may point out that the entropy and specific heat of the carriers are not approximately equal as for a nearly free electron gas, but tha the difference is very large suggests that the situation is more complicated. There is a possible change in the phonon spectrum at the critical temperatures as indicated by the crystal distortion and changes in the lattice constant. Furthermore, there is no a priori reason to believe that the lattice vibrations and the electronic spectrum can be treated separately. In fact, the failure of calculations based on independent particle models to predict even the order of magnitude of the observed quantities may indicate that electron phonon interactions are indeed important to the MIM transition in VIS.

REFERENCES

1. N. F. Mott and Z. Zinamon, Rep. Prog. Phys. 33, 881 (1970).
2. S. Doniach, Adv. Phys. 18, 819 (1969).
3. D. Adler, Rev. Mod. Phys. 40, 714 (1968).
4. N. F. Mott, Proc. Phys. Soc. (London) A62, 416 (1949).
5. J. C. Slater, Phys. Rev. 82, 538 (1951)
6. D. Adler and H. Brooks, Phys. Rev. 155, 826 (1967).
7. N. F. Mott, Phil. Mag. 6, 287 (1961).
8. W. Kohn, Phys. Rev. 133, 171 (1964).
9. J. Hubbard, Proc. Royal Soc. (London) A726, 238 (1963).
10. J. Hubbard, Proc. Royal Soc. (London) A277, 237 (1964).
11. J. Hubbard, Proc. Royal Soc. (London) A281, 401 (1964).
12. J. T. Sparks, T. Komoto, Rev. Mod. Phys. 40, 752 (1968).
13. R. F. Koehler (private communication).
14. H. Remy, Treatise on Inorganic Chemistry (Elsevier Pub. Co., New York, 1956), Vol. II, page 312.
15. G. Kullerud and R. Yund, J. Petrol. 3, 126 (1962).
16. J. T. Sparks, T. Komoto, J. Appl. Phys. 34, 1191 (1963).

17. J. T. Sparks, T. Komoto, J. Appl. Phys. 39, 715 (1968).

18. J. T. Sparks, T. Komoto, J. Phys Radium, 25, 567 (1964).

19. J. T. Sparks, T. Komoto, Phys. Lett. 25A, 398 (1967).

20. S. Anzai, K. Ozawa, J. Phys. Soc. (Japan) 24, 271 (1968).

21. D. T. McWhan et al., Phys. Rev. B5, 2522 (1972).

22. J. Norwood, et al., J. Appl. Phys. 42, 1476 (1971).

23. J. Norwood, M. Townsend, Solid State Comm. 9, 41 (1971).

24. M. Townsend, et al., J. Phys. C. 4, 598 (1971).

25. I. Tsubokawa, J. Phys. Soc. Japan 13, 1432 (1958).

26. F. A. Smith, J. T. Sparks, J. Appl. Phys. 40, 1332 (1969).

27. S. Anzai, K. Ozawa, J. Appl. Phys. 41, 3558 (1970).

28. Raccah and Goodenough (private communication).

29. N. Alsen, Geol. Fören. Förhands. 45, 606 (1923).

30. G. Levi, A. Baroni, Z. für Krist. 92A, 210 (1935).

31. M. Laffitte, Bull. Soc. Chim. (France) 1959, 1211.

32. T. Ohtani, et al., J. Phys. Soc. Japan 29, 521 (1970).

33. T. Ohtani, et al., J. Phys. Soc. Japan 29, 1588 (1970)

34. D. Adler, H. Brooks, Phys. Rev. 155, 826 (1967).

35. Methods of Experimental Physics (Academic Press, New York, 1959) Vol. VI, p. 147.

36. Powder Diffraction File, American Soc. for testing and Materials, 1963.

37. H. Levy, Acta. Cryst. 9, 679 (1956).

39. International Tables for X-Ray Crystallography (Kynoch Press, Birmingham, England, 1965) Vol. III, p. 201.

40. W. C. Hamilton, Acta. Cryst. 18, 502 (1965).

41. M. Buerger, Crystal-Structure Analysis, (John Wiley & Sons, Inc., New York, 1960) p. 542.

42. D. S. McKinney, J. Opt. Soc. America 38, 222 (1948).

43. H. E. Bennett et al., J. Opt. Soc. America 52, 1245 (1962).

44. J. Feinleib, J. Appl. Phys. 40, 1400 (1969).

45. D. Greenaway, Phys. Rev. Let. 9, 97 (1962).

46. H. R. Philipp, H. R. and E. A. Taft, Phys. Rev 113, 1002 (1959).

47. H. R. Philipp and E. A. Taft, Phys. Rev. 120 37 (1960).

48. L. Ladd, Technical Report HP-26, Office of Naval Research, pp. 100,101.

49. R. White, Mott, Phil Mag. 24, 845 (1971).

50. J. Kimball (private communication).

51. J. H. Tyler, J. L. Fry, Phys. Rev. B1, 4604 (1970).

52. D. E. G. Williams, The Magnetic Properties of Matter (American Elsevier Publishing Co., Inc. New York, 1965)pages 65-67.

APPENDIX

SPECIFIC HEAT OF NIS SAMPLE NUMBER 1

INCREASING TEMPERATURE

T ^{O}K	C J/m-^{O}K	T	C	T	C
220.225	44.67	255.004	48.06	267.469	66.39
221.416	44.74	255.328	47.81	267.731	67.07
223.193	44.88	255.571	48.11	267.993	67.92
224.667	45.14	255.948	48.09	268.255	68.15
225.548	45.11	256.055	48.18	268.517	68.31
227.595	45.35	256.580	48.19	268.779	68.70
228.468	45.39	256.849	48.26	269.040	69.39
229.049	45.43	257.118	48.44	269.562	70.45
230.207	45.58	257.386	48.58	269.719	70.50
231.074	45.67	257.655	48.74	269.875	70.59
232.512	45.96	257.923	48.87	270.031	71.05
234.374	45.88	258.192	49.04	270.188	71.36
234.944	45.96	258.459	49.17	270.266	71.56
235.514	45.70	258.727	49.31	270.579	72.12
236.083	45.95	258.995	49.45	270.735	72.70
236.651	46.16	259.262	49.70	270.878	72.76
237.218	46.14	259.530	49.85	271.021	73.89
237.783	46.23	259.797	50.06	271.177	74.12
238.913	46.33	260.063	50.17	271.333	74.75
239.476	46.40	260.330	50.58	271.489	75.81
240.038	46.40	260.596	50.77	271.567	75.87
240.600	46.49	260.863	51.18	271.645	76.11
241.160	46.61	261.129	51.37	271.567	75.87
242.558	46.69	261.396	51.73	271.723	76.86
243.116	46.74	261.661	51.93	271.801	77.46
243.673	46.76	261.927	52.56	271.879	77.88
244.506	46.51	262.192	52.99	271.957	78.30
245.061	46.60	262.458	53.41	272.034	78.63
245.614	46.65	262.723	53.50	272.190	79.67
246.168	46.74	262.988	54.35	272.268	80.06
247.271	46.84	263.253	54.83	272.346	80.82
247.822	47.02	263.782	55.44	272.423	81.64
248.371	47.02	263.782	55.98	272.501	82.09
248.920	47.13	264.047	56.47	272.579	83.02
249.743	47.26	264.311	57.24	272.656	83.69
251.041	46.93	264.575	57.89	272.734	84.39
251.286	47.03	264.839	58.75	272.812	85.07
251.776	47.16	265.103	59.51	272.734	84.39
252.021	47.03	265.367	60.04	272.890	85.92
252.266	47.30	265.630	61.23	272.967	86.76
252.674	47.35	265.893	62.18	273.045	87.45
253.000	47.46	266.156	63.02	273.304	91.61
253.163	47.57	266.419	63.68	273.382	92.14
253.976	47.69	266.682	64.48	273.459	93.44
254.517	48.08	266.945	65.24	273.537	94.76
254.761	47.95	267.199	65.93	273.615	95.75

T	C	T	C	T	C
273.692	97.29	275.922	346.65	276.914	222.53
273.770	98.88	275.948	364.96	276.939	218.54
273.808	99.79	275.974	396.67	276.965	210.92
273.963	102.38	275.999	440.79	276.990	204.32
274.041	104.90	276.025	494.98	277.016	200.39
274.118	106.59	276.051	566.56	277.042	196.48
274.196	108.91	276.076	637.14	277.068	193.52
274.273	110.12	276.102	688.65	277.093	188.45
274.351	113.02	276.128	721.52	277.119	184.46
274.428	115.60	276.154	739.42	277.145	181.33
274.505	118.19	276.179	748.05	277.170	177.35
274.583	120.38	276.205	779.95	277.196	173.85
274.660	124.09	276.231	818.27	277.221	170.99
274.738	127.19	276.256	898.45	277.260	167.29
274.815	130.89	276.282	996.95	277.298	163.71
274.892	134.94	276.308	1162.70	277.349	157.73
274.969	140.04	276.347	1518.95	277.375	154.78
275.098	149.49	276.355	1588.60	277.401	152.04
275.124	150.47	276.363	1838.88	277.426	149.96
275.150	152.40	276.370	2024.17	277.452	149.32
275.176	154.41	276.378	2728.31	277.529	143.00
275.201	155.85	276.388	3491.34	277.605	137.02
275.227	158.70	276.396	5371.79	277.682	131.43
275.253	161.61	276.403	3566.68	277.785	125.99
275.279	164.51	276.408	3121.27	277.887	120.53
275.304	166.15	276.419	2206.91	277.964	117.08
275.330	168.36	276.427	1660.75	277.964	117.08
275.356	172.40	276.434	1464.90	278.041	113.32
275.382	175.69	276.442	1176.24	278.117	110.14
275.407	178.46	276.450	1004.57	278.207	106.66
275.433	180.94	276.458	976.07	278.296	104.05
275.459	185.95	276.477	701.13	278.435	99.24
275.485	188.29	276.503	575.49	278.588	94.60
275.510	191.98	276.529	510.71	278.767	89.94
275.536	191.81	276.554	448.01	279.035	84.60
275.562	201.71	276.580	419.81	279.125	82.10
275.588	206.02	276.606	382.16	279.201	81.15
275.614	210.47	276.631	358.15	279.278	79.99
275.639	212.71	276.657	338.49	279.354	78.93
275.665	224.15	276.683	297.69	279.431	77.42
275.691	230.17	276.708	290.56	279.507	76.78
275.742	241.19	276.734	279.55	279.584	74.93
275.768	253.79	276.760	277.18	279.660	74.40
275.793	263.74	276.785	263.37	279.737	73.22
275.819	271.83	276.811	252.03	280.055	69.60
275.845	281.94	276.837	246.67	280.310	66.97
275.871	303.35	276.862	241.58	280.564	64.76
275.896	316.55	276.888	227.90	280.819	62.98

T	C	T	C	T	C
281.200	60.73	286.902	50.83	303.180	51.44
281.581	58.99	287.403	50.71	303.670	51.72
281.834	58.02	287.904	50.77	304.640	51.73
282.088	56.87	288.902	50.74	305.360	51.62
282.342	55.84	289.899	50.81	306.090	51.74
282.595	55.51	290.396	50.71	307.660	51.96
282.848	54.67	290.892	50.82	308.620	52.10
283.101	54.01	291.389	50.68	309.340	52.07
283.354	53.22	291.884	50.70	310.510	52.16
283.606	53.10	292.873	50.79	311.490	52.14
283.859	52.68	293.366	50.98	312.450	52.33
284.111	52.06	293.860	50.86	313.640	52.38
284.364	52.01	294.352	50.41	314.590	52.40
284.615	51.53	294.844	50.50	316.010	52.44
284.867	51.38	296.071	51.29	316.950	52.44
285.119	51.08	296.560	51.00	318.360	52.62
285.371	50.77	297.049	51.07	319.300	52.64
285.760	50.71	302.210	51.56	320.240	52.67
285.987	50.84	302.690	51.60	321.180	52.79

SPECIFIC HEAT OF NIS SAMPLE NUMBER 1
DECREASING TEMPERATURE

T °K	CJ/m-°K	T	C	T	C
219.329	44.74	254.517	48.08	265.380	72.77
220.225	44.67	254.761	47.95	265.459	73.59
221.416	44.74	255.004	48.06	265.538	74.02
230.207	45.82	255.328	47.81	265.617	74.35
223.193	44.88	255.571	48.11	265.696	75.01
224.667	45.14	255.948	48.09	265.775	76.40
225.548	45.11	256.055	48.18	265.854	77.08
227.595	45.35	256.930	55.64	265.933	77.58
228.468	45.39	258.272	56.86	266.012	79.09
229.049	45.43	258.540	57.19	265.972	80.55
230.207	45.58	258.808	57.56	266.169	82.65
231.074	45.67	259.075	57.73	266.918	128.66
232.512	45.96	259.343	58.06	267.036	139.00
234.374	45.89	259.610	58.38	267.155	148.78
234.944	45.96	259.877	58.89	267.181	150.14
235.514	45.70	260.143	59.20	267.207	153.33
236.083	45.95	260.410	59.43	267.233	155.24
236.651	46.16	260.677	59.95	267.260	156.17
237.217	46.14	260.943	60.43	267.286	157.93
237.783	46.23	261.209	60.82	267.312	160.01
238.913	46.33	261.475	61.50	267.338	162.33
239.476	46.40	261.741	61.99	267.364	164.99
240.038	46.40	262.007	62.48	267.391	166.98
240.600	46.49	262.272	62.78	267.417	169.06
241.160	46.61	262.538	63.74	267.443	171.85
242.558	46.69	262.803	63.93	267.469	174.18
243.116	46.74	263.067	64.65	267.495	174.75
243.672	46.76	263.333	65.64	267.522	176.02
244.506	46.51	263.782	66.80	267.548	177.88
245.061	46.60	263.968	67.01	267.574	181.36
245.614	46.65	264.047	67.04	267.600	183.97
246.167	46.74	264.153	67.50	267.745	188.42
247.271	46.84	264.232	68.52	267.810	198.03
247.822	47.02	264.311	68.63	267.836	201.60
248.371	47.02	264.390	68.67	267.863	202.98
248.920	47.13	264.469	69.21	267.889	204.12
249.742	47.26	264.549	69.59	267.915	206.50
251.041	46.93	264.588	69.60	267.941	211.82
251.286	47.03	264.668	69.66	268.020	214.57
251.776	47.16	264.747	69.72	268.046	217.57
252.021	47.03	264.826	69.97	268.072	220.07
252.266	47.30	264.905	70.68	268.098	224.81
252.674	47.35	265.063	71.44	268.124	228.82
253.000	47.46	265.142	71.76	268.150	229.77
253.163	47.57	265.221	72.24	268.177	231.29
253.976	47.69	265.301	72.30	268.203	233.85

T	C	T	C	T	C
268.229	238.41	268.046	70.27	272.060	52.60
268.255	245.81	268.098	69.77	272.216	52.44
268.308	252.01	268.150	69.46	272.372	52.28
268.360	267.14	268.203	68.63	272.527	52.28
268.386	272.22	268.255	67.81	272.683	51.90
268.412	274.28	268.308	66.84	272.838	51.81
268.438	277.68	268.373	66.61	272.993	51.68
268.465	285.59	268.438	65.97	273.304	51.53
268.478	282.98	268.491	65.45	273.537	51.25
268.504	280.01	268.543	64.73	273.692	51.28
268.530	293.84	268.595	64.54	273.847	51.05
268.556	309.85	268.648	64.57	274.002	51.23
268.582	307.52	268.765	63.30	274.234	51.03
268.609	315.88	268.844	62.66	274.389	50.84
268.635	321.39	269.027	61.39	274.544	50.85
268.661	336.84	269.210	60.15	274.699	50.78
268.687	348.54	269.288	59.97	274.854	50.82
268.713	364.25	269.366	59.68	275.008	50.71
268.739	375.81	269.445	58.62	275.163	50.27
268.765	390.19	269.562	58.66	275.472	50.46
268.797	423.10	269.679	58.11	275.626	50.53
268.812	439.40	269.758	57.89	275.781	49.97
268.828	464.22	269.836	57.77	275.935	50.45
268.844	488.24	269.914	57.36	276.089	50.38
268.859	513.38	269.992	57.04	276.243	50.18
268.875	542.69	270.071	56.63	276.398	50.25
268.891	604.47	270.149	56.57	276.552	50.16
268.903	614.29	270.227	55.99	276.860	50.08
268.910	672.79	270.305	55.93	277.424	50.03
268.918	703.70	270.383	55.69	278.550	49.99
268.926	767.75	270.461	55.74	279.571	50.00
268.934	858.73	270.540	55.28	280.590	50.02
268.942	900.22	270.618	55.05	281.606	50.11
268.949	1026.96	270.696	54.88	282.873	50.26
268.954	1227.79	270.774	54.48	283.884	50.28
268.961	1475.31	270.852	54.43	285.648	50.46
268.966	1590.70	270.930	54.49	286.651	50.48
268.970	2435.31	271.008	54.22	287.654	50.49
268.974	3284.91	271.086	54.47	288.653	50.54
266.511	200.90	271.164	54.10	289.401	50.61
266.630	151.41	271.242	53.73	290.644	50.78
266.800	350.17	271.320	54.03	291.636	50.80
267.036	103.35	271.398	53.66	292.626	50.90
267.246	89.70	271.476	53.64	293.613	50.81
267.430	83.13	271.554	53.24	295.335	51.09
267.561	79.21	271.632	53.28	296.316	51.12
267.719	75.89	271.710	53.07	297.293	51.15
267.993	71.45	271.905	52.86	298.999	51.35

SPECIFIC HEAT OF NIS SAMPLE NUMBER 2
INCREASING TEMPERATURE

T °K	C J/m-°K	T	C	T	C
35.296	2.90	141.610	36.55	218.280	45.01
37.373	3.45	145.223	37.25	218.880	45.23
40.390	4.26	147.597	37.67	219.478	45.13
42.336	4.81	153.418	38.58	220.076	45.23
45.158	5.74	155.704	38.87	220.672	45.45
45.158	6.09	157.967	39.19	224.520	45.44
48.741	7.01	162.427	39.85	225.108	45.52
50.456	7.59	164.626	40.07	225.695	45.60
33.165	2.39	166.805	40.29	226.281	45.68
36.341	3.15	170.037	40.71	226.866	45.87
39.397	3.97	171.106	40.74	227.449	45.61
42.336	4.91	169.680	40.96	228.032	45.89
46.974	6.64	171.815	40.88	228.613	45.99
49.604	7.27	173.933	41.24	229.194	46.10
52.121	8.34	178.116	41.78	229.773	45.85
54.527	9.32	181.209	41.87	230.352	45.86
56.821	10.37	183.252	42.07	230.929	45.88
59.007	11.54	187.292	42.50	231.506	45.95
61.804	13.24	189.289	42.76	232.081	46.05
63.836	14.00	190.282	42.76	232.656	46.00
65.838	14.66	193.241	42.92	233.230	46.07
67.811	15.36	194.220	43.02	233.802	46.21
70.719	16.52	197.138	43.42	234.374	46.20
72.625	17.01	199.067	43.28	234.944	46.21
74.783	17.93	200.982	43.59	236.083	46.30
78.187	18.82	202.885	43.98	236.651	46.42
80.887	20.21	206.653	44.22	237.218	46.36
82.657	20.75	208.520	44.30	237.783	46.58
85.272	21.73	210.374	44.59	238.349	46.53
86.989	22.18	205.716	44.04	238.913	46.64
90.360	23.19	206.341	44.11	239.476	46.59
92.016	23.89	206.965	44.13	240.038	46.66
96.074	25.34	208.829	44.48	240.600	46.77
99.240	26.20	209.448	44.35	241.720	46.74
102.339	27.19	210.066	44.44	242.279	46.87
105.375	27.99	210.682	44.50	242.837	47.05
106.870	28.45	211.297	44.46	243.394	46.99
111.270	29.69	212.523	44.65	243.951	47.14
114.135	30.50	213.134	44.62	244.506	47.36
118.339	31.62	213.744	44.66	245.061	47.21
121.082	32.43	214.353	44.71	245.614	47.49
123.782	32.90	214.960	44.79	246.168	47.52
129.056	34.31	215.567	44.74	246.995	47.48
131.636	34.61	216.172	44.78	247.546	47.40
134.179	35.23	216.775	44.87	248.097	47.67
136.688	35.73	217.378	45.06	248.646	47.78

T	C	T	C	T	C
249.195	47.85	269.379	62.77	277.014	270.71
249.743	48.02	269.640	63.07	277.039	273.77
250.290	48.20	269.901	63.80	277.116	299.55
250.836	48.18	270.422	64.90	277.142	305.33
251.381	48.35	270.683	65.49	277.167	308.70
251.926	48.57	270.943	66.61	277.193	313.58
253.285	48.41	271.203	67.97	277.219	323.29
253.827	48.67	271.463	68.45	277.244	333.01
254.369	48.96	271.723	69.81	277.270	341.82
254.909	48.98	271.982	70.83	277.295	349.28
255.449	49.09	272.242	72.11	277.321	385.30
255.988	49.49	272.501	74.86	277.347	392.15
256.527	49.55	272.760	75.56	277.372	369.99
257.064	49.68	273.019	78.48	277.398	378.66
257.601	49.84	273.537	82.26	277.424	388.55
258.138	50.13	273.795	85.05	277.449	393.90
258.165	51.09	274.054	87.70	277.475	400.01
258.433	51.11	274.312	92.32	277.500	409.90
258.701	51.20	274.570	99.06	277.526	425.85
258.968	51.33	274.969	106.31	277.577	402.97
259.235	51.55	275.047	108.55	277.603	426.79
259.770	51.85	275.124	110.29	277.628	430.64
260.037	51.99	275.356	117.91	277.654	434.04
260.304	52.29	275.433	121.35	277.705	420.99
260.570	52.60	275.510	125.49	277.757	419.60
260.836	52.87	275.588	127.34	277.782	417.69
261.103	52.88	275.665	130.89	277.808	411.84
261.369	53.18	275.742	134.74	277.833	406.45
261.635	53.32	275.819	139.00	277.859	400.29
261.900	53.63	275.896	144.06	277.885	391.86
262.166	54.13	275.974	147.82	277.910	385.55
262.803	54.19	276.051	152.69	277.936	388.18
263.067	54.97	276.128	158.26	277.961	370.80
263.729	55.89	276.282	169.92	277.987	364.02
263.994	56.06	276.359	177.71	278.013	354.52
264.258	56.40	276.436	185.21	278.064	332.16
264.522	56.85	276.513	193.01	278.089	327.81
264.786	57.08	276.629	207.34	278.115	318.90
265.050	57.45	276.654	209.93	278.141	310.44
265.314	57.68	276.680	214.03	278.166	304.41
265.577	58.05	276.706	217.52	278.192	299.90
265.840	58.14	276.731	220.57	278.217	291.89
266.104	58.66	276.757	225.12	278.243	284.04
268.072	60.95	276.783	229.37	278.269	270.40
268.334	61.36	276.808	233.02	278.384	249.34
268.595	61.62	276.834	237.58	278.460	252.70
268.857	62.21	276.962	260.07	278.537	219.33
269.118	62.36	276.988	266.30	278.614	206.23

T	C	T	C	T	C
278.690	195.15	282.772	60.14	290.942	51.04
278.767	184.57	282.899	59.09	291.190	50.84
278.844	174.18	283.025	59.13	291.438	51.01
278.920	166.53	283.152	57.77	291.686	51.06
278.997	159.18	283.657	55.59	291.933	51.08
279.035	148.63	283.909	54.64	292.181	51.23
279.227	136.98	284.162	53.93	292.428	51.22
279.303	132.66	284.414	53.19	292.675	51.29
279.380	128.34	284.666	52.77	292.848	51.88
279.456	123.60	284.918	51.99	292.848	51.73
279.533	120.59	285.169	51.59	292.996	51.76
279.571	118.37	285.414	51.13	293.120	51.19
279.724	111.08	285.439	51.04	293.860	51.36
279.851	105.95	285.439	51.04	294.598	51.48
279.979	101.58	285.464	50.95	296.071	51.76
280.106	97.45	285.489	50.93	296.804	51.61
280.234	93.28	285.949	51.15	297.781	51.76
280.361	89.90	286.200	51.09	297.781	51.51
280.488	86.58	286.451	51.14	298.513	51.62
280.742	83.22	286.701	51.18	299.398	51.79
280.870	78.91	286.952	51.02	300.133	51.82
280.997	76.96	287.203	51.00	300.866	51.90
281.124	74.94	287.704	50.77	301.598	51.98
281.251	73.27	288.203	50.84	303.788	52.17
281.378	71.44	288.453	50.86	305.242	52.22
281.505	69.38	288.703	50.55	306.691	52.20
281.632	68.81	288.952	50.75	308.136	52.13
281.759	67.47	289.201	50.84	308.875	52.21
281.885	66.34	289.450	50.84	314.110	52.86
282.012	65.05	289.699	50.89	316.478	53.02
282.139	64.11	289.948	50.87	318.834	53.06
282.265	62.91	290.197	51.07	321.178	53.35
282.519	61.35	290.446	51.09	323.510	53.44
282.646	60.47	290.694	51.01	325.831	53.72

REFLECTANCE OF NiS

300°K, c axis perpendicular to surface

E(ev)	R(%)	E(ev)	R(%)	E(ev)	R(%)
3.54	16.5	2.480	33.2	1.879	44.4
3.44	16.7	2.431	34.2	1.851	45.0
3.35	17.0	2.348	35.0	1.824	45.0
3.26	17.3	2.340	35.8	1.797	45.2
3.18	18.5	2.296	36.9	1.771	55.6
3.10	20.0	2.255	37.4	1.746	56.1
3.024	21.2	2.214	38.5	1.722	56.8
2.952	22.6	2.175	39.1	1.699	57.0
2.884	23.7	2.138	39.9	1.677	57.6
2.818	24.5	2.102	40.7	1.653	58.1
2.756	25.8	2.063	41.6	1.590	60.0
2.696	27.3	2.000	42.3	1.550	60.0
2.640	29.0	1.968	43.0	1.512	61.5
2.583	30.3	1.938	43.7		
2.531	31.7	1.908	43.7		

	c axis ⊥ surface			c axis ∥ surface		
	300°K	238°K	142°K	300°K	235°K	142°K
E(ev)	R(%)	R(%)	R(%)	R(%)	R(%)	R(%)
1.426	55.3			69.3	56.1	56.9
1.405		45.8	40.8	70.1	57.0	57.7
1.383	56.1		40.0	70.4	57.0	57.4
1.361	56.4	45.0	40.6	70.7	57.2	57.4
1.338	57.0	45.1	40.9	70.4	58.0	57.6
1.315	57.3	45.0	41.1	69.4	58.0	58.5
1.292	56.0	44.5	40.1	69.9	57.2	58.1
1.267	56.1	44.5	40.5	70.5	57.5	57.3
1.244	58.0	45.0	40.8		57.9	56.7
1.220	58.1	45.5	41.1	72.3	57.9	58.2
1.196	57.6	46.1	42.1	73.5	57.9	57.3
1.171	59.4	46.8	43.0	73.6	58.0	57.9
1.145	59.2	46.9	43.3	74.7	58.2	58.3
1.119	60.2	47.2	42.2	75.4	59.7	58.6
1.092	61.8	47.5	43.4	76.8	59.9	59.4
1.066	62.4	48.3	44.2	77.4	60.1	59.5
1.038	63.3		44.8	76.3	61.0	60.5
1.010		50.8	46.8	78.6	61.8	61.3
.982	63.6	50.9	47.2	78.5	60.2	59.7

.953	64.1	51.4	47.7	79.9	60.5	60.2
.924	66.4	52.0	47.9	80.7	60.8	60.7
.893	67.2	52.8	48.2	81.5	62.2	61.2
.864	67.9	54.0	49.1	82.5	62.3	62.5
.833	69.6	54.7	50.4	83.7	62.6	62.7
.802	71.2	56.4	51.2	84.6	63.3	62.9
.771	72.8	57.5	52.3	85.2	63.4	64.2
.739	73.7	58.2	53.1	86.3	63.7	63.6
.709	73.7	59.0	53.7	86.7	63.9	63.6
.678	75.3	60.0	54.1	86.7	63.5	63.4
.648	76.3	60.4	55.3	88.9	65.0	63.8
.618	77.2	61.5	55.6	88.5	64.3	63.8
.589	77.4	61.7	56.6	88.3	64.6	64.0
.562	77.6	61.5	56.5	88.8	64.7	63.3
.536	78.3	61.0	56.6	88.6	64.2	63.2
.511	78.5	61.0	55.8			
.488	76.6	59.2	53.9	87.4	64.4	62.1
.467	75.3	58.2	53.6	86.9	64.6	61.2
.477	75.3	57.4	53.4			60.0
.429	75.0				66.1	60.8
.383	71.8	54.4	50.8	86.0	64.9	62.8
.370	71.3	54.2	49.8	86.6	65.5	61.5
.358	71.1	53.2	48.7			
.347	69.3	52.3	48.3			
.337	71.1	53.0				
.276	70.0	52.9	47.9	83.9	64.8	62.0
.265	70.5	53.2	48.1	84.2	63.5	61.8
.256	70.4	53.1	48.0	84.7	63.6	61.4
.247	70.5	52.8	47.4	84.5	63.1	62.6
.239	71.6	53.3	48.1	85.0	65.1	62.8
.231	71.7	52.9	47.7	84.6	64.8	62.6
.225	72.3	52.9	47.9	85.2	64.6	61.5
.219	72.3	53.1	47.9	85.9	64.6	61.3
.213	72.8	53.8	48.0	87.1	65.2	62.2
.208		53.9	48.3	88.2	65.0	62.3
.203	72.9	54.2	48.2	88.6	64.6	62.2
.201	72.2	53.7	47.6		64.2	
.191	75.0	54.9	48.8	89.4	65.4	62.1
.183	76.4	54.7	48.6		65.7	62.8
.177	77.3	55.5	49.2	91.7	65.5	62.8
.166	78.1	55.7	49.1	93.8	63.6	61.3
.156	79.7	56.3	49.0	94.8	66.5	63.1
.148	79.2	56.0	48.8	94.9	65.9	62.7
.142	79.2	56.2	48.6		63.6	61.5
.136	80.2	56.1	48.3		66.0	65.3
.128	79.4	55.6	48.4			64.3

VITA

Jeffrey F. Trahan was born in New Orleans, Louisiana on April 4, 1941. His secondary education was completed at Alcee Fortier High School in New Orleans and in 1959 he enrolled at Tulane University from which he received a Bachelor of Science degree in Physics in 1963. The following three years were spent in the U. S. Army after which he enrolled for graduate study in physics at Louisiana State University in the fall of 1966. He received a Master of Science degree in physics in January of 1969. In July of 1964 he was married to the former Alice Jean Lonberger and they have two children. He is a member of the American Physical Society, the American Institute of Physics and has been elected to Sigma Pi Sigma and Phi Kappa Phi honor societies. He is a full member of the Society of Sigma Xi and is presently a candidate for the degree of Doctor of Philosophy.

EXAMINATION AND THESIS REPORT

Candidate: Jeffrey Francis Trahan

Major Field: Physics

Title of Thesis: Experimental Studies of the Metal-Nonmetal Transition in Nickel Sulfide

Approved:

R. G. Goodrich
Major Professor and Chairman

Max Goodrich
Dean of the Graduate School

EXAMINING COMMITTEE:

Joseph Callaway

Edward Zdanis

John Kimball

William Lamb

Date of Examination:

May 12, 1972